University of Zurich[UZH]

# Modelling climate sensitivity of debris-covered glaciers

GEO 511 Master's Thesis

**Author**
Florian Hardmeier
16-726-283

**Supervised by**
Prof. Dr. Andreas Vieli
James Ferguson

**Faculty representative**
Prof. Dr. Andreas Vieli

30.04.2022
Department of Geography, University of Zurich

University of Zurich[UZH]

# Modelling climate sensitivity of debris-covered glaciers

GEO 511 Master's Thesis

Florian Hardmeier
florian.hardmeier@uzh.ch

Department of Geography
University of Zurich

**Supervised by**
Prof. Dr. Andreas Vieli
James Ferguson

**Faculty representative**
Prof. Dr. Andreas Vieli

April 30, 2022

# Acknowledgements

I want to give thanks most of all to my thesis supervisor, Prof. Dr. Andreas Vieli, who guided me through this project. I am thankful for giving me the hard choice between several interesting topics, to organizing the amazing field work campaign to Zmuttgletscher, and helping me out immensely in countless meetings throughout the evolution of this thesis. The expertise in the field, recommendations of literature, and broad knowledge about the modelling process were essential for me. I would also like to thank James Ferguson, my co-supervisor, for introducing me to the DEBISO model he wrote himself, giving me the solid knowledge of the model I needed to perform my own experiments. I would like to thank Boris Ouvry for giving his perspectives and knowledge on field work, glaciers, supraglacial streams, and supraglacial food. I would like to thank Simon Farsky and Adrien Wehrlé for being great companions in the field work, and our symbiotic data collection process. I would like to thank Dimi for proofreading and my friends and family for supporting me in one way or another.

# Abstract

The common occurrence of debris-covered glaciers in high-mountain areas makes their response to climate change relevant. The insulating effect of debris cover on surface melt causes debris-covered glaciers behave differently from debris-free glaciers, warranting the use of a specialized model for predictions. In this thesis, the 2D flowline DEBISO model (Ferguson and Vieli, 2021) is used in assessing the response of debris-covered glaciers to abstract and realistic climate change. The model calculates the transport and effect of debris cover, while incorporating the formation of ice cliffs on stagnant termini as a melt-enhancing process in retreat. Two new additions to the model are made and analyzed: the curve of insulation by debris cover thickness is fit to field and literature data, and the formation of ice cliffs in the entire ablation area through supraglacial streams is added to the model. Results show that previous estimates might have overestimated the insulation effect. Response to climate changes shows significant lag consistent with observations and previous studies, which is heavily dependent on parameters like size, debris cover, and bed geometry. The lag in response leads to a dichotomy in retreat between easy re-advance for short-term warming, and more difficult re-advance following long-term warming like measured and projected climate change over the 20th and 21st century. As a consequence of this lag, length response from short-term changes in climate is often minimal, making the establishment of a relationship of volume as a derivative of climate possible. Both new additions to the model resulted in a significantly weakened insulating effect, leading to behavior in retreat and advance more similar to debris-free glaciers.

# Contents

# List of Figures

# List of Tables

Chapter 0

# List of abbrevations

**Abbrevations**

| | |
|---|---|
| ELA | Equilibrium Line Altitude |
| GLAMOS | Glacier Monitoring Switzerland |
| IPCC | Intergovernmental Panel on Climate Change |
| m a.s.l. | Meters above sea level |
| SIA | Shallow Ice Approximation |
| SSP | Shared Socioeconomic Pathway |

**Variables from the modelling experiments**

| | |
|---|---|
| $\tau_v$ | E-folding volume response time |
| $A$ | Amplitude (sinus wave) |
| $\lambda$ | Wavelength (sinus wave) |
| $\varphi$ | Phase lag (sinus wave) |
| $e$ | Euler's number ($\approx 2.72$) |

**Variables from the DEBISO model**

| | |
|---|---|
| $a$ | Suface mass balance |
| $\tilde{a}$ | Elevation-dependent debris-free mass balance |
| $a_{max}$ | Maximum surface mass balance |
| $a_s$ | Summer mass balance |
| $A$ | Glen's flow law rate factor |
| $b$ | Bed elevation |
| $D$ | Debris cover thickness |
| $D_0$ | Characteristic debris cover thickness for Østrem curve |
| $\mathrm{d}t$ | time step |
| $\mathrm{d}x$ | Horizontal grid size |
| $f_{red}$ | Runoff reduction factor |
| $g$ | Gravitational acceleration |
| $h$ | Glacier surface elevation |
| $H$ | Ice thickness |
| $n$ | Glen's constant / exponent |
| $Q_{grid}$ | Cumulative runoff by grid point |
| $Q$ | Cumulative runoff |
| $u$ | Ice celocity |
| $x$ | Distance along the glacier |
| $\lambda$ | Cryokarst area fraction |
| $\lambda_m$ | Maximum cryokarst area fraction |
| $\rho$ | Density of ice |
| $\sigma$ | Strain rate |
| $\tau_d$ | Driving stress |

Chapter 1

# Introduction

## 1.1 Motivation

Glaciers are commonly thought of as massive, slowly creeping structures of ice, with the blue and white colors of that ice giving them their characteristic look. But many glaciers present themselves very differently. Under the right circumstances, steep headwalls and slopes can deliver debris onto a glacier's surface through avalanching (Ferguson and Vieli, 2021). In the accumulation zone of a glacier, this debris is buried under new firn. It is then englacially transported downstream, until it resurfaces in the ablation zone. Generally, debris cover increases in thickness towards the terminus (Mölg et al., 2019), as melt increases and debris is transported dynamically with the ice.

Debris cover changes the parameters of the ablation process at the glacier surface. There are two main processes influencing surface ablation in opposite ways. One of them is a melt enhancement effect due to the increase in albedo compared to clean ice. The other is an insulation effect due to absorption of incoming shortwave radiation, which is dominant with thick debris layers (Østrem, 1959; Richardson and Brook, 2010). The subsequent question is how strong these effects are with varying debris cover thickness and how much they reduce surface ablation.

Despite the fact that debris should have an overall insulating effect, some studies have provided evidence that debris-covered glaciers have similar mass balances to debris-free glaciers (Nuimura et al., 2012; Gardelle et al., 2013; Pellicciotti et al., 2015; Brun et al., 2016). Using energy balance models, this anomaly has been suggested to be caused by the formation of ice cliffs on stagnating tongues of debris-covered glaciers (Sakai et al., 2000; Steiner et al., 2015; Miles et al., 2016). Ice cliffs generally appear when the surface slope is too steep for the debris to remain on it (Moore, 2018). These circumstances can develop through a variety of processes (Kneib et al., 2021) resulting in different forms, collectively referred to as *cryokarst* features (Ferguson and Vieli, 2021).

Debris-covered glaciers are most prevalent in high-elevation areas such as the Karakoram and Himalaya, where around 10 percent of glacier area is covered by debris (Bolch et al., 2012). In the Everest region, debris covers around 25 percent of glaciated area (Vincent et al., 2016). This means that debris-covered glaciers represent a substantial part of glaciers in these areas. Generally, glaciers act as natural buffers of hydrological seasonality, with people downstream already now heavily depending on meltwater in the dry summer and early autumn months (Bolch et al., 2012).

And in the face of climate change, predicting changes of glaciers over the 21st century is very important. Related challenges include the socio-economic consequences of glacier loss (Rowan et al., 2015), the contribution to sea-level rise (Gardner et al., 2013), and altered risk of glacial lake outburst floods (Bolch et al., 2012), while providing an opportunity for better general understanding of glacier response to climate variability (Richardson and Brook, 2010). As long-term data corresponding to the long response times of debris-covered glaciers are rare (Ferguson and Vieli, 2021) and present-day trends cannot simply be extrapolated into the future (Rowan et al., 2015), numerical modelling is required.

For this application, a standard glacier model needs to incorporate a debris routine, developing englacial and supraglacial debris and reproducing the feedback on surface mass-balance (Rowan et al., 2015). Such an approach is taken by Ferguson and Vieli (2021) in their DEBISO model, which serves as the basis for the experiments conducted in this thesis. Their model is a simplified version of the two-dimensional model using shallow ice approximation (SIA) dynamics by Anderson and Anderson (2016), with the goal of creating a simple, efficient model to approximate the complex physical processes of debris-covered glaciers. A more detailed overview is provided in section 2.4 (Modelling).

Ferguson and Vieli (2021) have integrated a cryokarst routine into the DEBISO model, tying the formation of cryokarst features to *driving stress* (Benn et al., 2012; Ferguson and Vieli, 2021). It essentially assumes that when a part of a glacier is in a stagnant state, it is harder for a glacier to dynamically compensate differences in surface topography such as cryokarst features.

## 1.2 Objective and Research Questions

### 1.2.1 Østrem curve

**Research question 1:** How well do field measurements agree with literature and the Østrem curve used in the model?

Many studies have provided combined quantitative measurements of ablation and debris cover thickness (Mattson et al., 1993; Mihalcea et al., 2006; Hagg et al., 2008; Brook et al., 2013; Groos et al., 2017). For this thesis, additional data were collected on Zmuttgletscher, Switzerland. The details of the data collection are provided in section 3.1. One of the aims of this thesis is to combine all the data from various glaciers to find a realistic Østrem curve that fits the data best. This curve is then used in the debris routine of the DEBISO model, which in its default version employs a user defined value.

### 1.2.2 Climate sensibility

**Research question 2:** How do debris-covered glaciers react to real climate history and scenarios?

This thesis also aims to thoroughly test the DEBISO model against various climate inputs, comparing debris-covered glaciers to debris-free glaciers in a controlled setting. The experiments build and expand on the simple step-change and random climate experiments already conducted by Ferguson and Vieli (2021). The model is tested with various types of climate inputs, where not only the influence of long-term trends, but also of short-term changes on glacier geometry is tested. Finally, in an attempt at using real climate history and projections, a realistic response of debris-covered glaciers to contemporary climate change is simulated and compared to debris-free glaciers.

### 1.2.3 Cryokarst

**Research question 3:** What are the main factors in cryokarst formation? How can they be integrated into a model?

Cryokarst formation is still rather poorly understood, and a multitude of processes having some influence in the formation of cryokarst are presented in various studies (Kneib et al., 2021). Another aim of this thesis is to gain an overview of the scattered explanations of cryokarst formation. An analysis of which processes could potentially be integrated into the DEBISO model, and considerations whether integrations would fit the scope of this simple model are necessary.

Chapter 2

# Background

## 2.1 Debris input

As for a glacier's ice itself, debris on top of it does not simply emerge from the ice out of nowhere. There need to be processes causing this material to abandon its static position and enter transport within and on the glacier. There are three main processes contributing to supraglacial debris. The two direct sources include basal erosion and bordering rockwalls. Lateral moraines can serve as an indirect third source of supraglacial debris (Van Woerkom et al., 2019). Though the relative contribution of these three processes is dependable on local conditions, basal erosion is generally thought to be the one of least importance, as erosive processes on rockwalls and moraines are highly active (Van Woerkom et al., 2019) in the environments where debris-covered glaciers are most prevalent.

Rockwall erosion is difficult to quantify, as long-term erosion rates are highly variable spatially and temporally. Events are irregular and often catastrophic, and the influence of other periglacial processes makes it difficult to estimate erosion from exposure dating. Overall, rockwall erosion rates are estimated to be on the order of 1 mm per year. (Heimsath and McGlynn, 2008). Erosion events such as rockfall, rock avalanches or landslides can be triggered by processes like extreme rainfall or seismic events (Van Woerkom et al., 2019). During glacial retreat rockwalls become increasingly exposed to erosive processes and lose stability. Some large singular events have been at least partially attributed to current glacier melting (Hartmeyer et al., 2020), but some argue the role of rockwall debuttressing has been overemphasized (Reznichenko et al., 2011).

Both low-magnitude rockfalls (Hartmeyer et al., 2020) and catastrophic rock avalanches (Reznichenko et al., 2011) contribute to the transport of supraglacial debris onto the accumulation area (Anderson and Anderson, 2018). Remobilization of moraine material is of greater importance below the equilibrium line altitude (ELA), particularly during glacial retreat. As the glacier surface descends lower than the moraine crest, the moraine slopes become susceptible to mass transport processes such as debris flows (Van Woerkom et al., 2019).

## 2.2 Supraglacial debris

As already mentioned in chapter 1, the presence of debris on a glacier surface influences its thermal characteristics. Supraglacial debris alters the ablation rate of the underlying ice compared to clean ice, primarily dictated by the thickness of the debris cover (Østrem, 1959; Mattson et al., 1993; Nicholson and Benn, 2006; Nicholson et al., 2018). Because the debris originates from local sources and does not distribute equally across the glacier, it is concentrated in some areas before being transported further. As these structures are buried in the accumulation area, they form discrete debris-rich bands called septa (Kirkbride and Deline, 2013). The debris follows the dynamic movement of the glacier before eventually melting out in the ablation area.

The debris typically still emerges as elongated bands or transverse septa (Kirkbride and Deline, 2013), as much of the original structure is conserved during englacial transport. This leads to a heterogeneous distribution of supraglacial debris (Mölg et al., 2020). After melting out, debris is dispersed over the glacier surface. This can happen through the migration of emerging septa, which is caused by changes in geomorphological factors upstream, englacial changes in the septum structure and glaciological factors such as surface lowering or stagnating ice (Kirkbride and Deline, 2013). In a second step, debris can be dispersed over short distances – in the order of 10 meters – through local slope development, which is caused by differential debris distribution in the first place. For these reasons, debris cover tends towards a layer of uniform thickness (Kirkbride and Deline, 2013).

Østrem (1959) was the first to establish an empirical relationship between debris thickness and ablation rates, which is why it is referred to as the *Østrem curve*. In his and many subsequent studies, it was found that debris had a melt enhancing effect on the underlying ice for very thin (1-2 cm) or discontinuous cover, and an insulating effect for thicker debris layers (Østrem, 1959; Mattson et al., 1993; Mihalcea et al., 2006; Nicholson and Benn, 2006; Hagg et al., 2008; Dobhal et al., 2013). Debris thickness has been found to be the dominant factor in ablation of debris-covered glaciers (Nicholson et al., 2018), but there is still quite some variation between individual glaciers and studies. This can at least partly be attributed to other factors such as local climate and debris properties, such as albedo, lithology, texture and moisture content (Nicholson and Benn, 2006; Nicholson et al., 2018).

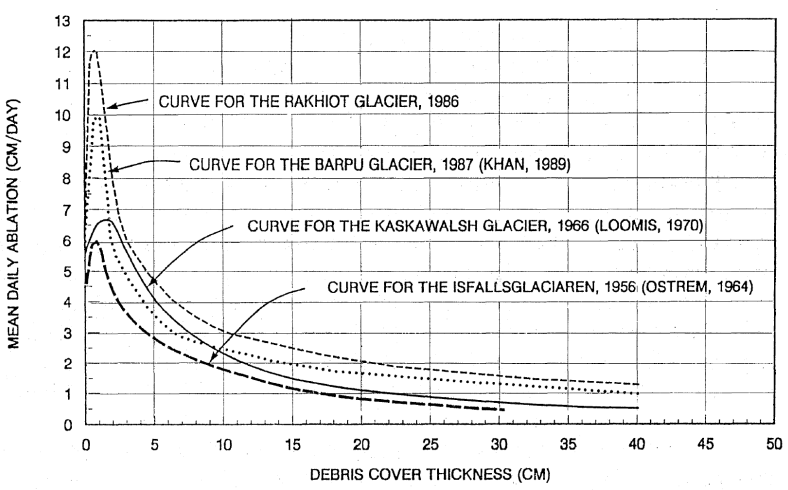


**Figure 2.1:** *Examples of Østrem curves from empirical measurements of debris cover thickness and ablation rates of several glaciers (Mattson et al., 1993).*

## 2.3 Cryokarst features

On many debris-covered glaciers, mass loss in the current warming period has been found to be quite similar to clean-ice glaciers, frequently termed the *debris cover anomaly* (Gardelle et al., 2013; Pellicciotti et al., 2015; Buri et al., 2021). There is however a tendency for the tongues of glaciers towards thinning rather than retreating (Rowan et al., 2015; Mölg et al., 2019; Buri et al., 2021). These two observations have been connected to the formation of ice cliffs and supraglacial ponds on the glacier surface, which expose bare ice to the surface and have been shown to substantially increase local melt rates, with melt being estimated to be 3 to 8 times higher there compared to surrounding debris-covered areas (Sakai et al., 2002; Reid and Brock, 2014; Buri et al., 2016; Miles et al., 2016; King et al., 2020; Rounce et al., 2021; Kneib et al., 2021).

The formation of ice cliffs has been attributed to several processes. These include collapsing englacial conduits, slope oversteepening for example from locally variable melt rates, crevasse opening, and undercutting or melt enhancement by supraglacial streams and ponds (Benn et al., 2012; Reid and Brock, 2014; Moore, 2018; Nicholson et al., 2018; Kneib et al., 2021). Locally variable melt rates occur for example when debris is distributed heterogeneously, as discussed in section 2.2. Crevasse formation is associated with strong longitudinal extension as at ice falls (Miles et al., 2016), with fracture occurring when a certain *strain rate* is reached (Vaughan, 1993). Crevasses themselves expose ice faces to a degree, but can also interrupt supraglacial streams and drain water into the glacier (Mölg et al., 2020). Supraglacial channels form meandering valleys with walls getting steeper until debris slides off (Mölg et al., 2020). The resulting surface moves

sideways both through backwasting by increased atmospheric melt (Kneib et al., 2021) or continuous undercutting by the stream that can eventually lead to a collapse. Undercutting from streams primarily occurs in areas of thin (less than 20 cm) debris cover (Anderson et al., 2021b). Supraglacial ponds can form and expand ice cliffs through thermal undercutting of the cliff face and even calving for large ponds (Watson et al., 2017). Pond formation and drainage is closely related to the englacial drainage system, as ponds can both form by collapse of and drain into englacial conduits (Benn et al., 2017). The formation of ponds correlates strongly with areas with stagnant dynamics (Anderson et al., 2021b).

All of these processes are strongly connected to the glacier dynamics and drainage system, allowing approximations of the amount and persistence of ice cliffs from dynamic properties. However, different glaciers render varying results. On Zmuttgletscher, a debris-covered alpine glacier, stagnation seems to have enabled a consistent drainage network, inhibiting dynamic readjustment of topographical differences (Mölg et al., 2020). Contrary to this, up-glacier surging behavior resulting in a reorganisation of the drainage network is suggested to have a big influence on the formation of cryokarst features on Urdok Glacier in the Karakoram (Kneib et al., 2021). This makes it difficult to ascribe a single property or process to the formation of cryokarst features.

## 2.4 Modelling

Measurement periods of glaciers generally are really short compared to their response times and only allow research with conditions that are set and often unknown. This small window into glacier behavior can be significantly magnified using models. For predictions of the future state of a glacier and any experiment outside the preexisting data, modelling is deemed essential (Ferguson and Vieli, 2021). Numerical models for glacier dynamics in particular can act as a simplified sandbox version of a real glacier, with real processes represented by parameters and formulas.

Many existing glacier models are designed for clean-ice glaciers, which makes them unfit for debris-covered glaciers (Rowan et al., 2015). Models specifically designed for debris-covered glaciers have only been emerging in recent years. Early attempts at modelling debris-covered glaciers struggled with boundary conditions (e.g. Konrad and Humphrey, 2000). A second approach was coupling a numerical glacier model with a debris surface transport model, treating the glacier as a conveyor belt (e.g. Vacco et al., 2010). Rowan et al. (2015) developed the first model using coupled debris-ice dynamics for the examination of one particular glacier. An important realization from this implementation was that diagnosing the effects of different processes on glacier responses can be difficult, as multiple processes can lead to similar outcomes (Anderson and Anderson, 2016). The subsequent approach by Anderson and Anderson (2016) aimed to eliminate as

many variables as possible to take a look at debris-covered glaciers in a more sterile setting, where observations can be more easily attributed to individual parameters. One example of that is looking at the isolated effect of debris cover on glacier dynamics and length (Anderson and Anderson, 2016).

Including cryokarst features in debris-covered glacier modelling today constitutes another research gap. As the physical processes behind the formation of cryokarst are not fully understood yet, the simple approach by Ferguson and Vieli (2021) shown in section 3.2.4 being the first integration of a cryokarst routine into a numerical debris-covered glacier model.

## 2.5 Study area

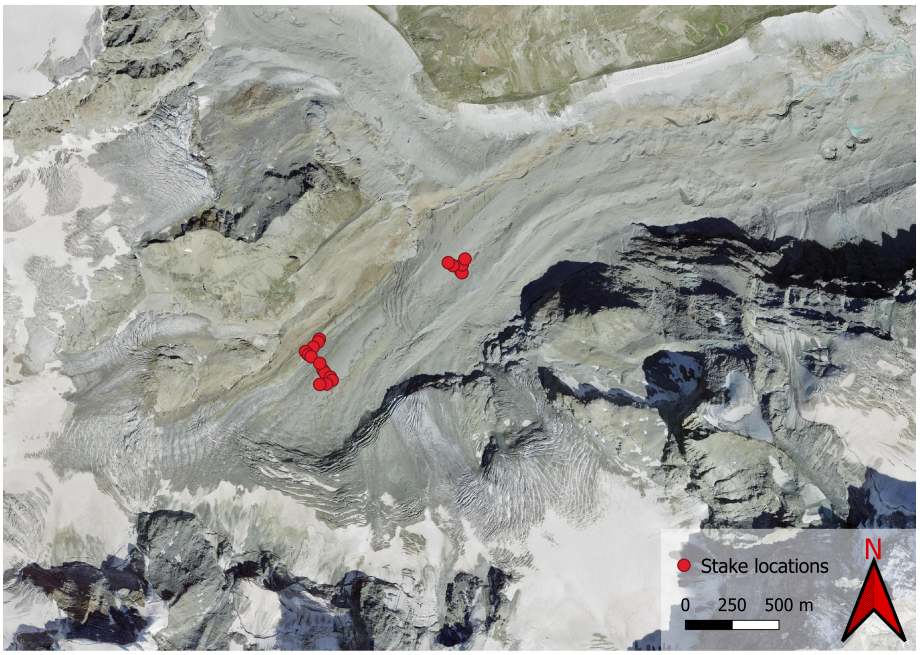


**Figure 2.2:** *Aerial view of Zmuttgletscher and its tributaries (Swisstopo, 2020). All positions of ablation stakes of the 2021 field work are marked in red (more in section 3.1.1).*

Zmuttgletscher is a debris-covered glacier in the western Swiss Alps, ranging in elevation from around 2240 to 4150 m a.s.l., being surrounded by the steep headwalls of the surrounding mountains and ridges. Including all its tributaries, the surface area added up to 15.74 $km^2$ in 2016, being substantially debris-covered in its ablation area (Mölg et al., 2019). Due to warming since the mid 19th century, Zmuttgletscher has mostly had a negative mass balance, causing thinning (Mölg et al., 2019) and retreat of more than 1 km.

The glacier has some interesting unique characteristics. One of them is the lower tongue becoming almost stagnant since the end of the LIA. Large debris-covered glaciers often exhibit low flow velocities due to decreased driving stress in their flat tongues even in steady-state conditions (Anderson and Anderson, 2016). Still, Mölg et al. (2019) attribute the decrease in dynamic activity to changes in climate rather than inherent effects of debris cover. Sustained thinning since the LIA has resulted in a reduction in ice thickness, which in turn reduces driving stress.

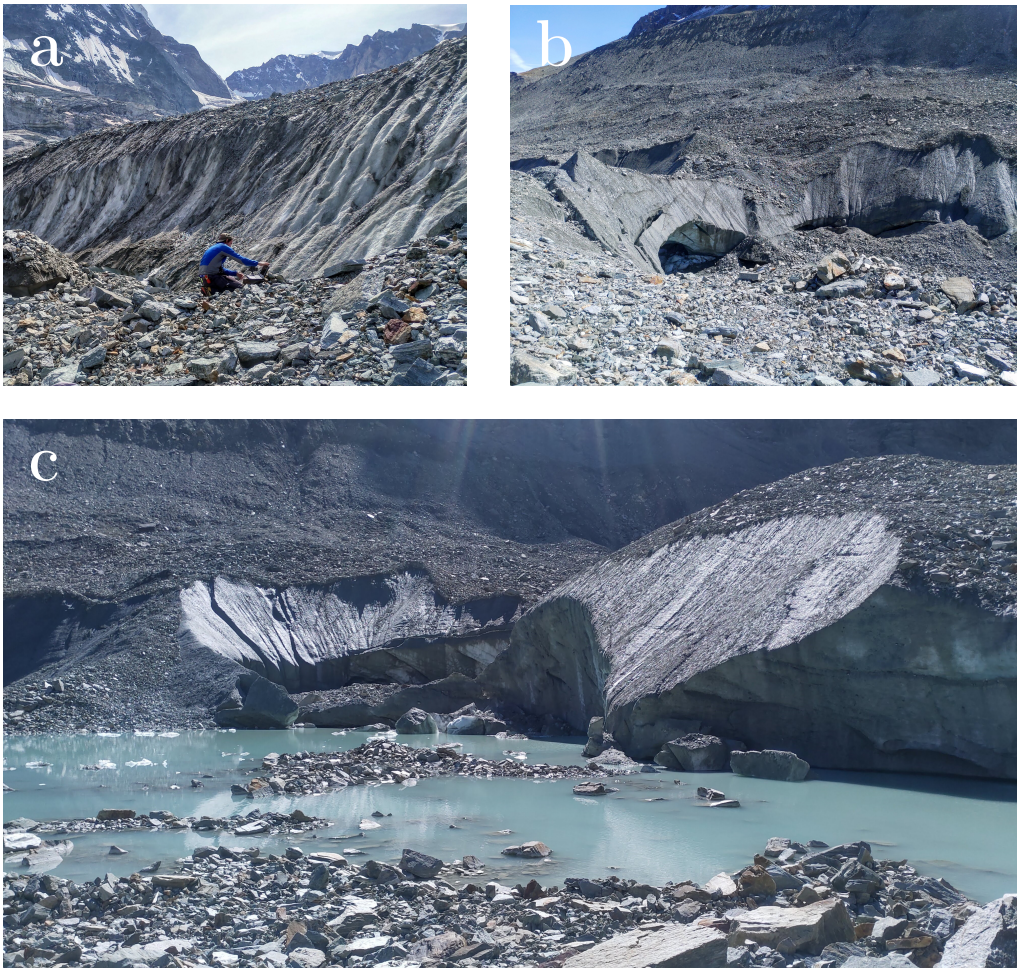


**Figure 2.3:** *Ice cliff formed by a supraglacial stream in the upper ablation area of Zmuttgletscher (a), large ice cliffs in the lower ablation area (b), and terminal ice cliff with small lake (c).*

In the current warming period, Zmuttgletscher has undergone major changes regarding debris cover. The area of debris-covered surface has increased by about 19% – from ~13% to ~32% since the end of the LIA – with no evidence of particularly large rockfalls (Mölg et al., 2019). The coinciding occurrence of temporal

variations in the rate of debris cover extent change and climatic signals suggests that the increase in debris cover extent is likely connected to the effects of temperature increase and decreasing ice flow velocities (Mölg et al., 2019). At around 15 centimeters over much of its ablation area, Zmuttgletscher's debris cover is also relatively thin compared to other debris-covered glaciers. This may be enough to reduce glacier thinning and terminus reatreat, but decoupling from climatic influences may only be limited. In fact, surface changes and flow velocities show a direct reaction to climatic change (Mölg et al., 2019).

Cryokarst features are found on Zmuttgletscher in areas of compressional flow such as flat and stagnating parts of the glacier. Correspondingly, most ice cliffs are found on the lower tongue (Mölg et al., 2019). Their formation is most often associated with the presence of supraglacial streams, but also with ponds and collapsing englacial conduits and cavities (Mölg et al., 2019). Large ice cliffs at the terminus contribute significantly to the steady retreat contrary to other debris-covered glaciers, where mostly thinning occurs. The contribution of ice cliffs on volume loss is also not as large as on other comparable glaciers, as their area is small and the debris layer is rather thin already (Mölg et al., 2019).

Chapter 3

# Methods

## 3.1 Field work on Zmuttgletscher

In the summer of 2021, a campaign of several field work trips was conducted on Zmuttgletscher. Though explicitly not the main focus of this thesis, the field work provided both data on the relationship between ablation and debris cover was collected to complement data from literature (section 3.1.1) and qualitative insights and observations of the processes involved on the surface of a debris-covered glacier (section 3.1.2).

### 3.1.1 Ablation and debris thickness measurements

The main goal of the measurements of ablation and debris cover thickness was providing data to find a representative Østrem curve, coming up in section 3.2.3, to then be used in the DEBISO model. Using PVC ablation stakes, ablation was measured over several weeks at 20 locations. Debris thickness was measured multiple times in the immediate vicinity of the stakes to counterbalance bias from local variability on the scale of centimeters. To exclude the influence of air temperature differences as much as possible, these locations were distributed across the glacier at similar elevations and spanning as much of the debris thickness spectrum found on Zmuttgletscher. For reference, two stakes were placed at clean-ice locations. To increase the amount of data, stakes in a second cluster about a kilometer downstream – placed there for other research projects – were included, as seen in Figure 2.2.

### 3.1.2 Qualitative observations

Another part of the field work was examining glacier morphology and specifically cryokarst features on Zmuttgletscher as described by Mölg et al. (2019). These are some of the key observations and additions to their descriptions as summarized in section 2.5:

- Ice cliffs originating from supraglacial streams develop not only near the terminus, but also in flat parts of the upper ablation area. Mölg et al. (2019) describe a high occurrence of cryokarst features downstream of topographic steps, which corresponds to the observations. Additionally, it holds true that these features disappear in the extensive areas on topographic steps themselves, as runoff enters the glacier more easily.

- In the lower ablation zone, collapse of large en- and subglacial channels seems to be the dominant process producing ice cliffs, as the associated cryo-valleys are much deeper than further upstream.

- Supraglacial streams do not create incisions into the surface on clean-ice areas, contrary to their counterparts in debris-covered areas at similar elevations. In theory this also makes sense, as the discrepancy in ablation rates is not as large on clean-ice surfaces.

- Supraglacial ponds can be found on Zmuttgletscher, but they are much more rare than streams, which was also observed by Mölg et al. (2020). The ponds can fill up and drain over short timescales, making their contribution to increased ablation highly variable.

- Moraine ridges on the glacier, as clearly visible in Figure 2.2, have lower ablation rates than surrounding areas. This leads to the formation of large longitudinal depressions between them, where runoff is concentrated in supraglacial channels and distinct sub-catchments form (Mölg et al., 2020). Ice cliff formation is therefore more pronounced in these valleys compared to the ridges.

- In the upper ablation area of Zmuttgletscher, supraglacial streams only accumulate a limited amount of runoff before inevitably entering the glacier through moulins or crevasses. Still, relatively small streams can form quite large ice cliffs (e.g. figure 2.3(a)).

## 3.2 Model components

### 3.2.1 Model inputs and outputs

In a DEBISO model run, a number of variables are calculated and some of them stored as an output for visualization. This section provides a short overview of these variables to facilitate understanding of later plots.

With all the inputs in table 3.1, most of them constants, the model can be run over a defined duration, with climate variation given by the ELA. A glacier can be modelled from an initial state of no ice or start off at the end-state of a previously modelled glacier.

**Table 3.1:** *Variables and values used as model parameters (Ferguson and Vieli, 2021).*

| Parameter | Name | Value | Units |
|---|---|---|---|
| ELA | Equilibrium line altitude | 3000–3100 | m |
| $\rho$ | Density of ice | 910 | kg $m^{-3}$ |
| $g$ | Gravitational acceleration | 9.80 | m $s^{-2}$ |
| $c$ | Debris volume concentration | 0–0.005 | - |
| $A$ | Glen's flow law rate factor | $1 \times 10^{-24}$ | $Pa^{-3}s^{-1}$ |
| $n$ | Glen's constant / exponent | 3 | - |
| $D_0$ | Characteristic debris thickness | 0.05–0.1497 | m |
| $a_{max}$ | Maximum surface mass balance | 2 | m $yr^{-1}$ |
| $\gamma$ | Surface mass balance gradient | 0.007 | $yr^{-1}$ |
| $H^*$ | Terminal ice thickness threshold | 30 | m |
| $\lambda_m$ | Maximum cryokarst fraction | 0–0.2 | - |
| $\mathrm{d}t$ | Time step | 0.01 | yr |
| $\mathrm{d}x$ | Horizontal grid size | 25 | m |
| $\tau_d^+$ | Upper driving stress threshold | 110 | kPa |
| $\tau_d^+$ | Lower driving stress threshold | 60 | kPa |
| $\theta$ | Bed slope | 0.1 | m $m^{-1}$ |
| $\theta_c$ | Headwall slope | 1 | m $m^{-1}$ |

The model's outputs shown in table 3.2 are only a small selection from all values the model calculates, but they fully contain the glacier geometry and dynamic state across the time and space given to the model. From these values, basic information on the glacier such as total volume or extent can easily be calculated. The outputs can be stored for later visualization.

**Table 3.2:** *Model output variables.*

| Parameter | Name | Units |
|---|---|---|
| $H$ | Ice thickness | m |
| $D$ | Debris lyer thickness | m |
| $\overline{u}$ | depth-averaged ice velocity | m $yr^{-1}$ |
| $a$ | Surface mass balance | m $yr^{-1}$ |
| $Q$ | Accumulated runoff (new) | m $yr^{-1}$ |

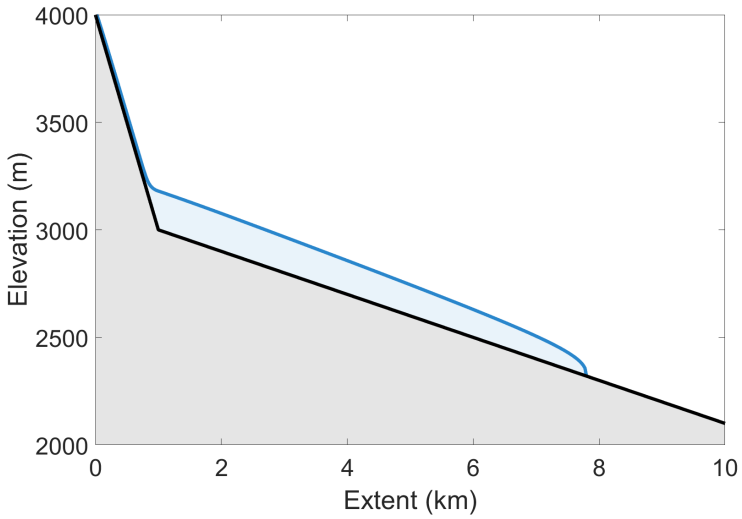


**Figure 3.1:** *Exemplary visualization of the glacier geometry output of a model run. The glacier is represented in blue on an exaggerated bed (the slope is only 10%).*

### 3.2.2 Basic DEBISO model

This section serves as a short overview of the mathematical backbone of the glacier model used for the later experiments. The model developed by Anderson and Anderson (2016) was also the basis for the DEBISO model by Ferguson and Vieli (2021) used in this thesis. Both use a 2D flowline version of the shallow ice approximation (SIA), a simple model for calculating dynamics from glacier geometry. The DEBISO model computes a depth-averaged ice velocity $\overline{u}(x,t)$ based on the glacier's geometry *(3.1)* and the change in ice thickness $H$ based on the velocity field and the mass balance $a(x,t)$ *(3.2)*, given by

$$\overline{u} = \frac{2A(\rho g)^n}{n+2} H^{n+1} \left|\frac{\partial h}{\partial x}\right|^{n-1} \frac{\partial h}{\partial x}, \tag{3.1}$$

$$\frac{\partial H}{\partial t} + \frac{\partial(\overline{u}H)}{\partial x} = a, \tag{3.2}$$

where $\rho$ is the density of ice, $g$ is gravitational acceleration, $A$ and $n$ are the rate factor and exponent from *Glen's flow law*, respectively, and $h(x,t) = H + b$ is the glacier surface elevation for a given bed elevation $b(x)$ (Ferguson and Vieli, 2021).

Debris is added to the model in a very simple way. It is assumed that there is a uniform debris concentration $c$ throughout the glacier. A melt-out source term

is calculated from $c$ and the local mass balance $a$. The debris that has melted out is then transported along the surface. The main input of the model is the ELA, which determines the elevation-dependent surface mass balance $\tilde{a}(z)$ given by

$$\tilde{a}(z) = min(\gamma(H + b - ELA), a_{max}), \tag{3.3}$$

with $\gamma$ being the *mass balance gradient* and $a_{max}$ being a maximum mass balance to realistically represent the ceiling in accumulation at a certain elevation. The influence of debris cover thickness $D$ on the mass balance is determined through a simple calculation from Anderson and Anderson (2016), given by

$$a = \tilde{a}\frac{D_0}{D_0 + D}, \tag{3.4}$$

with $D_0$ being a free parameter representing an Østrem curve. This approach neglects the melt enhancing effect of very thin debris cover, assuming it is negligible compared to the insulation effect of thicker debris.

At the terminus, debris is transported out of the system via a debris-free terminal ice cliff. Once ice thickness is below a certain threshold, the critical ice thickness $H^*$, all debris is assumed to slide off.

### 3.2.3 Østrem curve

The default implementation of the Østrem curve in the DEBISO model uses equation 3.4 with an arbitrary standard value of $D_0 = 0.05m$. Following up on the first research question, data from the 2021 Zmuttgletscher field work was combined with debris thickness and ablation measurements from 6 studies (Brook et al., 2013; Groos et al., 2017; Hagg et al., 2008; Mattson et al., 1993; Mihalcea et al., 2006; Richardson and Brook, 2010). Literature data originated from 5 individual glaciers in the Karakoram, the Tian Shan and in New Zealand (see Figure 3.2(a).

Figure 3.2(a) shows all the data collected in one plot. It is clear that most data points approximately follow a curve of decreasing melt with increasing debris thickness. There are some outliers and some distinct differences between glaciers. One can also see that the data density is much better for thin debris layers. There definitely is an argument that there is no universal Østrem curve that approximates all glaciers equally well, but it is a necessary assumption to make if we want to look at debris-covered glaciers in a more isolated and general way.

In a second step (Figure 3.2(b)), the default Østrem curve is plotted onto the data points. The curve clearly does not fit the data well, strongly overestimating the insulating effect of the debris. This validates the need for an improved Østrem

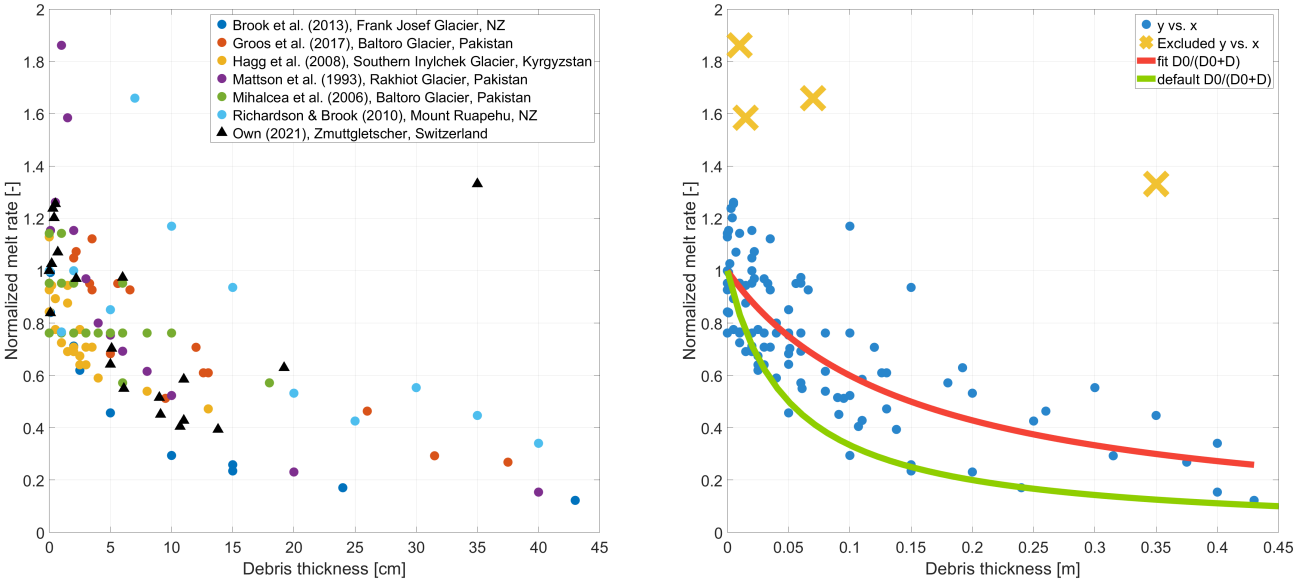


**(a)** **(b)**

**Figure 3.2:** *Debris thickness and normalized melt rate (relative to clean ice) from Zmuttgletscher field work and literature (a). Debris thickness and normalized melt rate data, default $D_0$ curve, fit $D_0$ curve and points excluded from the analysis (b).*

curve. To fit this curve to the data, the same equation (3.4) was used with $D_0$ as the free parameter. A first fit attempt was made, but outliers had a strong effect on the resulting curve. This lead to the decision to remove points diverging from this initial curve by more than a threshold of 0.5 normalized melt, as visualized in Figure 3.2(b).

Two of these points originate from Mattson et al. (1993) looking at very thin debris ($1 - 2cm$). Another excluded data point was from Richardson and Brook (2010), whose melt rates generally are higher than the ones from other glaciers. The authors acknowledge this as well and struggle to explain the differences, discussing geothermal activity at Mount Ruapehu as a possible explanation. The last data point was one from our own field work on Zmuttgletscher. It is a very interesting case, as it was placed right on top of an ice cliff (see figure 3.4 in the appendix), which melted back over the measurement period. As cryokarst is taken into account separately (section 3.2.4), it made more sense to leave this measurement out.

The final fit Østrem curve shown in red in figure 3.2(b) uses a $D_0$ of about 0.15m. This means that the insulation effect from debris cover is about three times less strong when this curve is used, or rather it takes three times more debris to get the same amount of insulation. It represents the data well and shows a much more restricted insulating effect of the debris layer on ablation.

### 3.2.4 Cryokarst implementations

In the standard version of the DEBISO model written by Ferguson and Vieli (2021) there is a simple cryokarst implementation. It uses driving stress $\tau_d$ as an indicator for cryokarst formation. This is not based on any analysis of individual ice cliffs forming, but rather on the general observation that cryokarst features commonly occur near the termini of stagnating debris-covered glaciers (Pellicciotti et al., 2015; Brun et al., 2016; Watson et al., 2017). These parts are areas of decreased ice velocities and driving stress (Benn et al., 2012), which are both dependent on ice thickness. Driving stress is defined by

$$\tau_d = \rho g H \frac{\partial h}{\partial x}, \tag{3.5}$$

and is essentially a combination of ice thickness and surface slope. The effect of cryokarst on surface ablation is implemented by defining a fraction of the glacier's surface that is comprised of cryokarst features, called cryokarst area fraction $\lambda$. For this fraction, debris-free ablation $\tilde{a}$ is assumed, whereas the rest of the area has the reduced ablation $a$ from equation 3.4. The model defines a first threshold of $\tau_d$, under which cryokarst features can start forming. From this point, $\lambda$ increases linearly as $\tau_d$ decreases until a second threshold is reached. At this point, no additional cryokarst is formed and $\lambda$ keeps stable at a maximum area fraction $\lambda_m$ (Ferguson and Vieli, 2021). This calculation is visually represented in figure 3.3(a).

As described in section 2.3, many processes are involved in cryokarst formation. And in the field work on Zmuttgletscher it became apparent that supraglacial streams play a big role in the formation of cryokarst, especially in the upper ablation area. There, undercutting by supraglacial streams initiates and maintains ice cliffs. The streams meander and migrate over the surface throughout the melting season, creating areas of higher melt rates on the exposed ice cliffs compared to debris-covered surfaces.

In a first approximation ice cliff size roughly correlates with stream discharge, leading to the assumption that more runoff leads to increased formation of ice cliffs. In the upper ablation area, driving stress might not necessarily be below the threshold defined by the standard implementation in the model, but low debris cover thicknesses lead to high enough melt rates to increase stream flow (Anderson et al., 2021b). Another factor to consider is crevasses interrupting catchments of

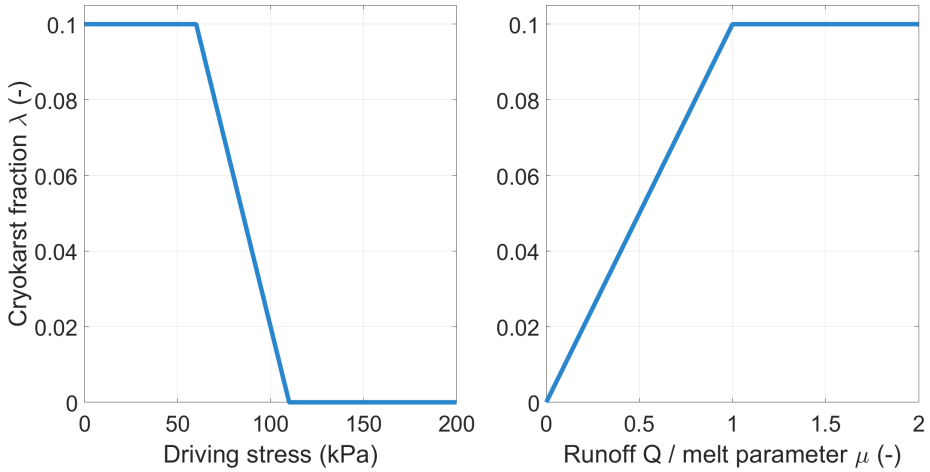


**Figure 3.3:** *Default cryokarst implementation calculating the cryokarst area fraction $\lambda$ from driving stress (a). New cryokarst implementation using the cumulative surface runoff $Q$ to calculate $\lambda$ (b).*

supraglacial streams, resetting the cumulative runoff by diverting streams into the glacier.

These processes have been integrated in this study into a new, abstractly process-based cryokarst routine. It is meant to replicate the process of runoff accumulation on the glacier, not physically accurate but rather as an abstract value to distinguish high-runoff areas from low-runoff areas, which correspond to areas of increased and decreased occurrence of ice cliffs, respectively. In a first step, local summer ablation $a_s$ in the ablation area is calculated as a factor of the annual mass balance $a$. The ratio $\frac{a_s}{a}$ was calculated from measurements of $a$ and $a_s$ on 9 alpine glaciers (GLAMOS 1880-2021). The accumulation area was categorically excluded from the routine, as no debris cover can develop there – and no cryokarst correspondingly. To approximate the formation of crevasses, a strain rate $\sigma$ was computed, given by

$$\sigma = \frac{\partial \overline{u}}{\partial x}. \tag{3.6}$$

The strain rate is then used to identify areas of extension ($\sigma > 0$) and compression ($\sigma < 0$). In areas of extension, runoff is lost from the surface as water enters crevasses. The reduction of runoff is then defined through the factor $f_{red}$ given by

$$f_{red} = 1 - \frac{\sigma}{max(\sigma)}. \tag{3.7}$$

Runoff is then accumulated along the surface, where at any point $i$ on $x$ the local summer balance $a_s$ is multiplied by the local reduction factor $f_{red}$. This value is carried over and added to the next grid point $i+1$, creating the cumulative runoff $Q_{grid}$, which has to be multiplied with the grid size $dx$ to account for the grid size area. After all this, we end up with a cumulative runoff $Q$ in $m^3yr^{-1}$.


**Figure 3.4:** *Ice cliff formation by undercutting in a meander of a small supraglacial stream in the upper ablation area of Zmuttgletscher. Ablation stake from the Zmuttgletscher field work that melted out during the measurement period and was excluded from the Østrem curve analysis (see section 3.2.3).*

As discussed earlier, it is assumed that more runoff corresponds to the formation of more and larger ice cliffs, but a certain saturation point exists. At this point incision from the stream is large enough for it to become englacial (Reid and Brock, 2010; Jarosch and Gudmundsson, 2012), therefore no additional cryokarst is formed beyond that point. This is also corroborated by the observations made in section 3.1.2. Including a physically-based incision rate (e.g. Fountain and Walder, 1998) into this calculation was considered, but deemed unfit for the abstract nature of the routine. These assumptions lead to the final implementation

shown in figure 3.3(b). The cryokarst area fraction increases with runoff, until the melt parameter $\mu$ is reached at the maximum cryokarst area fraction $\lambda_m$, which is the level it stays at for larger runoff values. The default value for $\lambda_m$ is 10% (Ferguson and Vieli, 2021), which is consistent with fractional area observations (Mölg et al., 2019; Steiner et al., 2019; Anderson et al., 2021a). $\mu$ is a free parameter that basically indicates how large a supraglacial stream can get before entering the glacier, with a default value of 10% (Ferguson and Vieli, 2021).

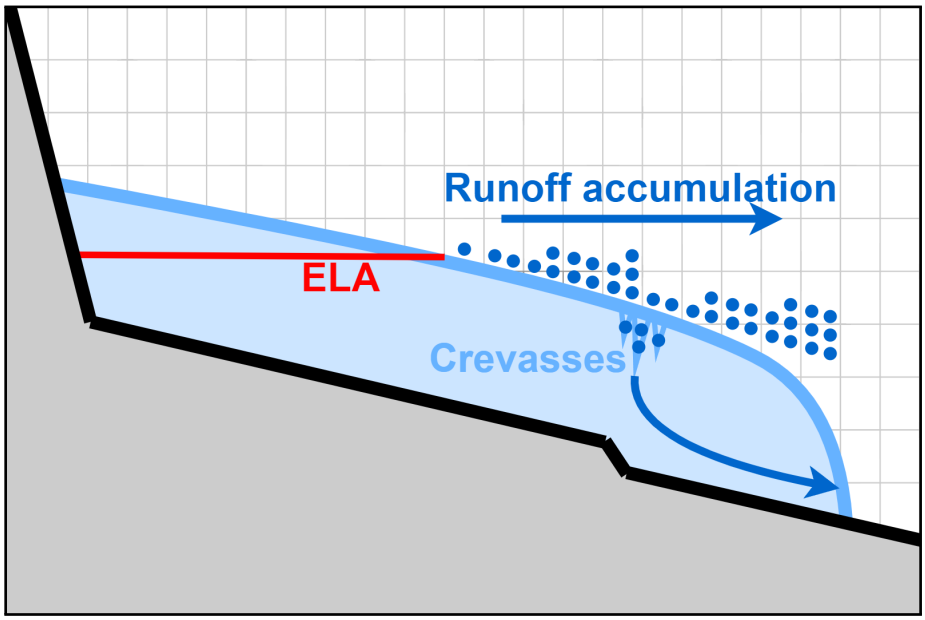


**Figure 3.5:** *Conceptual representation of the new meltwater cryokarst routine. Water starts accumulating in the ablation area and can enter the glacier at areas with a high strain rate, where crevasses form. One blue circle represents meltwater from one grid point.*

Chapter 4

# Results

Corresponding to the three main research questions, experiments and their results focus on testing the new Østrem curve (section 4.1), testing the model against various climate inputs (section 4.2), and comparing different implementations of cryokarst (section 4.3). As a non-essential addition, some experiments are also conducted for a real glacier, Zmuttgletscher (section 4.4). An overview of all experiments is given in table 4.1.

## 4.1 Østrem curve

In section 3.2.3, most of the results of the Østrem curve analysis were already presented. The only remaining experiment to make further statements about the first research question is experiment A1 from table 4.1(a), graphically represented in figure 4.1. To compare the default and new Østrem curves, a simple step-change experiment is conducted, where the ELA is suddenly raised by 100 meters, which would correspond to a warming of about 1.1°C (Lüthi, 2014). After 1000 years, the ELA is restored to its initial value. Three versions of the model are compared: the default version with a $D_0$ of 0.05m, the new data-oriented version using a $D_0$ of 0.1497m, and a completely debris-free version. Looking back at figure 3.2(b), a higher $D_0$ means a weaker debris insulation effect.

As shown in figure 4.1 the largest glacier in equilibrium (before year 500) is obtained with the default version, also showing the slowest response time of both volume and length. The shortest glacier is the debris-free glacier, which starts its retreat instantly after the ELA step-change and quickly reaches equilibrium after both retreat and advance. The newly implemented Østrem curve is right between the other two versions. The behavior after retreat and advance however is very close to the default debris-covered glacier. Both show a characteristic hesitation to retreat as volume already starts decreasing after warming, an effect that was described by Ferguson and Vieli (2021) and will also be visible in later experiments. During advance, behavior initially is very similar between all three

**Table 4.1:** *Summary of modelling experiments performed.*

**(a)** *Østrem curve*

| No. | Description | Section | Figures |
|---|---|---|---|
| A1 | step-change: Default vs. new Østrem curve | 4.1 | 4.1 |

**(b)** *Climate sensitivity*

| No. | Description | Section | Figures |
|---|---|---|---|
| B1 | step-change: Varying debris concentration | 4.2.1 | 4.2 |
| B2 | step-change: Varying bed slope | 4.2.1 | 4.3, 4.4 |
| B3 | Sinus: Varying amplitude & wavelength | 4.2.2 | 4.5, 4.6 |
| B4 | Linear temperature increase | 4.2.3 | 4.7, 4.8 |
| B5 | Real climate history & projections | 4.2.4 | 4.9, 4.10, 4.11, 4.12 |

**(c)** *Cryokarst*

| No. | Description | Section | Figures |
|---|---|---|---|
| C1 | step-change: Comparison between cryokarst implementations | 4.3.1, 4.3.2 | 4.13, 4.14, 4.16, 4.17 |
| C2 | real climate history & projections and cryokarst implementations | 4.3.1 | 4.15 |

**(d)** *Zmuttgletscher*

| No. | Description | Section | Figures |
|---|---|---|---|
| D1 | Sinus on Zmuttgletscher bed geometry | 4.4 | 4.18 |
| D2 | Real climate history on Zmuttgletscher bed geometry | 4.4 | 4.19, 4.20, 4.21 |

versions. But as the debris-free glacier already is back to equilibrium, both debris-covered glaciers keep growing steadily. All these effects are further described in sections 4.2.1 and 4.2.2.

## 4.2 Climate sensitivity

### 4.2.1 Step-change experiments

The first experiment is basically a repetition of the ones already conducted by Ferguson and Vieli (2021). It is meant to help assessing the influence of debris cover on glaciers in the most controlled way possible. The experiments shown in figure 4.2 look at the influence of debris concentration $c$ on the transient response of

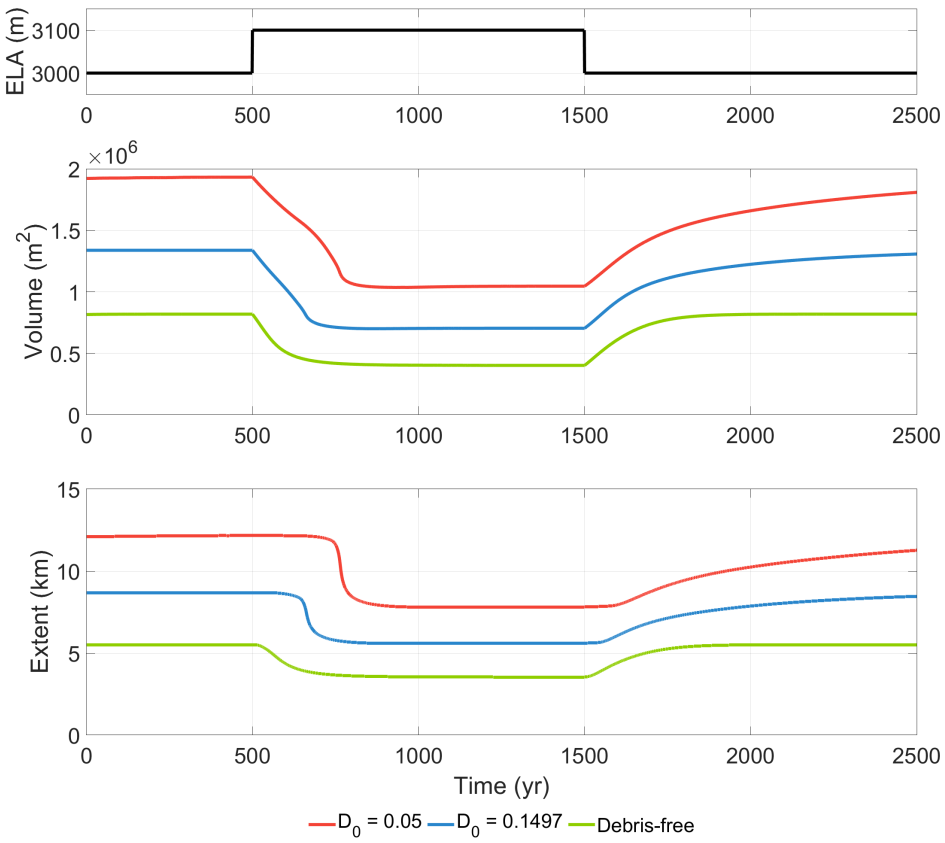


**Figure 4.1:** *Step-change experiment (A1) using the default (red) and new (blue) Østrem curves, as well as a debris-free glacier (green). The three plots show ELA change, and the corresponding volume and length response, respectively.*

the glacier geometry and the debris layer on its surface. The default debris concentration of 0.25% is compared with half and double the amount of debris with the same step-change experiment done in section 4.1.

First of all, differing debris concentration results in different sizes of glaciers in equilibrium. The glacier with the most debris therefore must be the largest. This would indeed be the case, the ELA for the $c = 0.5\%$ glacier had to be raised by 100 meters to avoid it exceeding the array bounds. After the sudden warming in year 500, a few observations can be made. Right after the change, volume starts decreasing, which is nicely seen in the first about 5 kilometers of the glacier, whereas length stays constant, lagging behind the climate forcing. As the glacier is thinning and debris is melting out, debris cover thickness increases at first. It peaks and then drops exactly as the glacier dramatically retreats multiple kilometers within just a few years. This effect can be seen for all three

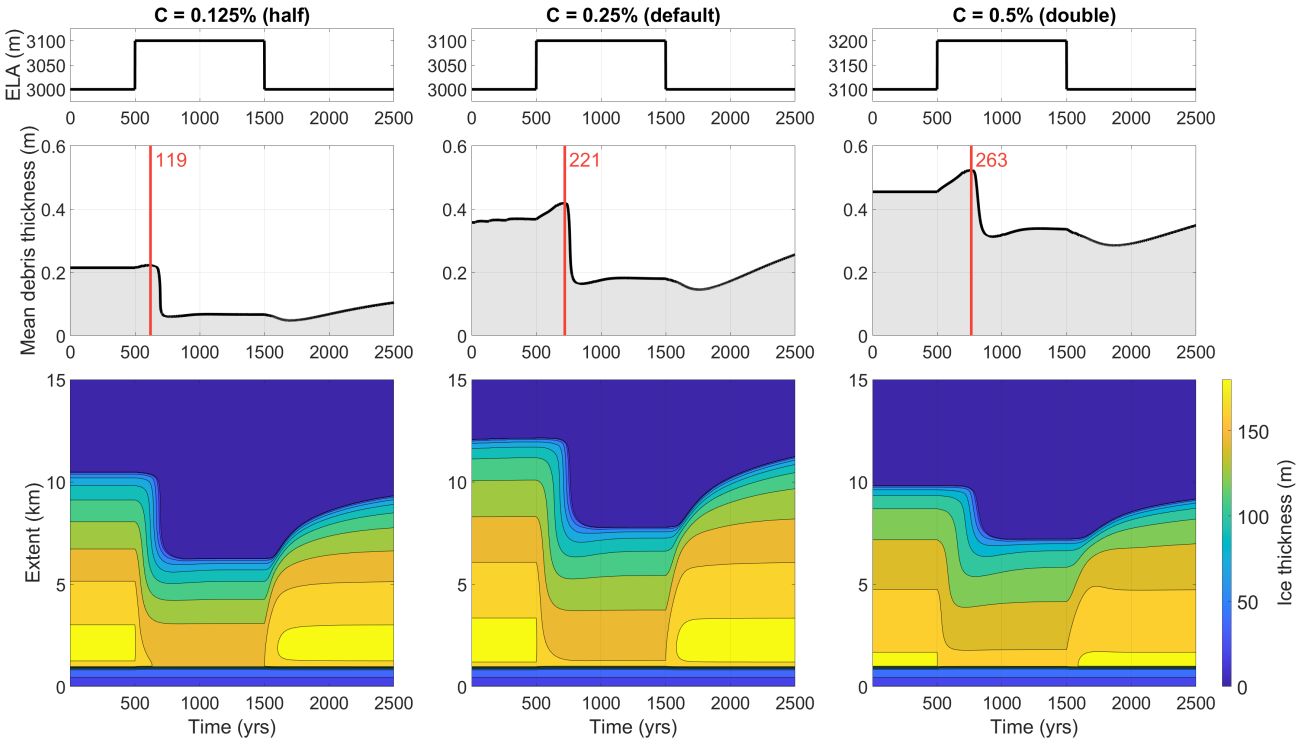


**Figure 4.2:** *Step-change experiment (B1) using three different debris concentrations (0.125%,0.25% and 0.5%). The plots in the first row show ELA change, the second row shows the mean debris thickness across the entire glacier surface, and the third is a contour plot of the ice thickness for simultaneous visualization of length and volume.*

concentrations – but with differing magnitude and time lag. As shown in table 4.2, it takes over a hundred years longer (262 years) for the $c = 0.5\%$ glacier's terminus to respond to warming compared to the $c = 0.125\%$ glacier (160 years) and over 70 years longer to respond to cooling. The loss in volume caused by warming strongly differs as well. The $c = 0.125\%$ glacier lost about 50% of its mass, whereas the $c = 0.5\%$ glacier only lost about 35%.

Generally, there is an asymmetry between advance and retreat response, which was also described by Ferguson and Vieli (2021). This will also be seen in following experiments. Table 4.2 clearly shows that advance always takes longer than retreat for debris-covered glaciers, provided the warming is strong and continuous enough for severe retreat and debris offloading.

It is also interesting that the glacier with the least debris loses most of its debris layer after warming, as large parts of the ablation area are lost, but the one with the most debris can retain most of it. For all three concentrations, a dent in

debris thickness before and after the adjustment to the new, warmer equilibrium state is observed, coinciding with an overshoot in volume. Both features are most pronounced for the $c = 0.5\%$ glacier. During advance, regaining the lost debris cover takes time and is not finished after the remaining 1000 years of modelled time. This slow increase in debris cover correlates with a steady advance of the terminus irrespective of the quickly ($< 500$ years) balanced accumulation area.

**Table 4.2:** *Response times during advance and retreat after an ELA step-change of 100 meters, for varying debris concentration and bed slope.*

| **Debris concentration** | *Advance e-folding volume response time (yrs)* | *Retreat e-folding volume response time (yrs)* |
|---|---|---|
| *0.125% (half)* | 383 | 160 |
| *0.25% (default)* | 398 | 217 |
| *0.5% (double)* | 455 | 262 |
| **Bed slope** | *Advance e-folding volume response time (yrs)* | *Retreat e-folding volume response time (yrs)* |
| *10% (default)* | 398 | 217 |
| *20%* | 122 | 93 |
| *30%* | 61 | 51 |

In experiment B2, the influence of bed slope on a debris-covered glacier is considered. Figure 4.3 shows the results in the same way as figure 4.2 did for debris concentration. Many of the same effects observed in experiment B1 can also be seen here, namely the increase, dramatic drop, and overshoot of debris cover as well as the overshoot in volume.

Bed slope clearly affects glacier size, as elevation drops much faster along the glacier. It is therefore simultaneously the effect of glacier size that is looked at in this experiment. The slope and size affects dynamics, leading to much faster ice velocities and faster response times to climate forcing. This is not exclusive to debris-covered glaciers, as small glaciers generally respond more quickly to changes in climate (Bahr et al., 1998).

Volume response times decrease strongly with increasing slope during advance and retreat. While the typical steep drop in retreat and slow rise in advance are still found, mean debris thickness barely drops for steep sloped glaciers, as the glacier response is fast but minimal.

Looking at the geometry (figure 4.4(a)) of the glaciers resulting from this experiment, it becomes more clear how steep-sloped glaciers are less affected by changes in ELA. All glaciers retreat to a quite similar extent in terms of elevation, but the area affected is much larger for flat-sloped glaciers, leading to further horizontal retreat. Figure 4.4(b) shows how this affects debris cover on flat-sloped glaciers.

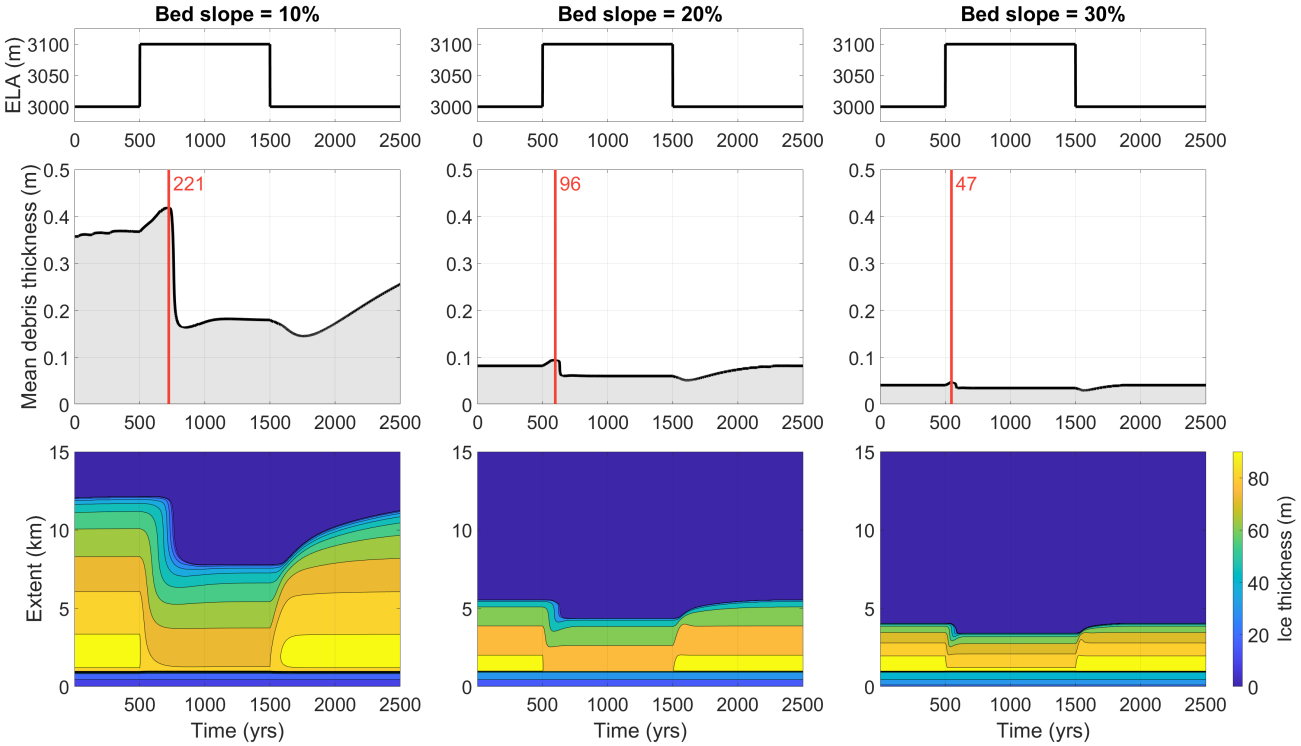


**Figure 4.3:** *Step-change experiment (B2) using three different bed slopes (10%,20% and 30%). The plots in the first row show ELA change, the second row shows the mean debris thickness across the entire glacier surface, and the third is a contour plot of the ice thickness for simultaneous visualization of length and volume.*

### 4.2.2 Sinus wave experiments

The next set of experiments (B3) is meant to be a further step from the step-change experiment towards realistic climate forcing. Climate is always changing and ELAs are always moving up- and down-glacier. A sinus wave forcing embodies this while still providing a very controlled setting, where observations can easily and directly be attributed to forcing or other factors. In section 4.2.1, substantial time lags between forcing and response were observed. The sinus experiments allow controlling the timescale and magnitude of changes in forcing through a wavelength $\lambda$ and an amplitude $A$, offering insight into the effects of these lags in an ever changing climate.

For this purpose, many ELA wavelengths – between 10 and 1000 years – and amplitudes – between 10 and 500 meters – were tested in the model. To show significant differences without using extreme values, only wavelengths of

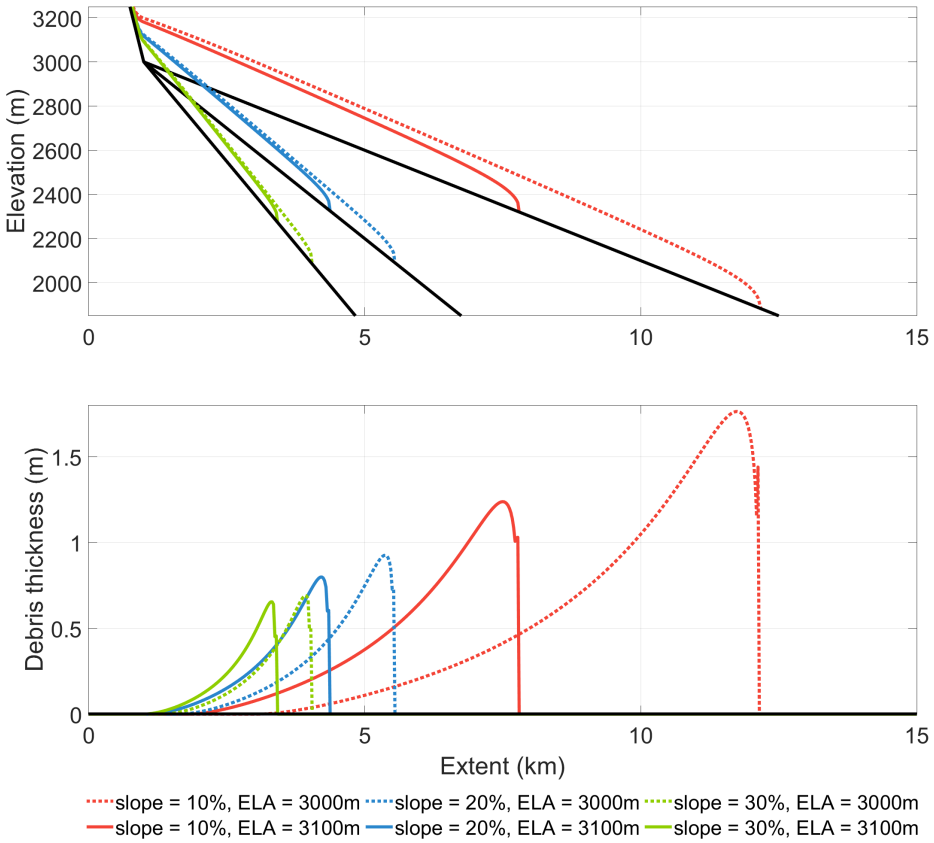


**Figure 4.4:** *Steady-state glacier geometry for the three bed slopes (10%, 20%, 30%) used in experiment B2 and ELAs of 3000 and 3100 m a.s.l. (a). Debris cover thicknesses along these glaciers (b).*

100 and 500 years and amplitudes of 50 and 250 meters are shown in the figures. Three combinations were evaluated: low-$\lambda$-low-$A$, high-$\lambda$-low-$A$ and low-$\lambda$-high-$A$. These ELA curves can be found in figure 4.5(a) or 4.6(a).

Figures 4.5 and 4.6 show volume and length response of debris-free and debris-covered glaciers, respectively, to the three ELA forcings.A maximum and a minimum are marked at years 1625 and 1875, as well as the corresponding minima and maxima in volume and length. The difference between these peaks and their response peaks is denominated as the *phase lag* $\varphi$. It is a similar but not identical quantity to response time in the step-change experiment, providing information about time lag. Phase lag values are compiled in tables 4.3 and 4.4. The amplitudes of volume and length response seen in the figures are found in table 4.5.

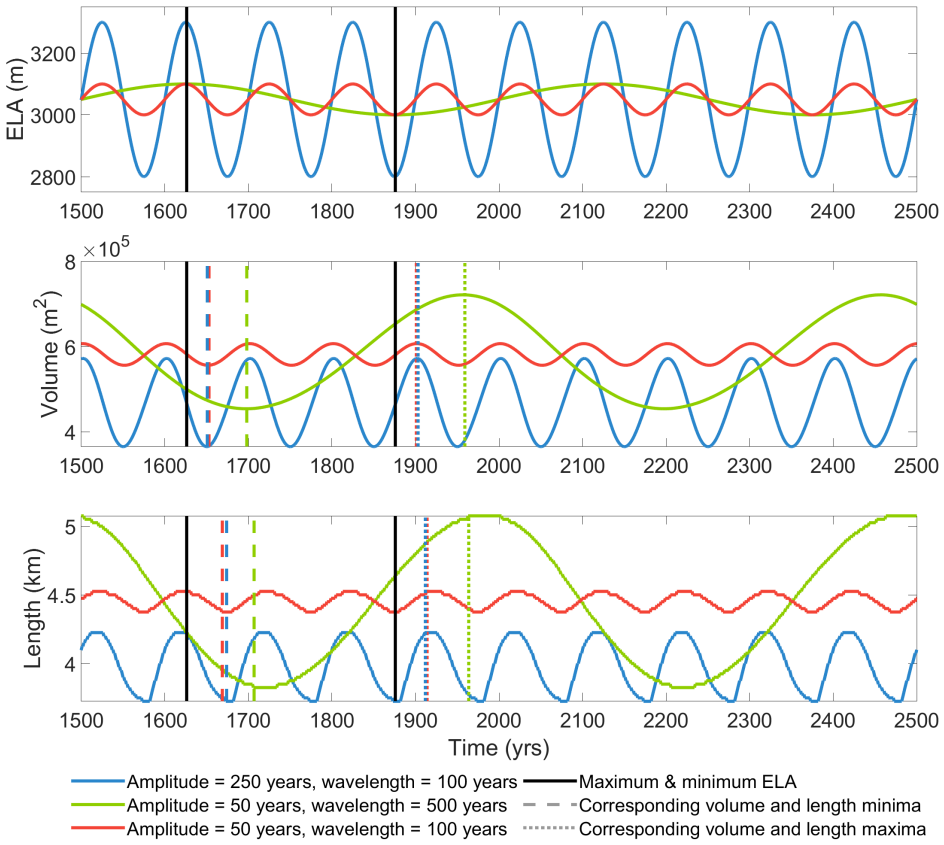


**Figure 4.5:** *Sinus wave experiment (B3) on a* ***debris-free*** *glacier, using three combinations of wavelength $\lambda$ and amplitude $A$. The plots show ELA, volume and length response, as well as phase shifts during advance and retreat.*

Looking at the response of debris-free glaciers to the sinus wave ELA (figure 4.5) and the corresponding phase lags, we see that volume response is very much sinusoidal as well, with peaks shifting about a quarter of a phase (~25 years) for the 100 year wavelength, but much faster relative to the wavelength (~75 years) for the 500 year wavelength. Length changes are shifted a bit more and asymmetric. Advance is actually faster than retreat for the 100 year wavelength, most clearly visible for the low-$\lambda$-high-$A$ curve. This effect only seems to show for short wavelengths, as length response to the 500 year wavelength is even slightly faster in retreat than advance. This suggests that there is a certain lag between volume and length response of around 10 to 15 years that is not strongly influenced by wavelength or amplitude. Length changes in retreat are a notable exception caused by the asymmetry described above.

Volume and length responses to the high-amplitude ELA clearly show lower values than their low-amplitude counterparts. This is likely a remnant of the initial conditions of the experiment. Each glacier comes out of a constant climate before the sinus wave experiment. As we start at model time zero, the ELA starts off by rising. In this initial retreat phase, volume and length drop and then plateau at a lower value than at the start. For the high-amplitude ELA, this effect is stronger, as it starts off with an intense warming phase.

**Table 4.3:** *Volume response phase lags for sinus experiments (B3) with varying wavelength $\lambda$ and amplitude $A$ for a debris-free and a debris-covered glacier.*

| **Debris-free** | *Advance $\varphi_V$ (yrs)* | *Retreat $\varphi_V$ (yrs)* |
|---|---|---|
| *$A$ = 50m, $\lambda$ = 100 yrs* | 25 | 27 |
| *$A$ = 250m, $\lambda$ = 100 yrs* | 27 | 25 |
| *$A$ = 50m, $\lambda$ = 500 yrs* | 83 | 72 |

| **Debris-covered** | *Advance $\varphi_V$ (yrs)* | *Retreat $\varphi_V$ (yrs)* |
|---|---|---|
| *$A$ = 50m, $\lambda$ = 100 yrs* | 25 | 25 |
| *$A$ = 250m, $\lambda$ = 100 yrs* | 27 | 25 |
| *$A$ = 50m, $\lambda$ = 500 yrs* | 111 | 132 |

**Table 4.4:** *Length response phase lags for sinus experiments (B3) with varying wavelength $\lambda$ and amplitude $A$ for a debris-free and a debris-covered glacier.*

| **Debris-free** | *Advance $\varphi_L$ (yrs)* | *Retreat $\varphi_L$ (yrs)* |
|---|---|---|
| *$A$ = 50m, $\lambda$ = 100 yrs* | 38 | 43 |
| *$A$ = 250m, $\lambda$ = 100 yrs* | 36 | 48 |
| *$A$ = 50m, $\lambda$ = 500 yrs* | 88 | 81 |

| **Debris-covered** | *Advance $\varphi_L$ (yrs)* | *Retreat $\varphi_L$ (yrs)* |
|---|---|---|
| *$A$ = 50m, $\lambda$ = 100 yrs* | -* | -* |
| *$A$ = 250m, $\lambda$ = 100 yrs* | -* | -* |
| *$A$ = 50m, $\lambda$ = 500 yrs* | 225 | 234 |

For a debris-covered glacier (figure 4.6), the response to the sinus wave forcing looks quite different. But starting with similarities, volume phase lag values for the 100 year wavelength are identical to the debris-free glaciers at ~25 years or a quarter wavelength. And in this case, the quarter-wavelength rule more or less holds true for the 500 year wavelength as well, with phase lag being slightly

shorter during advance (111 years) than retreat (132 years). These values are much higher than for the debris-free glaciers, which can be explained with the difference in size, as the debris-covered glaciers are much larger.

Length response, and how different it is compared to volume response, nicely shows one of the main effects of debris cover. For short wavelengths, the sinus wave climate barely has any influence on the glacier's length, even for the high amplitude. The amplitude of the changes is within the grid size $dx$ of 25 meters, rendering any calculation of phase shift impossible. The 500 year wavelength curve looks interesting, showing a mix between a sinus wave and the asymmetric advance and retreat patterns seen in the step change experiment. When at its longest, the extent plateaus and falls back quickly during retreat. Advance is then relatively slow in comparison, but phase shift values end up very similar, just below half-wavelength.

In this experiment, it is the volume and length response to the 500 year wavelength that is vertically shifted to a lower value than the other two curves. Once again, this can be attributed to the initial conditions. But as short-term changes (100 year wavelength) do not have as much of an influence on volume and length, especially, only the long-term changes can strongly impact the results through this modelling artifact.

**Table 4.5:** *Volume and length response amplitudes for sinus experiments (B3) with varying $A$ and $\lambda$ for a debris-free and a debris-covered glacier.*
**Amplitude is equal to or less than dx (25m), so no peaks can be measured.*

| **Debris-free** | $A_V$ $(m^2)$ | $A_L$ $(m)$ |
|---|---|---|
| $A$ = 50m, $\lambda$ = 100 yrs | $0.51 * 10^5$ | 150 |
| $A$ = 250m, $\lambda$ = 100 yrs | $2.07 * 10^5$ | 500 |
| $A$ = 50m, $\lambda$ = 500 yrs | $2.67 * 10^5$ | 1250 |

| **Debris-covered** | $A_V$ $(m^2)$ | $A_L$ $(m)$ |
|---|---|---|
| $A$ = 50m, $\lambda$ = 100 yrs | $0.41 * 10^5$ | 0 - 25* |
| $A$ = 250m, $\lambda$ = 100 yrs | $1.30 * 10^5$ | 0 - 25* |
| $A$ = 50m, $\lambda$ = 500 yrs | $2.33 * 10^5$ | 1075 |

When we compare amplitudes of length and volume response between the debris-free and debris-covered glaciers (table 4.5), the debris-covered glaciers' amplitudes are always smaller, even though they are much larger. The biggest difference can be seen in low-$\lambda$-high-$A$ changes, where the volume amplitude is 37% smaller than for the debris-free glacier.

Debris thickness (figures A.1, A.2 and A.3) also shows some interesting patterns. While the low-$\lambda$-low-$A$ glacier keeps a constant debris cover thickness

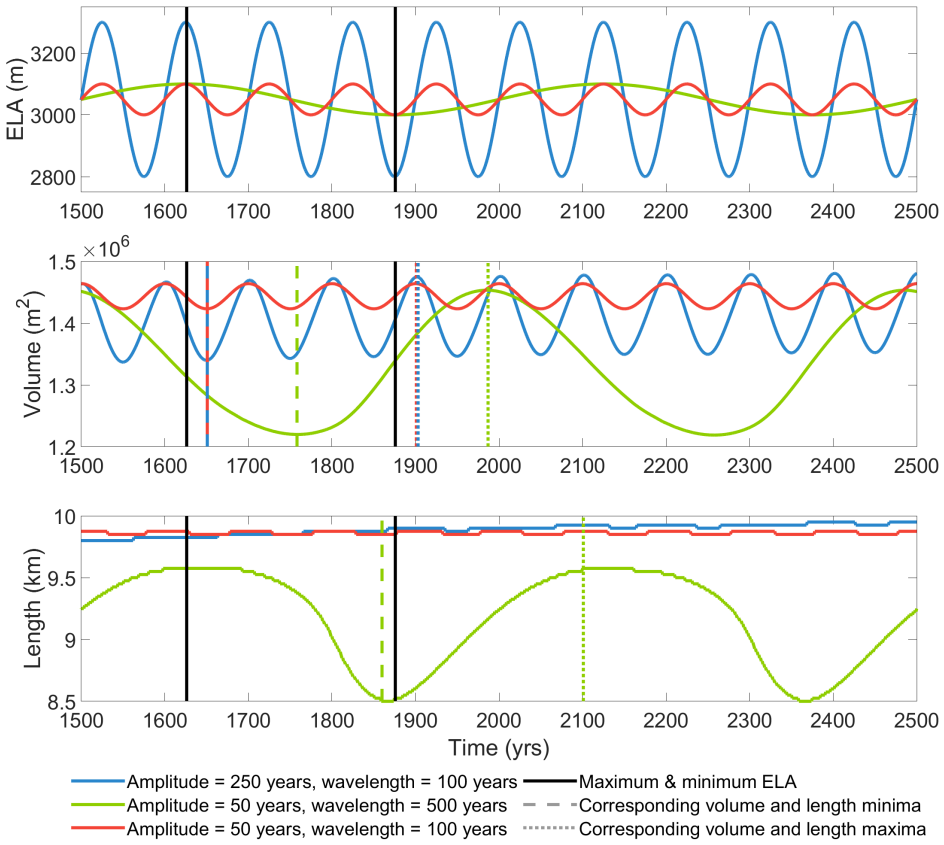


**Figure 4.6:** *Sinus wave experiment (B3) on a* ***debris-covered*** *glacier, using three combinations of wavelength $\lambda$ and amplitude $A$. The plots show ELA, volume and length response, as well as phase shifts during advance and retreat.*

throughout the experiment, the low-$\lambda$-high-$A$ glacier's debris cover increases slightly in thickness. The high-$\lambda$-low-$A$ glacier loses debris cover over time, as the terminus substantially retreats. Still, all of these changes are minor compared to the step-change experiment.

### 4.2.3 Linear temperature increase

The linear increase ELA experiment (B4) is a short stopover on the way to real climate data. It makes the transition from the abstract experiments done so far to a – very simple – representation of climate change in the 20th and 21st centuries. The experiment assumes a constant ELA throughout the LIA, followed by a period of constantly rising temperatures between 1850 and 2090, which is then followed by another constant ELA phase, as depicted in figure 4.7(a).

The temperature values used for the difference in ELA between 1850 and 2090 originate from the intermediate SSP2 scenario in the IPCC's Sixth Assessment Report (Masson-Delmotte et al., 2021).

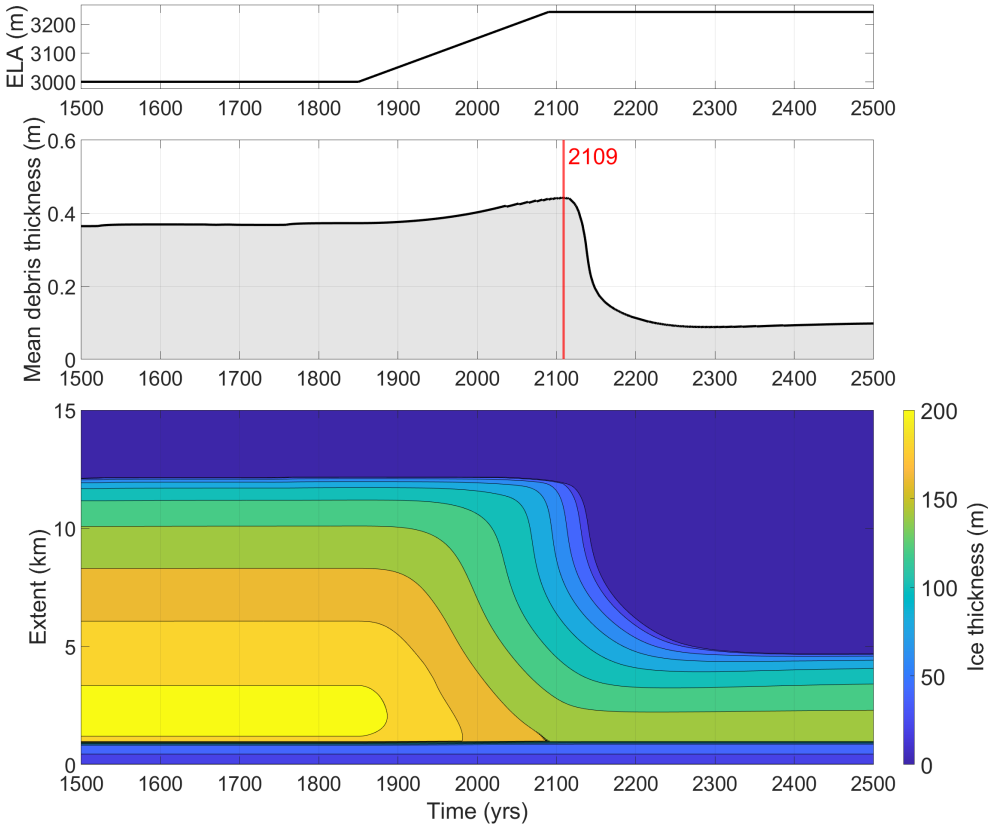


**Figure 4.7:** *Linear increase experiment (B4) with SSP2 projected warming on a debris-covered glacier. The plots show ELA, debris cover thickness, and a contour representation of ice thickness.*

The linear increase experiment is quite similar to the step-change experiment, and results also look similar correspondingly. A debris-free glacier (figure 4.8(a) starts melting away instantly after the initiation of the warming phase. Length remains constant for a few decades before retreating steadily and reaching a new equilibrium around the year 2200. The debris-covered glacier remains at the same extent for the entire warming phase, retreating dramatically shortly after, but not quite as fast as in the step-change experiment. A new equilibrium is reached only after the year 2300. In figure 4.8(b) we can nicely see how the accumulation area adapts to the change as fast as on a debris-free glacier, but the thinning tongue holds out for 150 years.

In a sub-experiment, different levels of natural climate variability on the scale of 10 years were added onto the linear increase. Results (figure A.5) indicate the same response that was already observed in section 4.2.2: The accumulation area responds to short-term changes, making the total volume somewhat variable. But the changes are just too short-lived to have any effect on the terminus position, as length response times are more on the scale of centuries than decades.

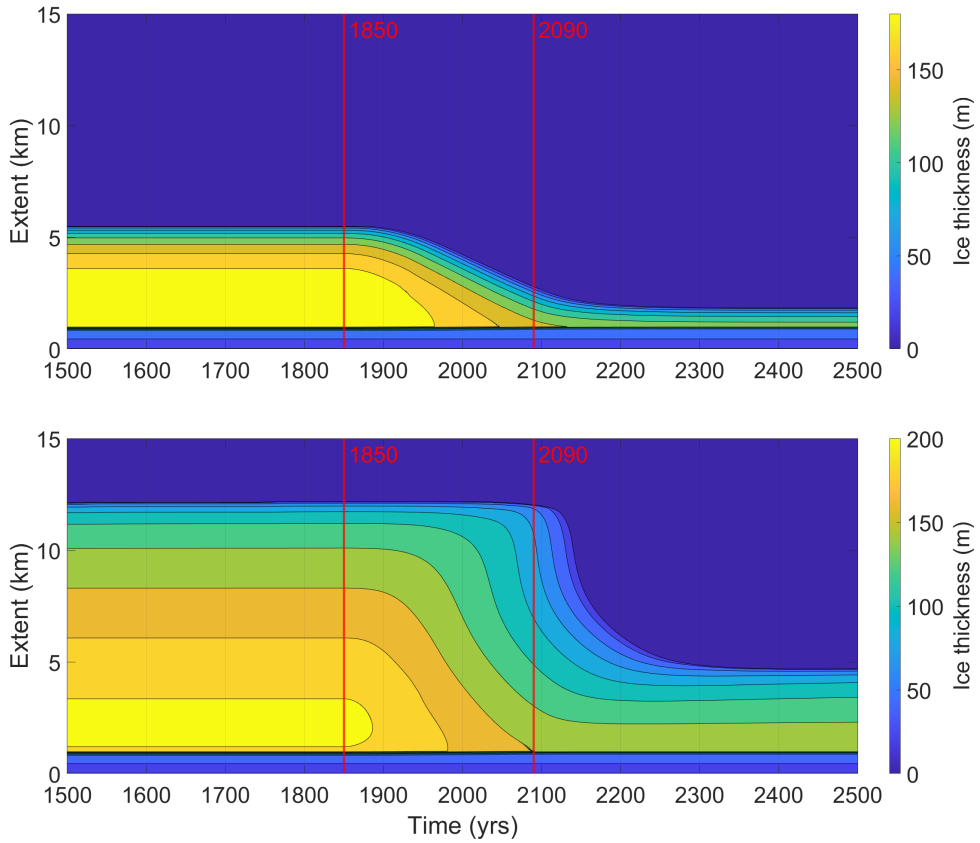


**Figure 4.8:** *Linear increase experiment (B4) with SSP2 projected warming on a debris-free (a) and a debris-covered (b) glacier. Both plots show a contour representation of ice thickness. The start and end date of the temperature increase are marked in red.*

### 4.2.4 Real climate history and projections

Moving on to the real climate history and projections experiments (B5), the final step to a climate input as realistic as possible is taken. It is also the main experiment of the thesis and is analyzed in the most detail accordingly. For

this purpose, a climate reconstruction from historical alpine glacier extents by Lüthi (2014) is combined with three climate projections from the IPCC's Sixth Assessment report (Masson-Delmotte et al., 2021). The corresponding ELA curve starts of in year 0 A.D. at an ELA of 3000 m a.s.l. for all experiments.

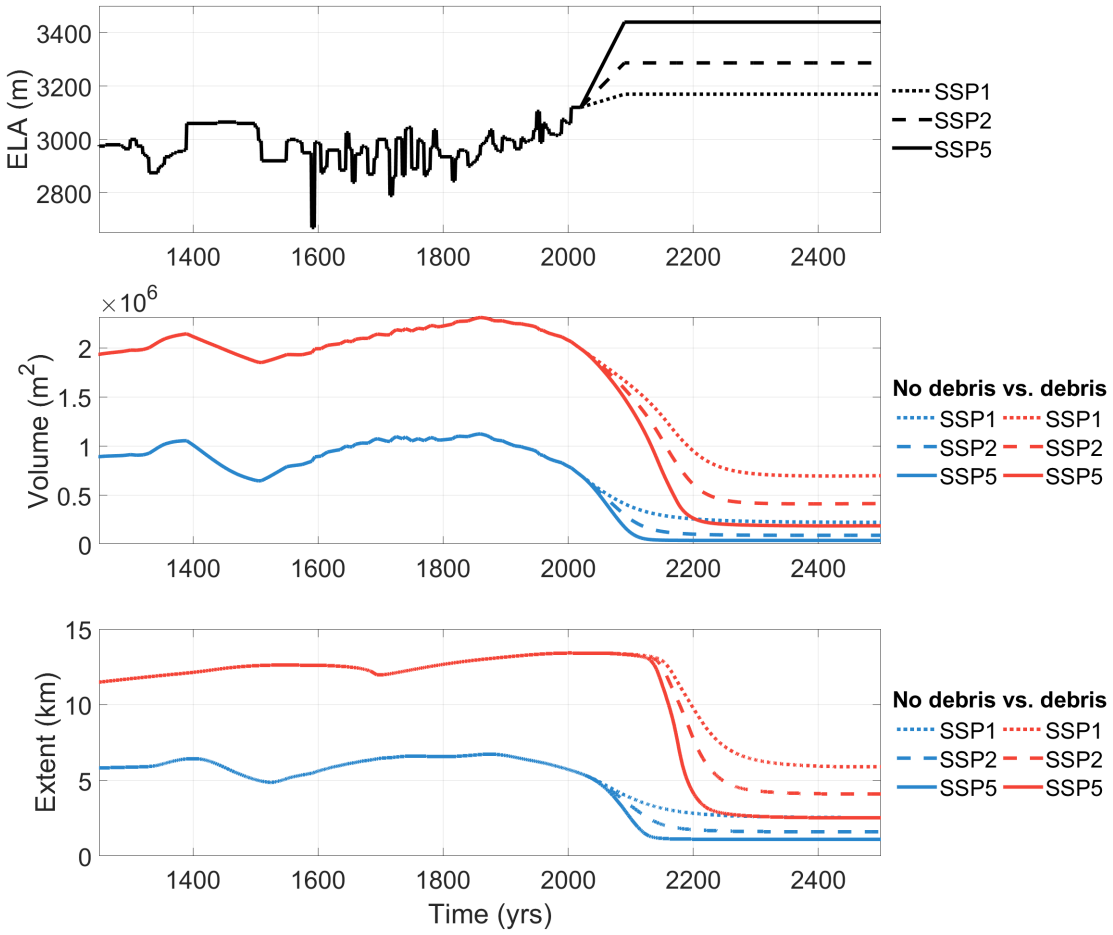


**Figure 4.9:** *Real climate history and projections experiment (B5) for a debris-free and a debris-covered glacier, using the IPCC's SSP1, SSP2 and SSP5 projections (Masson-Delmotte et al., 2021). The plots show ELA, volume and length response between years 1250 and 2500.*

The three climate projections represent a range of predictions, with SSP1 being the most optimistic and SSP5 the most pessimistic $CO_2$ emission scenario. The global climate model ensemble computes projected temperature differences between 2020 and 2090 of +0.55°C, +1.85°C and +3.55°C, respectively. The three resulting ELA curves are shown in figure 4.9(a). Similarly to experiment B4,

projected temperature increase is represented as a linear increase from 2020 until 2090 and under the assumption that temperature stabilizes from 2090 onward. This decision was made to enable observing a finite retreat that can clearly be attributed to the warming between 1850 and 2090.

Going in chronological order, we see an increase in volume during the LIA between 1500 and 1850. As length – especially of the debris-covered glacier – has an additional lag behind climate, a small retreat around the year 1700, originating from the last warmer phase between 1400 and 1500, is still visible.As temperatures increase in the 20th century, volume responds fast, with the debris-free glacier also responding quickly. After 2020, differences in volume response between projections appear immediately. The debris-covered glacier keeps advancing as a late reaction to the coldest LIA phase, and then suddenly retreats around the year 2130. Until then, the projections do not have any influence on length. During and after retreat, projections result in very different outcomes.

The debris-free glacier ends up almost completely melted away regardless of projection. Similar, severely reduced volumes and lengths are found after the SSP5 warming for the debris-covered glacier, but the other two projections (SSP1 & SSP2) end up strongly impacted, but still at a length of around 4 to 6 kilometers.

In section 4.2.3 it was already mentioned that natural variability might not have a significant influence on the glacier. To get a clear answer to whether these short-term changes have any significant influence, a comparison between the linear increase projection and the same climate with variability added is shown in figure 4.10. The amplitude of the natural variability is computed from the natural variability of the historic climate data from Lüthi (2014) by calculating the standard deviation from long-term (50 year) trends. This deviation (33m/0.37°C) then acts as the mean value of a normally distributed variability added onto the ELA curve.

Volume response shown in figure 4.10(b) shows no apparent difference between the two variants for both a debris-free and a debris-covered glacier. In figure 4.10(c), the difference between volume responses is shown in relation to volume. This confirms that variability changes the volume by less than one percent over the whole duration, with length being even less affected ($< dx$). It is quite surprising that even for volume, variability makes barely any difference, which justifies neglecting short-term variability in subsequent experiments for simplicity.

Figure 4.11 looks at how the debris layer is impacted by historical and projected climate change. One interesting feature before the current warming stands out during the small retreat described earlier, which is caused by a warm period before 1500 and manages to impact the terminus only around the year 1700. In the upper ablation area (around 5 kilometers) an anomaly of unusually high debris cover thickness appears just after the year 1500. It then slowly propagates downstream, reaching the terminus around the year 1700. Retreat and this

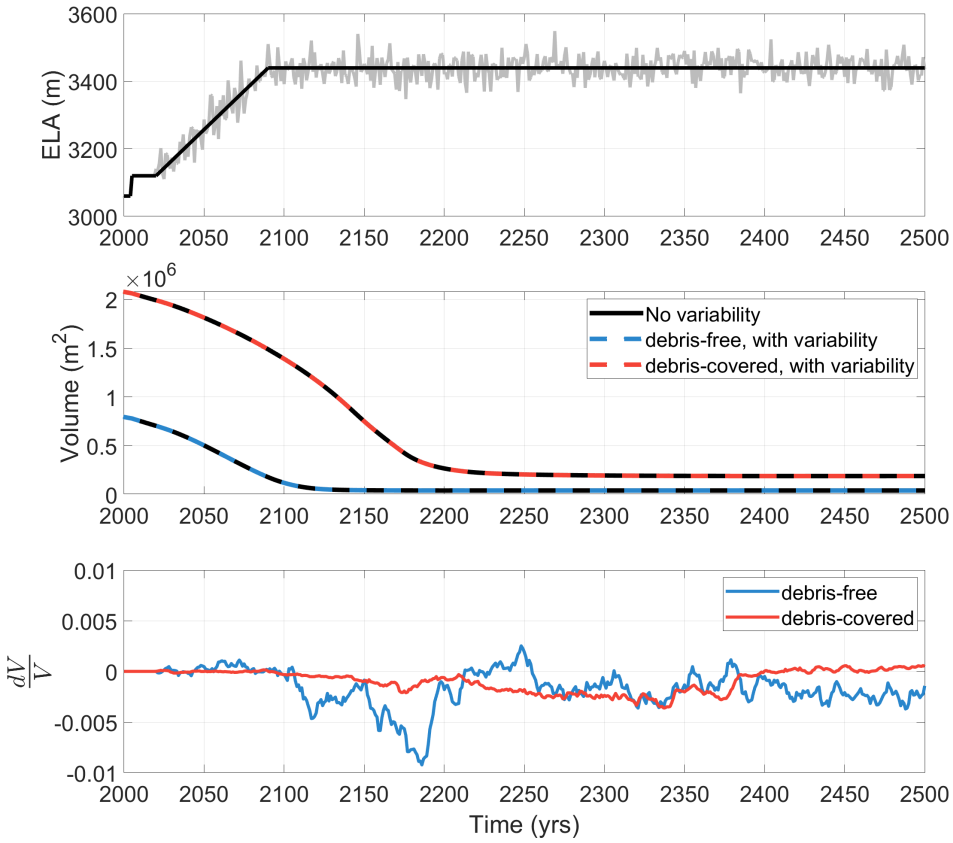


**Figure 4.10:** *Significance of natural variability for volume response. The plots show ELA with and without variability (a), volume response of a debris-free and a debris-covered glacier, both with and without variability (b), and the volume difference made by adding variability relative to the volume (c).*

anomaly are clearly connected, as it is also observed following a previous warm period between 1400 and 1500. Debris thickness then decreases during the LIA advance, before increasing – once again – at first in the upper ablation area and propagating along the glacier. If the warming in the 20th century were followed by a period of cooling, the same debris cover enhancing effect seen at the start of the LIA would be possible. But the projections show no such development. After peak extent is reached at the start of the 21st century, the terminus starts retreating slowly at first – similarly to before 1700 – and drops dramatically over the course of the 22nd century. In the process, debris cover is cut off from the glacier, which is nicely visible in figure 4.11 where debris thickness contour lines intersect with the terminus instead of running parallel. In the SSP5 projection the most debris is lost in relative terms, but all scenarios lead to a majority of

debris cover being offloaded in the rapid retreat phase. After warming, debris cover starts recovering slowly.

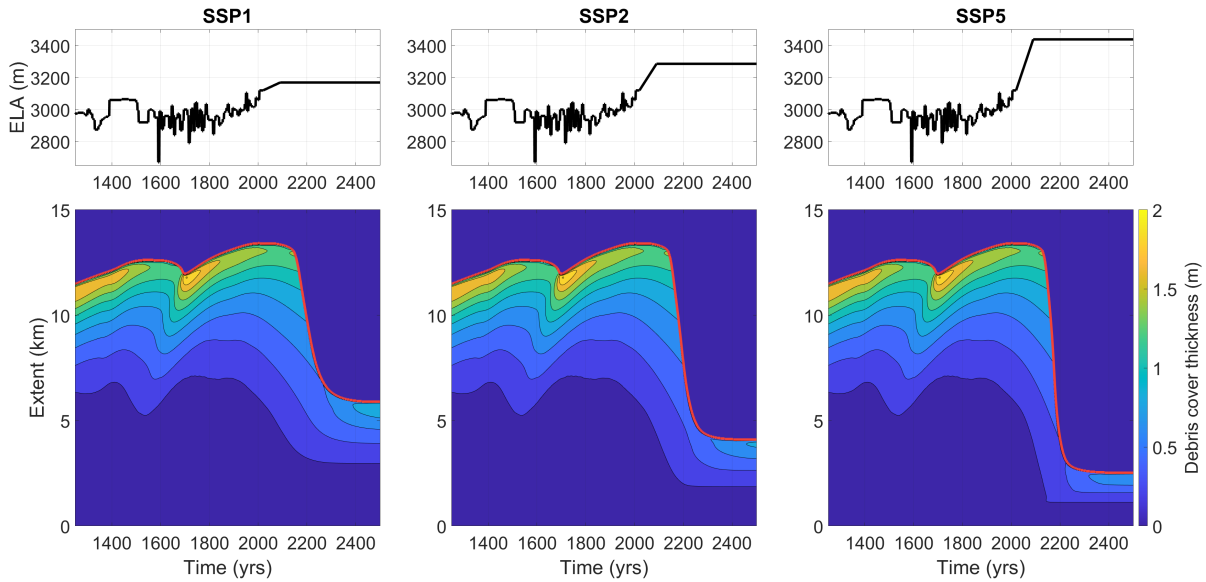


**Figure 4.11:** *Debris cover thickness of a debris-covered glacier during the real climate history and projections experiment (B5) for all three projections (SSP1, SSP2, SSP5). Plots show ELA (top) as well as contour representations of debris cover thickness (bottom). The glacier extent is marked in red.*

To understand the glacier's reaction to the climate more deeply on a dynamic level, we need to look at the dynamic properties of the glacier over time. Namely driving stress and ice velocity can give a better insight into when, where and how the glacier is impacted by the climate forcing. It also reveals areas of *dead ice*, which in this context denominates stagnating areas of the glacier, where ice cannot be replenished by dynamics. Driving stress and ice velocity patterns will look similar, as both are mainly dependent on surface slope and ice thickness (see equations 3.1 and 3.5).

Figure 4.12 compares these properties for a debris-free and a debris-covered glacier. Similarities between the two glaciers can be found in the general pattern of high driving stress and ice velocities during advance, and the opposite during retreat. There is however a difference in the propagation of changes along the glacier. On the debris-free glacier, changes in dynamics are instantly distributed along the entire length of the glacier, whereas the debris-covered glacier takes time for these variations to reach the terminus, which exactly coincides with the lag on length reaction.

The observation from previous experiments that the debris-free glacier is much more reactive to changes in climate can also be made here. The effect of cooler

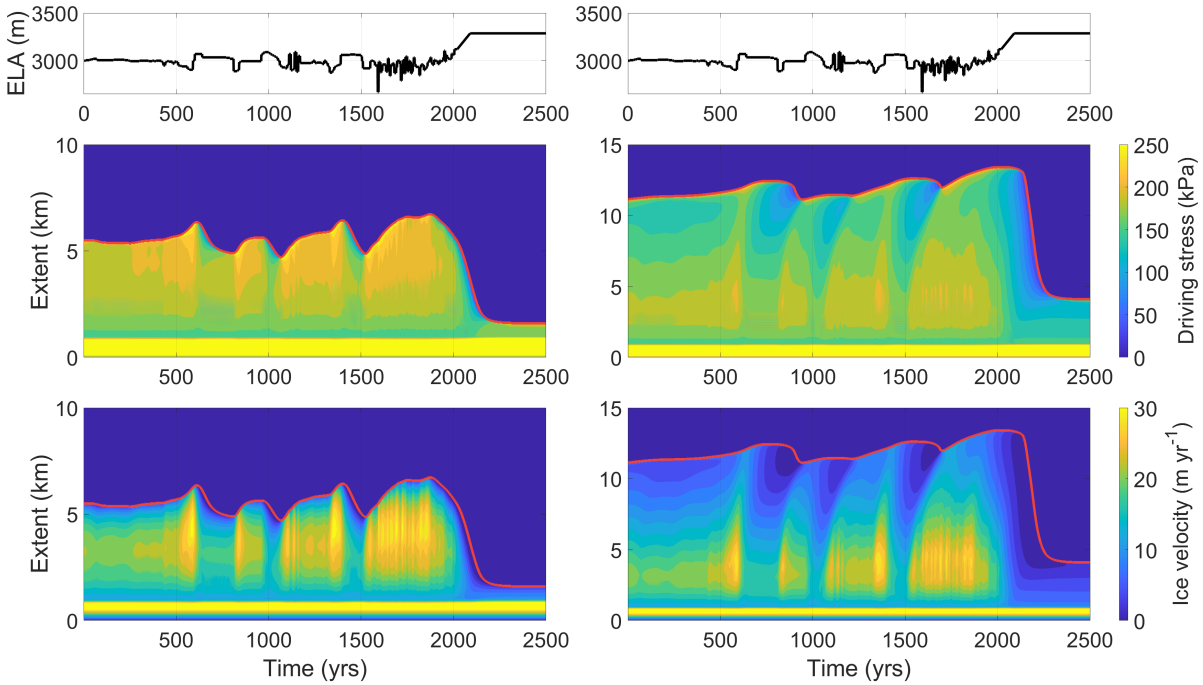


**Figure 4.12:** *Dynamic evolution of a debris-free and a debris-covered glacier during the real climate history and projections experiment (B5). Plots show ELA (top) as well as contour representations of driving stress (middle) and ice velocity (bottom). The glacier extent is marked in red.*

periods having a longer-lasting effect on the debris-covered glacier than warmer periods (Ferguson and Vieli, 2021) can also be found here. While the debris-free glacier's length stays more or less constant over the first 2000 years of model time, the debris-covered glacier grows by about a kilometer over the same time frame.

Driving stress and ice velocity values are generally lower for the debris-covered glacier, as the debris cover enables larger, flatter glaciers with elongated tongues. The gap between the already close to stagnant dynamics in the lower ablation area and entirely stagnant dead ice is small, and quickly bridged during retreat. In every one of the four retreat phases observed over the entire model time, dead ice appears. For the debris-free glacier, ice velocities only approach zero in the immediate terminus area during retreat.

## 4.3 Cryokarst

### 4.3.1 Differences between implementations

After testing the model against various climate inputs, we turn our attention towards the third research question. This section presents an evaluation on the cryokarst modules established in section 3.2.4. We differentiate between four versions of cryokarst implementation: the base model without any cryokarst (denominated as "No-CK"), the default driving stress driven implementation ("Default"), the solo version of the new runoff-based implementation ("Melt-only"), and an additive combination of the default and melt-only versions ("Default+melt"). These versions are tested in experiment C1, which steps back to use a simple step-change ELA to isolate the effect of cryokarst on the results.

**Table 4.6:** *Response times during advance and retreat after an ELA step-change of 100 meters, for the different cryokarst implementations (Experiment C1).*

| **Cryokarst implementation** | *Advance e-folding volume response time (yrs)* | *Retreat e-folding volume response time (yrs)* |
|---|---|---|
| *Default* | 398 | 217 |
| *No Cryokarst* | 383 | 245 |
| *Melt* | 217 | 138 |
| *Default + melt* | 217 | 132 |
| *Debris-free* | 134 | 77 |

In a first step we look at volume response times to the step-change warming and cooling, shown in table 4.6 and figure 4.13. The melt-only version applied here uses a $\mu$ of 1250 $m^3 yr^{-1}$, sensibility to this parameter is analyzed later (figure 4.17). The longest response times are taken by the no-CK and default versions, showing barely any difference. During retreat, the default version only seems to have a strong influence on the volume in the late stages. The sudden collapse of the lower tongue they both share happens 150 years earlier for the default cryokarst, but only after more than $1 - \frac{1}{e}$ of totally lost volume (e-folding volume response time $\tau_v$) is already lost.

Melt and default+melt versions start off with a smaller glacier to begin with, as this implementation affects ablation not only during retreat but in all states. Both versions also show a much earlier and less dramatic retreat in length, starting another 150 years earlier than the default version. Length response lags behind volume response only by about 50 years in these versions. Volume response time is also faster, but this might be an effect brought along with the size of the glacier. Generally, there is barely any difference between the two versions. Only during retreat does the default+melt version respond slightly faster. The debris-free glacier displays a simultaneous decrease in both volume and length,

as we already know from previous experiments. During advance the differences should mostly be caused by glacier size, as no cryokarst version explicitly affects advance behavior. The only other factor to consider would be the slow and steady continuation of advance over centuries as the debris layer rebuilds, as discussed in section 4.2.1.

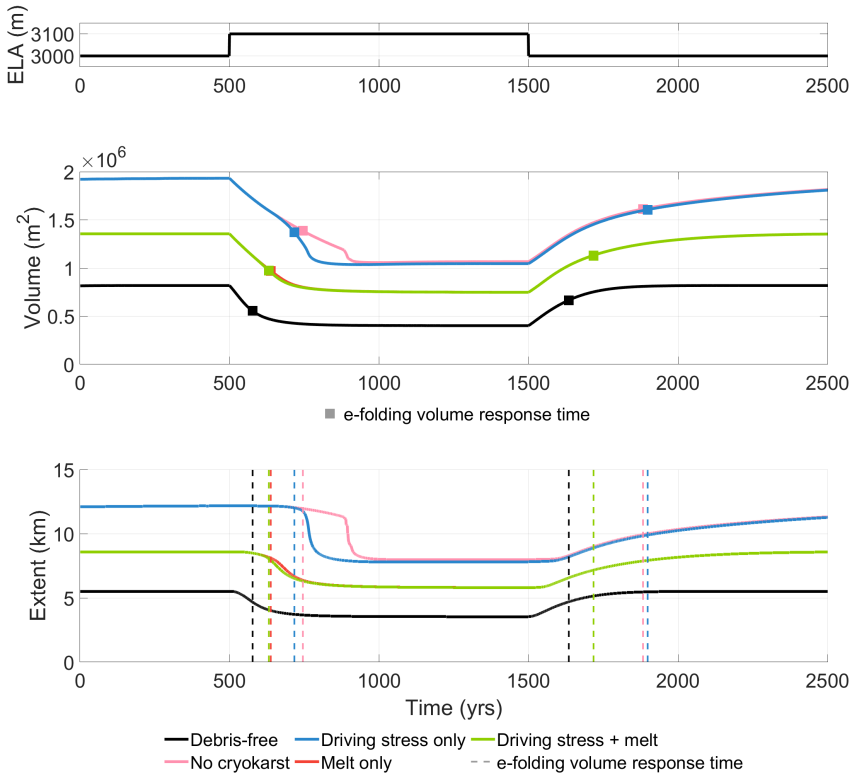


**Figure 4.13:** *Step-change experiment (C1) with glaciers using all versions of cryokarst implementation (no-CK, default, melt-only & default+melt) as well as a debris-free glacier. The plots show ELA, Volume and length response, with $\tau_d$ marked.*

The effect of the four versions on retreat and general behavior is further illustrated with the distribution of mass balance over space and time in figure 4.16. The reversal of the mass balance gradient on the lower tongue from debris cover insulation is apparent for both the no-CK and default versions. The increased ablation shortly before retreat is clearly visible for the default version and – in a reduced amount – the default+melt version. Both the melt-only and default+melt versions do not exhibit a reversal of the mass balance gradient, as the cryokarst strongly counteracts the debris insulation effect over the whole duration.

An interesting feature is also an apparent undershoot of mass balance right after the step-change warming and an overshoot after cooling, best visible in the melt-only and default+melt versions. The origins of these features will be extensively discussed in chapter 5.

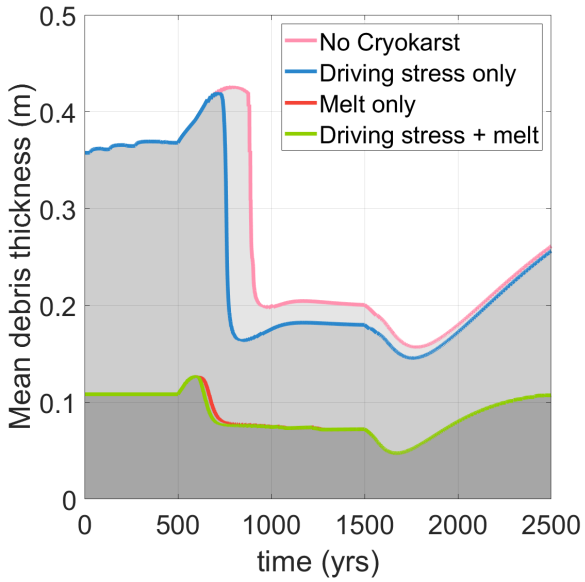


**Figure 4.14:** *Debris cover thickness in step-change experiment C1 for all cryokarst implementations.*

As seen before in both the step-change and real climate experiments, the manner of retreat is quite relevant to the state of the debris layer after retreat. And because the cryokarst implementation is a critical factor in how fast the terminus retreats, debris layers react differently depending on which version is used. Figure 4.14 shows that the no-CK and default versions lose about half of their debris layer in the sudden retreat as a consequence of the step-change warming. Because the melt-only and default+melt versions produce much smaller glaciers, they also build up less of a debris layer. However, this layer is much more persistent, as only about 20% of debris cover is lost in retreat, and the original layer thickness is quickly recovered after re-advance. Interestingly, no-CK and default debris layers show both overshooting features described in the first step-change experiments. The other two versions however only feature such a dent during advance, which might be connected to the decreased speed of retreat as well.

With the general differences between the cryokarst versions sorted out, we can look at how they affect a glacier with a real climate history and the three projections. Experiment C2 uses the climate input from experiment B5 (section 4.2.4) and compares three glaciers: a debris-free glacier and two debris-covered

glaciers with default+melt and default cryokarst versions, respectively. Figure 4.15 shows a tangible representation of the states these three glaciers are modelled to be in for the years 1850, 2022 and 2090.

In 1850, at the peak – and beginning of the end – of the LIA, glacier sizes and shapes are already quite different. While the accumulation zones are similar because of the absence of debris cover there, the debris-covered glaciers can grow longer, flatter tongues. The increased cryokarst area of the default+melt version somewhat inhibits this, finding itself halfway between the other two glaciers. In 2022, the debris-free glacier has already substantially retreated, whereas the debris-covered glaciers only show some thinning. And in 2090, we see similar results between the three projections, with differences in temperature increase having much more of an impact on the debris-free glacier. Both the debris-free and default+melt cryokarst glaciers have retreated strongly by this point, but the latter still holding more of its initial volume and length. Only the default cryokarst glacier still holds strong, showing no retreat yet, regardless of projection.

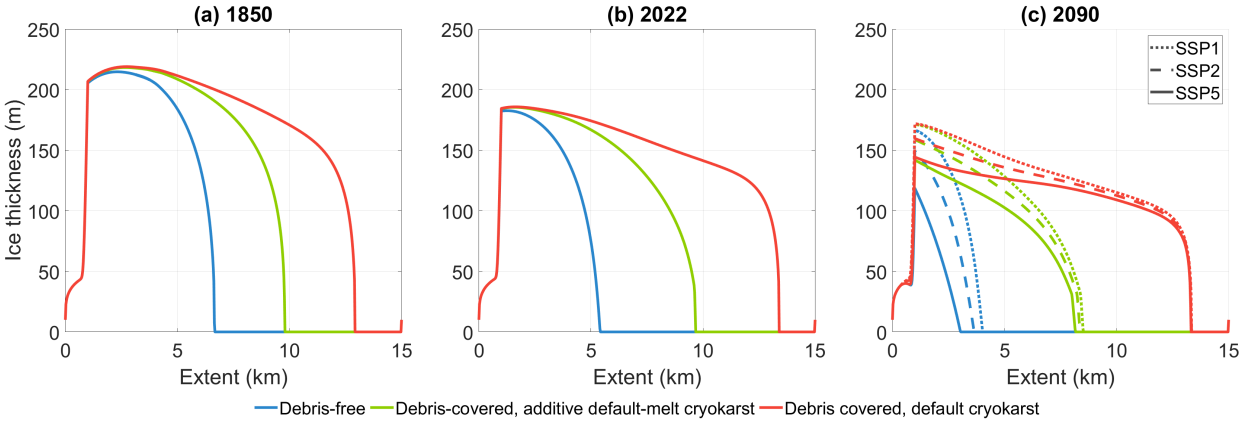


**Figure 4.15:** *Ice thicknesses resulting from the real climate history and projections experiment (C2) using default and default+melt cryokarst versions and a debris-free glacier*

### 4.3.2 Sensitivity of the melt parameter

One can imagine that the melt parameter $\mu$ is quite decisive for the amount of cryokarst formed through the melt version. Figure 4.17 shows how sensible volume and length are to changes in $\mu$. The value used in previous figures and analyses was 50 $dx$ or 1250 $m^3 yr^{-1}$. This is based on the field observation that even small streams can create large ice cliffs, and that streams usually only reach a certain size before entering the glacier. Looking at the maximum runoff over the whole glacier, it is above this threshold at all times. This means that there

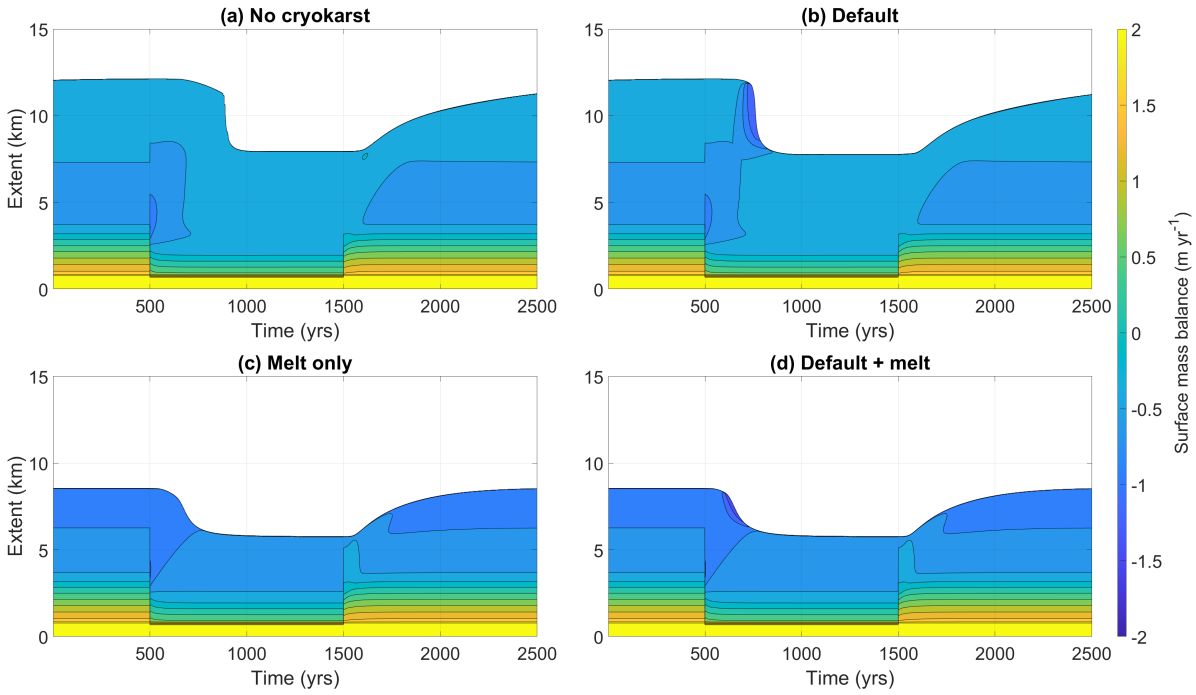


**Figure 4.16:** *Step-change experiment (C1) with glaciers using all versions of cryokarst implementation (no-CK, default, melt-only & default+melt). The plots show a contour representation of surface mass balance a over time and space.*

is always a part of the glacier where the maximum cryokarst area fraction $\lambda$ is reached. The high value of 500 $dx$ or 12,500 $m^3yr^{-1}$ is set around the all-time high of maximum runoff, so $\lambda$ is rarely reached, but most areas exhibit some cryokarst. Finally, there is an intermediate value of 200 $dx$ or 5000 $m^3yr^{-1}$, where the areas with a high amount of runoff will almost always reach $\lambda$, and a lot of area still ranging between zero and $\lambda$.

The pattern in maximum cumulative runoff (figure 4.17(b)) is also a nice reflection of the glacier's adaptation to climate. As local runoff is a factor of mass balance, it makes sense that cumulative runoff will behave similarly, increasing after warming and decreasing after cooling. But as the glacier gets shorter, less runoff can accumulate during the warm phase, so retreat leads to a lower maximum runoff and vice versa.

Changing $\mu$ does have a significant effect on volume and length, especially changing to the largest value results in a larger glacier. In terms of quantity, volume and length increase by about 10% when $\mu$ is multiplied by 10. These changes are substantial but not in the range of the differences between default and melt cryokarst versions (~35%) or between debris-free and debris-covered glaciers (~40-60%). Behavior in retreat is very similar between the three values, with the lower two taking more time to fully reach a new balance after retreat. The differences in length are also somewhat larger in the warm phase than in the cold phases.

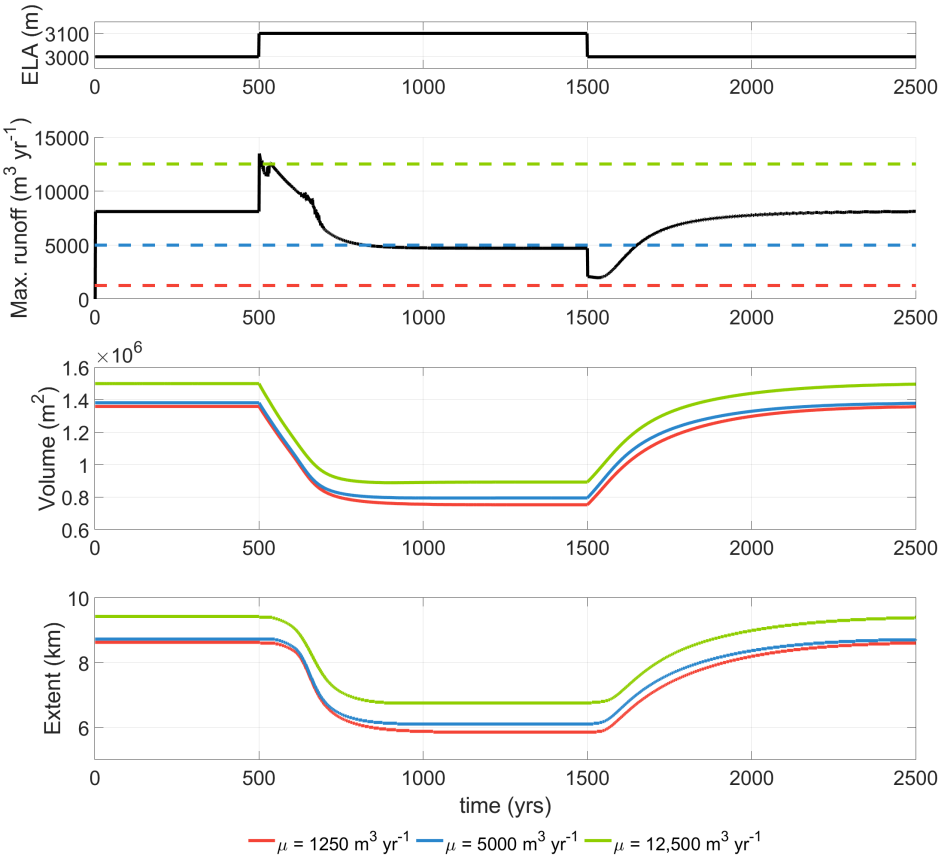


**Figure 4.17:** *Step-change experiment (C1) with varying values of the melt parameter $\mu$ (1250 (50 dx), 5000 (200 dx) & 12,500 (500 dx) $m^3yr^{-1}$). Plots show ELA (a), the highest runoff value over the whole glacier (b), as well as volume (c) and length (d) response. $\mu$ values are also marked in plot b.*

## 4.4 Zmuttgletscher

This section applies some of the experiments that were done on an abstract bed geometry in previous sections to a real example. For this purpose, a simplified approximated bed geometry of Zmuttgletscher (Mölg et al., 2020; Grab et al., 2021) was used.

### 4.4.1 Sinus experiment

In a first step, a sinus wave ELA is used by the model – with all values set to the default – to get a general sense of what the impact of a more complex bed on the glacier looks like. Figure 4.18 shows the results of this experiment with a wavelength of 500 years and an amplitude of 50 meters. Interestingly, the thickest part of the glacier is found in the ablation area, contrary to the abstract geometry, where ice thickness continuously decreased along the glacier. The flat bed below the ablation area enables temporary ice thicknesses of up to 200 meters, a value never reached on the abstract geometry. There is also much more variability in ice thickness caused by topographic features creating heterogeneous gradients along the glacier. Steep areas are thinner and more dynamic, whereas flat areas are thicker and more stagnant. This also causes more areas of compression and extension to appear throughout the glacier. That might have some impact on runoff accumulation, which is not of importance here, but will be in the second experiment (D2).

Changes reach the terminus, but once again cooling periods seem to have more of an impact than periods of warming, leading to a net increase in length. The flat terrain in the terminus region also favours advance and the build-up of a thick tongue. The delayed propagation of changes along the glacier observed on the abstract geometry can also be found here. For shorter wavelengths (figure A.6), changes do not reach the terminus. Apart from that, the glacier behaves similarly in terms of dynamics and reaction to ELA forcing.

### 4.4.2 Real climate history and projections

The final experiment (D2) considers the impact of real climate history and projections on a glacier on the Zmuttgletscher bed topography. The objective is to have somewhat of an application case for the model and to compare results to real measurements. In this process, we might get an indication of which combination of parameters and implementations represents actual changes to debris-covered glaciers the best. It is also important to emphasize that this is not an attempt at accurately modelling Zmuttgletscher, but rather at using more realistic and complex circumstances than with the abstract topography.

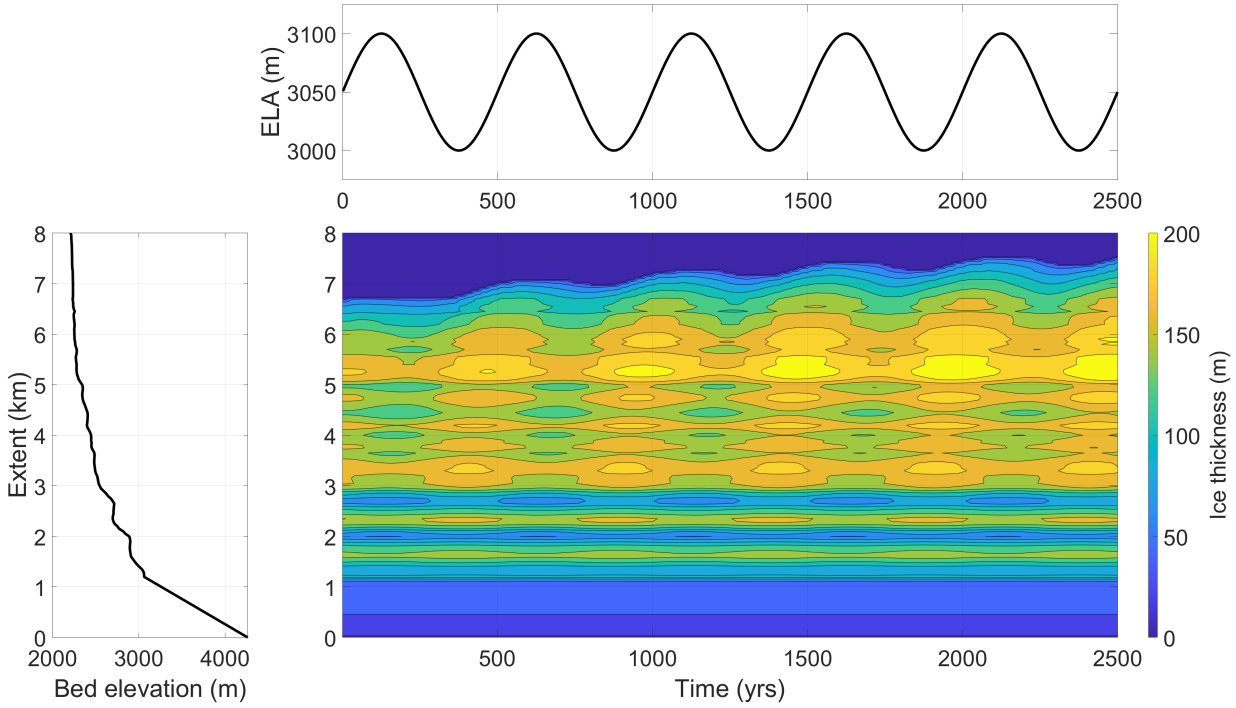


**Figure 4.18:** *Sinus wave experiment (D1) on the Zmuttgletscher geometry, using $\lambda = 500$ years and $A = 50$ meters. Plots show ELA, bed topography, and a contour representation of ice thickness over time and space.*

Figure 4.19 shows how a debris-covered and a debris-free glacier respond to real climate history and future projections. Some of the common themes of earlier experiments show up again here. The plateau and delayed drop-off in length for the debris-covered glacier reappears. In this case, retreat was even a bit too fast for the model to handle. In the SSP5 scenario, a large part of the glacier – basically the entire ablation area – is cut off from the upper part, leading to model failure (see figure 4.20). Either way, the continued development of the glacier in this scenario would be quite simple: the glacier length is instantly reduced to the length of the upper part, and the lower part melts away quickly, as it cannot sustain itself, and becomes an isolated chunk of dead ice. First signs of such cutoffs can be observed in areas of thin ice thickness on Zmuttgletscher as well.

Comparing this experiment to its equivalent on the abstract geometry, shown in figure 4.9, we see that the glacier on the Zmuttgletscher geometry generally is much less responsive to changes in volume and extent. Features like the small retreat around the year 1700 do not appear here. Between 1500 and 2100, the extent of the debris-covered glacier stays almost constant with a slight increase. There are however some other interesting features, like the irregular speed of

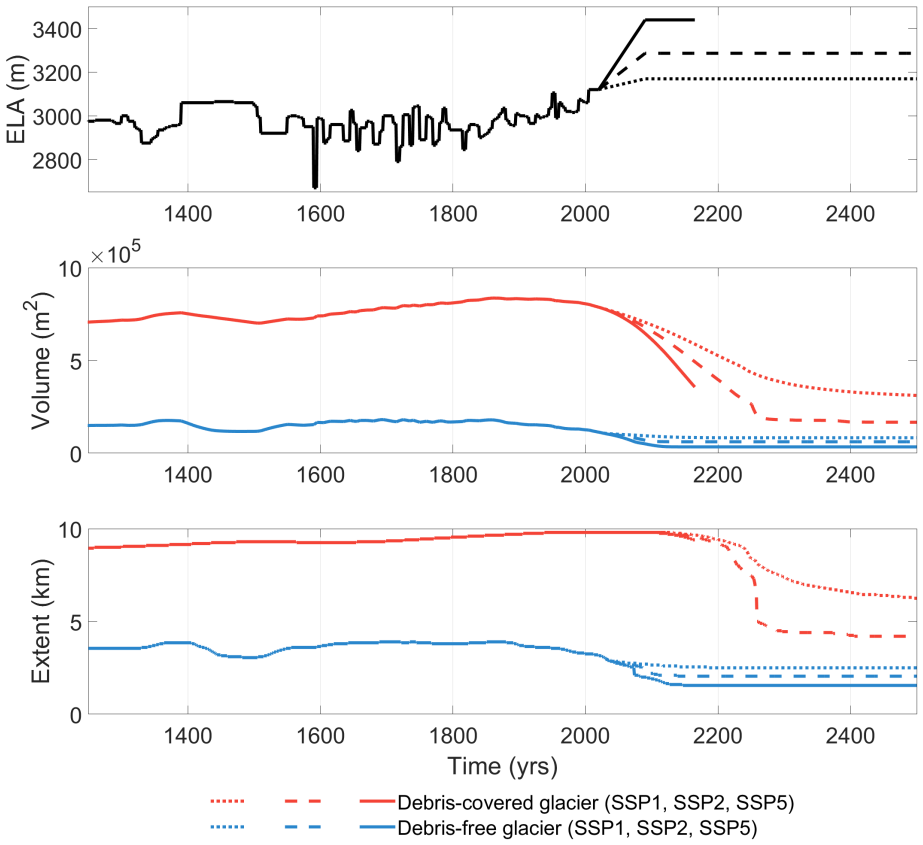


**Figure 4.19:** *Real climate history and projections experiment (D2) on Zmuttgletscher bed geometry. Plots show ELA, as well as volume and length response between years 1250 and 2500. The SSP5 response is incomplete due to a cutoff feature shown in figure 4.20.*

retreat as the terminus passes topographical features. Also, retreat of the debris-covered glacier is initiated even later (around year 2200) and impacts the length of the glacier less than on the abstract geometry. In this sense, the topography of the Zmuttgletscher bed is perfect for resilience against warming: the thick tongue on flat ground remains stationary during small short-term changes and is constantly replenished through dynamic replacement from the steep upper ablation and accumulation area. And in case the tongue collapses, the steep terrain protects against further retreat.

In the final sub-experiment we try to match the metaphorical fingerprint of Zmuttgletscher's retreat over the last 140 years, which is the measurement period for length changes by GLAMOS. Figure 4.21 shows three of these attempts. The default model, the model with all new implementations – including the new

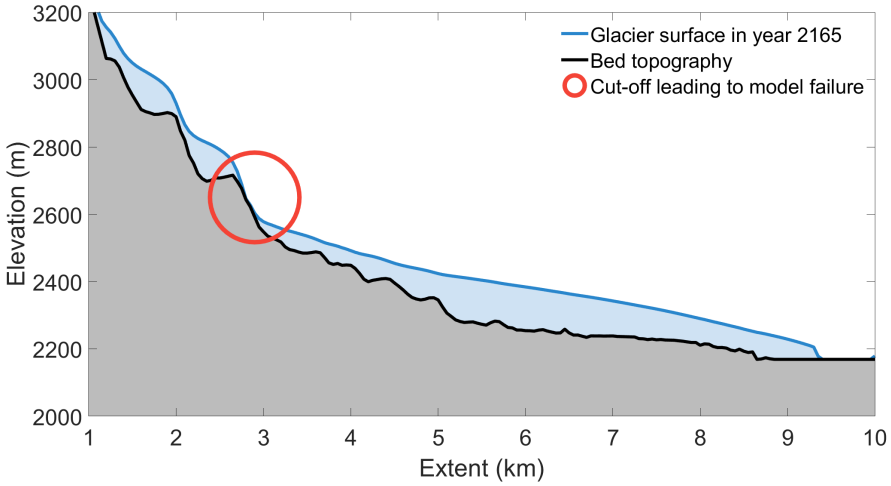


**Figure 4.20:** *Glacier geometry in model year 2165 of the SSP5 branch of the real climate history and projections experiment (D2), right before the cutoff event in the area marked in red.*

Østrem curve and the default+melt cryokarst version – and the same, but with an ELA lowered by 100 meters to create a larger glacier.

Surprisingly, the behavior of Zmuttgletscher is most similar to a completely debris-free glacier. But all models cannot recreate the real retreat of Zmuttgletscher perfectly, with the one including the new implementations being the best guess for a debris-covered glacier. The big difference between models is the timing of retreat initiation. The default model is even still in advance when real measurements already show retreat. The lowered-ELA version shows that this timing highly depends on the size of the glacier. Zmuttgletscher is certainly much longer than 5 kilometers, which makes its fast retreat relative to the models quite mysterious. Attempts at changing debris concentration, the maximum cryokarst area fraction, and ELA were all unsuccessful in reproducing the retreat pattern of Zmuttgletscher. As mentioned before, it is not the goal to replicate Zmuttgletscher, and the model configuration certainly is inadequate for that, making this failed experiment an expected overestimation of the model's capabilities.

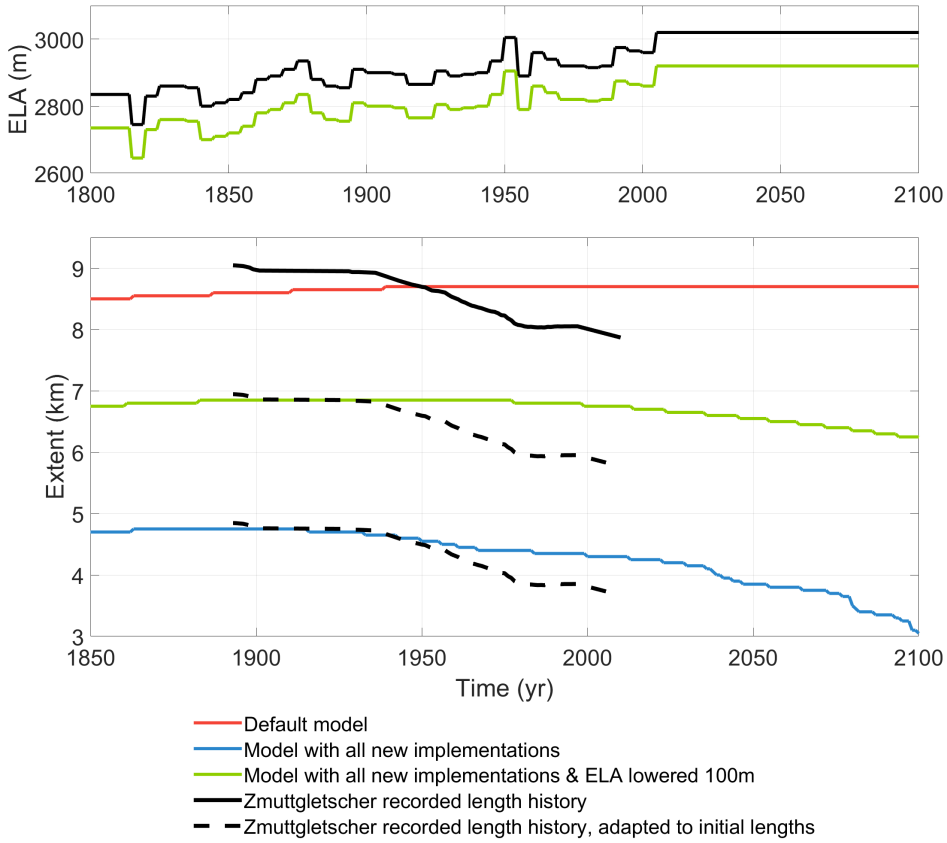


**Figure 4.21:** *Attempt at replicating length measurements at Zmuttgletscher with the real climate history experiment (D2). Plots show ELAs and length responses of different model configurations compared to real length measurements (GLAMOS 1880-2021).*

Chapter 5

# Discussion

In the previous chapter, a multitude of experiments were conducted, looking at various aspects of the DEBISO model. The data and figures that were showcased focused mostly on the transient response to changes in climate and testing newly adapted model routines. In this chapter, the goal is to consolidate insights on the model and debris-covered glaciers from the modelling results, and set them into the context of previous studies, field observations, and model limitations.

## 5.1 Influence of model parameter choices

Some of the key parameters that were considered in the experiments – excluding climate – were debris concentration, the Østrem curve, bed topography, and the cryokarst implementations. Additional parameters analyzed already by Ferguson and Vieli (2021) include maximum cryokarst area fraction and the driving stress thresholds for cryokarst. As cryokarst will be discussed separately in section 5.3, focus in this section will lie on the first three parameters.

It was established that changes in debris concentration lead to vast differences in glacier size in equilibrium, an observation shared by Ferguson and Vieli (2021). The general limitations of the use of a debris concentration will be discussed later in section 5.5. Response times, as well as mass loss as a consequence of warming, are also strongly affected by debris concentration. Volume response to warming is delayed more by increased debris concentration than response to cooling, which indicates an asymmetric response. As a consequence, cooling periods are remembered more than warming periods (Ferguson and Vieli, 2021), an effect that gets stronger the more debris is present. Debris cover thickness is dependent on debris concentration accordingly, roughly complying with the *intercept theorem*, where the shape of a glacier's debris cover thickness along the glacier is equal and scalable.

As shown in Figure 5.1, debris cover thickness is more or less equal at a fixed point along the grid when varying debris concentration, as excess debris is transported to the additional area from the increased length. This leads to the

conclusion that for a given ELA and bed topography, debris cover thickness at a point along the glacier is predefined, and that debris concentration only dictates glacier length. The relationship between extent and debris cover thickness is convex-concave-up because of decreasing ice velocities towards the terminus (Anderson and Anderson, 2018; Ferguson and Vieli, 2021). This effect is counteracted by differential melt due to debris cover, meaning that less melt from thicker debris cover towards the terminus leads to less melting-out of debris, which would then favor a concave-convex-up shape. This is nicely summarized by Nicholson et al. (2021) as the net effect between melt-out and the dynamic processes of advection and compression/extension. In the upper ablation zone, where debris cover is thin, melt-out dominates, whereas the dynamic effect dominates in the lower ablation zone (Anderson and Anderson, 2016).

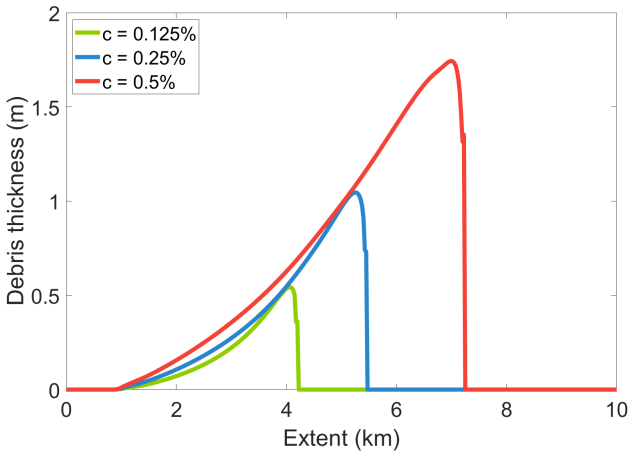


**Figure 5.1:** *Debris cover thickness along the glacier at a constant ELA of 3100 m a.s.l., using three debris concentrations (0.125%, 0.25% & 0.5%).*

Consequently, debris cover thickness is also partly dictated by the Østrem curve. Figure 4.1 also shows that the choice in $D_0$ is critical for glacier size, with the new data-driven approach essentially halving the effect of debris cover on volume and extent compared to the default Østrem curve. Anderson and Anderson (2016) compared $D_0$ values between 0.035m and 0.165m, noting a 110% length enhancement from the highest to the lowest $D_0$, which is consistent with the results here. They also found glacier length to be increasingly sensitive to $D_0$ variation the closer to zero it gets (Anderson and Anderson, 2016). This makes a more thorough analysis on the relationship between debris cover and sub-debris ablation necessary for future modelling, especially as this one value forms the basis for all other experiments. The variability between individual glaciers in this relationship shown in figure 3.2(b) suggests that calculating an Østrem curve for real glaciers might require an analysis based on local data, or some sort of classification dependent on other environmental conditions.

Circling back to the research question regarding the Østrem curve, some clear answers can be given: the default curve using a $D_0$ of 0.05m fits neither the field measurements nor most literature data. It does however fit perfectly for a single glacier, Franz Josef Glacier (Brook et al., 2013), which showcases once again the large variability between individual glaciers. Field measurements on Zmuttgletscher agree well with literature data, with most data points found within one standard deviation. Only the single data point located at an ice cliff steps out of line as a symbol for the melting power of cryokarst features.

Topography affects debris-covered glaciers in a similar way to debris-free glaciers. The consequences in size and dynamics – with steep slopes leading to smaller and more dynamic glaciers – in turn influence the ability of the glacier to form a sizeable debris cover. Steep, small glaciers have less volume for debris to be contained in, less available surface for it to melt out, and faster ice velocities offloading the debris, leading to lower debris thicknesses seen in figure 4.3.

In figure 4.4(b) we once again observe the linearly scalable nature of debris cover thicknesses for different glacier sizes, as described for the debris concentration above. The change in slope does seem to somewhat distort the shape, but the peak debris cover thickness at the terminus is still determined by an approximately linear relationship between length and debris cover thickness. The effect of a complex topography on glacier response will be discussed in section 5.4.

## 5.2 Climate sensitivity of the DEBISO model

The second research question was intentionally worded rather broadly and ambiguously to encompass as many experiments as possible. In this section, climate experiments are again discussed in order of complexity from step-change to real climate experiments.

### 5.2.1 Retreat and advance dynamics

The first climate variations introduced were the step-change experiments, which mainly served the purpose of isolating the effect of the parameters described in the previous section. In terms of climate, the most important assessments concern response times and the asymmetric shape of length response to warming and cooling. The latter observation of a long-lasting length plateau after warming as a contrast to the more consistent advance after cooling is described as an effective hysteresis by Ferguson and Vieli (2021), leading to the selective memory effect shown earlier. The tendency to stagnate or advance during periods of repeated warming and cooling is also observed in the sinus wave and real climate history experiments.

Apart from the shape, e-folding volume response times contrarily are hundreds of years longer for advance than for retreat. This indicates an interesting dichotomy: For warming periods that fail to impact glacier length significantly – which here encompasses warm periods of over a hundred years – the glacier can recover easily in following cooler periods and even show net growth as a result of increased debris cover thickness during re-advance. If however a critical point in terms of warm period duration is crossed, the glacier can retreat dramatically. In the process, much of its debris cover is lost (e.g. figure 4.11), making re-advance a much slower process. In figure 4.1 we can very well see that advance (after year 1500) is similar between debris-free and debris-covered glaciers in shape at first, indicating a *climate-controlled* advance phase. The debris-free glacier is back to steady state after a few hundred years, whereas the debris-covered glacier keeps advancing steadily as debris cover is replenished, thus constituting a *debris-controlled* second advance phase.

During both retreat and advance following a step-change climate change, local overreactions in volume associated with similar features in debris cover thickness are observed. These curiosities can be explained by the need for adaptation to the suddenly different climate. After warming, the lowest part of the accumulation area now exhibits a negative mass balance. Ablation rates in this debris-free area and adjacent slightly debris-covered areas are suddenly much higher initially. In this period, these areas lose a lot of volume, accompanied by an increase in debris thickness, shown in figure 4.2. After a locally constant debris cover has been established, ice thickness in these areas slightly increases again. The opposite effect can be observed after cooling – but only for high debris concentration or steep bed slopes. Figure 4.16 might show some evidence for this interpretation of the anomaly. After cooling, ablation decreases in the ablation area, as temperatures are lower and debris cover is still thick as insulation. But another consequence of the cooling is decreased melt-out upstream, and the decrease in surface debris delivery to the lower ablation area eventually makes the debris layer thinner, increasing ablation in the process. These overreaction features are only observed on debris-covered glaciers and only in the step-change experiments, because it is only there that changes are fast enough to bring along these effects.

The change of dynamic properties such as driving stress and ice velocity is closely related to the lag of both volume and length and response times that were just discussed. Figures 4.12 and 5.2 nicely show the instantaneous effect of warming and cooling over the whole glacier in the debris-free case, leading to almost lag-less retreat. In the debris-covered case we observe that changes in climate manifest in the accumulation and upper ablation area, where debris cover is non-existent or thin. As the lower ablation zone is not impacted instantly, it takes time for thinner or thicker ice to dynamically flow downstream. The gradual flow of a thinning anomaly caused by warming can be observed in figure 4.11. As warming causes the melt-out of debris in an area that newly finds itself below the ELA, this anomaly of surfaced debris is transported with surface ice velocity,

until it reaches the terminus right as it retreats, therefore constituting somewhat of a proxy for the effect of warming travelling downstream.

As this anomaly travels downstream, it brings along lower driving stress – and therefore ice velocities too – as a direct consequence of the decreasing ice thickness. Near the terminus melt is also somewhat increased from the start of the warming, thinning out the tongue and lowering the ice thickness. When these two processes meet at the terminus, ice velocity drops close to zero, forming dead ice. After this point, ice can only melt away, leading to the initiation of actual retreat within a few decades. The climate might already be cooling again, but it is too late to prevent retreat entirely. As explained earlier, advance takes longer than retreat which is well visible in the triangular shape of dead ice features highlighted in figure 5.2. The vertical gradients in shown the figure after warming indicate that the dynamic effect of thinning in the accumulation area does have an instant impact on downstream dynamics that grows stronger the further down the thinning anomaly travels.

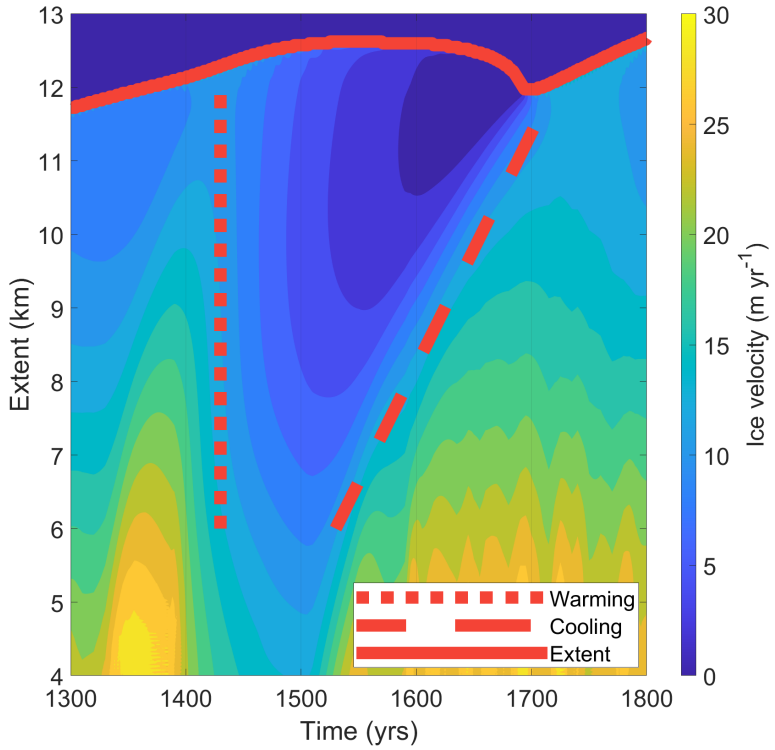


**Figure 5.2:** *Close-up excerpt from figure 4.12, showing the propagation of ice velocity decrease (warming) and increase (cooling) along the glacier, using the example of the 1400-1500 warm period and subsequent cooling.*

It was also shown that random climatic changes in the very short-term (10 years) virtually do not have any influence on both length and volume on debris-covered and even debris-free glaciers. This is however only tested for truly random variability and does not necessarily justify the conclusion that variability should not be considered at all. But a more detailed analysis of variability would go beyond the scope of this thesis.

### 5.2.2 Correlations of ELA, volume and length

The sinus wave experiment introduced two new properties of the forcing: a climate that is always changing but also repetitive. The ever-changing nature is a key step into the direction of real climate, moving along from the unrealistic concept of constant climate over hundreds of years. The cyclic nature of the experiment allows us to still estimate correlations and relationships between parameters and responses, providing meaningful information about the processes involved in glacier response to climate.

Generally, volume change over the whole glacier is essentially influenced by two factors: length change and mass balance. If we just neglect length change in a thought experiment, volume change only depends on mass balance. This means that when mass balance is at its most positive, volume increases the fastest, and vice versa. This leads to the conclusion that – if length change is neglectable – volume must be the first derivative of mass balance, adjusted by some factor and initial volume.

In the sinus wave experiments, this is exactly what is observed for short-wavelength (100 years) ELA changes. Length is too slow to react to the changes, therefore constituting a minimal influence on volume change. As shown in figure 4.6 and table 4.3, the theoretical relationship that was just established holds true – and is also surprisingly accurate for the long-wavelength (500 years) ELA. This might relate to the fact that the debris-covered glacier only loses about 10% of its length in this experiment. Increased amplitude would lead to a stronger influence of length change. This influence of length change can also nicely be seen in the debris-free case (figure 4.5), where short-wavelength responses obey the relationship, but the long-wavelength volume responds faster to the changes, as length retreats by over 20%.

These observations can be summarized in a general equation, predicting volume change – or at least the shape of the volume response curve:

$$\text{For } ELA = ELA_0 + A \sin\left(\frac{t}{\lambda}\right) \; : \; V \approx V_0 + c_a \cos\left(\frac{t}{\lambda}\right), \tag{5.1}$$

or more generally:

$$\text{For } ELA = f(t) \; : \; V \approx V_0 + c_a f'(t), \tag{5.2}$$

with $ELA_0$ being the initial and average ELA, $A$ the ELA amplitude, $\lambda$ the ELA wavelength, $V_0$ the initial and average volume, and $c_a$ an unknown constant given by mass balance. The equation holds true only if length change can be neglected for the effect on volume change. Where the threshold of length change starting to significantly influence volume change lies would be a subject for an additional analysis – but from the experiments we know it should lie somewhere between 10% and 20% of length lost. As a small side note, it can be observed that the initial volume and the average volume during the sinus wave experiment are not equal. This difference is an effect of the initial conditions described in section 4.2.2. Initial volume here means it is adjusted for this effect, making it equal to average volume.

Another interesting observation is the distorted waveform of the length response to a long-wavelength ELA change. As described in section 4.2.2, it constitutes a mix between the asymmetric response observed in the step-change experiments and the sinusoidal response observed in the debris-free sinus wave experiment. We see again that the time frame of ELA changes is the critical factor for retreat, indicated by the 100 year plateau visible in figure 4.6(c), as well as the non-reactive lengths in the short-wavelength experiments. Most of the retreat occurs as volume is already increasing again, and minimum length is reached when volume is increasing the fastest. Therefore, it conversely forms a distorted sinus, meaning maximum length is reached at the highest temperatures and minimum length at the lowest temperatures.

Of course the lag leading to this is highly dependent on debris cover thickness and how its effect on mass balance is defined. For a debris-free glacier, length shows almost no lag to volume, which in turn decreases the lag of volume to the ELA. In general, it is important to state that all of these observations have been made with a very specific set of parameters, and only a small subset of parameters being tested for their influence on the experiments. Especially the observations on length response are mostly a product of individual parameter values. This will be further elaborated in section 5.5.

### 5.2.3 Implications of the real climate experiments

The first attempt at actually approximating real climate was made in the linear increase experiment. In this experiment we got a first idea of the timing, shape, and magnitude of retreat caused by anthropogenic climate change. Results suggest that the timing – meaning the initiation – of retreat is mainly dictated by debris cover, with only small differences between step-change and linear increase experiments when using the same debris concentration. The following retreat phase is less dramatic in the linear increase experiment, with a fast initial retreat leading to about 50% of total length loss, and the second half lost in a slower fashion. This of course also dependent on the projection, with the SSP5 projection leading to a much faster retreat than the SSP1 projection.

The results shown for the real climate history and projections provide valuable information about the reaction of debris-covered glaciers to climate change. Meanwhile the three projections maintain some ambiguity for the future, showing how debris-covered glaciers react differently to a range of climate scenarios. In a first step however we take a look at the responses to climate history with a focus on the LIA. The ELA from climate reconstruction using glacial extents by Lüthi (2014) shows a warm period between 1400 and 1500 (e.g. figure 4.9(a)) and the subsequent initiation of the LIA cold phase lasting until about 1850. The volume and length responses to these changes described above indicate that volume response is quite similar between debris-free and debris-covered glaciers, whereas debris-covered glacier length response lags behind much more and is generally more resistant to climate changes. And as mentioned earlier, an increase in debris cover thickness after the retreat following the pre-LIA warm phase might help the glacier quickly recover in length during the LIA.

The tendency of debris-covered glaciers towards tongue thinning (Gardelle et al., 2013; Pellicciotti et al., 2015; Brun et al., 2018; Anderson et al., 2021b) rather than retreat observed in literature is supported by the results from both abstract and real climate experiments, where glacier thinning occurs during warm periods, with terminus retreat lagging behind. Looking back at the results in figure 4.9, we can observe that in the current glacier state in the year 2022, both debris-free and debris-covered glaciers have already lost substantial mass, whereas retreat has been relatively limited until now. Regardless of projection, a steep fall in volume between now and 2200 is computed, showing that length measurements of debris-covered glaciers might be deceptive about the real state of the glacier. In the unlikely case that a cool period should suddenly reverse climate change before ~2050, re-advance and regaining the former volume might be very much facilitated compared to a re-advance after the dramatic retreat, corresponding to the generally stagnating or advancing behaviour observed by Ferguson and Vieli (2021) and in the results about real climate history until now.

The basic proportions of the debris-covered glacier – using default parameters – being about twice as long and twice as voluminous as the debris-free glacier are more or less preserved from before until after retreat, of course with some lag. Hence debris-covered glaciers are equally impacted by high-magnitude, long-term climate change as it is projected by the IPCC (Masson-Delmotte et al., 2021). In the case of relatively low-magnitude, short-term changes like the 1400 to 1500 warm period, debris-covered glaciers react more slowly to the warming and re-advance more easily than debris-free glaciers.

Results regarding glacier dynamics over climate history and projections suggest that because debris cover causes climatic changes to have a heterogeneous impact across the glacier, and areas of lower ice thickness from the accumulation area first needing to flow down the glacier to have a strong impact on the terminus position. Simultaneously, the tongue is thinning, but at a lower rate than the accumulation area.

In terms of implications on the current and future state of debris-covered glaciers, the experiments show that debris cover can delay glacial retreat for a certain duration, which is dependent on local conditions and model parameters and should be investigated more thoroughly. However, glacier volume is much more relevant for the role of debris-covered glaciers as a water resource. Volume response does not show the same delay, with measurements already now showing substantial mass loss (Bolch et al., 2012; Gardelle et al., 2013; Pellicciotti et al., 2015; Brun et al., 2016). The experiments showed that regardless of projection, 21st century climate change will lead to the increased formation and collapse of stagnant tongues, causing immense loss of volume and eventually also debris cover and length.

## 5.3 Evaluation of the cryokarst implementations

Looking at figure 5.3, we can see that – with the default cryokarst version – features of increased ablation due to cryokarst only start to form around the year 2100 as a precursor to fast retreat. However, on real glaciers cryokarst features are already present now and contribute to thinning of debris-covered tongues (Brun et al., 2016; Kneib et al., 2021). This once again supports the need for a different cryokarst implementation. For this purpose, the melt version of the cryokarst module was introduced, which will be reviewed and compared against the default implementation in this section.

Figure 4.16 nicely summarizes the differences between the cryokarst versions. The default version only activates 200 years after warming, shortly before retreat. The melt version is always active, reversing the reversal of the mass balance gradient in the lower tongue, and is intensified during retreat, as runoff is increased. As a consequence of warming, the melt version leads to a faster and less steep

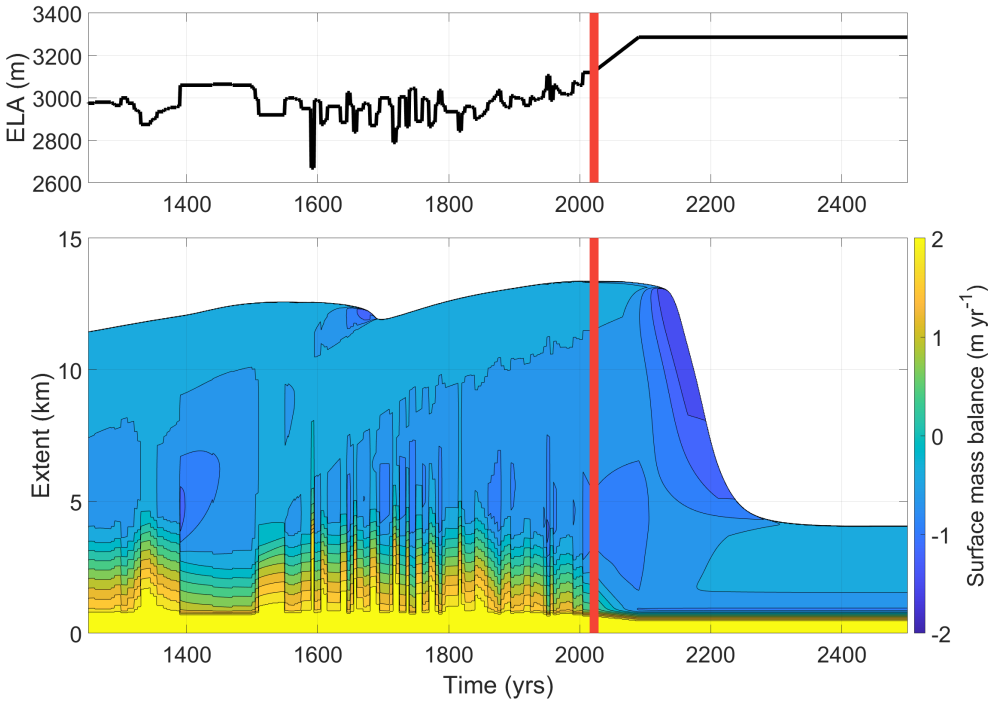


**Figure 5.3:** *Surface mass balance over time and space between years 1250 and 2500 of the real climate history and projections experiment (B5) using the SSP2 projection. The plots show ELA and a contour representation of surface mass balance. The red line indicates the year 2022.*

retreat, starting just 50 years after warming. Because the glacier is much smaller and less debris-covered already before warming and retreat is slower, less length and debris cover is lost in retreat, leading to a faster second advance phase after cooling.

In figure 4.13 we can see that for an additive default-melt version, the melt version dominates, as it produces a smaller stagnant lower tongue, which is the main working area for the default version based on driving stress. It also shows increased maximum runoff values early after warming, which are found in that same area, arriving earlier to the scene than the default version and melting away the ice in the lower tongue before it is completely stagnant. This would demand some re-balancing to ensure both versions have a significant effect on retreat behavior.

The conversion from accumulated runoff into cryokarst area fraction $\lambda$ is heavily dependent on the melt parameter $\mu$, which defines how much runoff has to accumulate to reach the maximum cryokarst area fraction $\lambda_m$. The sensitivity analysis for $\mu$ showed that there is some influence on glacier dimensions, but

retreat and advance behavior remains the same. One possible addition could have been considering a variation where small amounts of runoff do not cause any cryokarst formation, and whether that would have a strong effect on the upper ablation area. This was purposely avoided, as field observations (section 3.1.2) showed that even small amounts of runoff can lead to the formation of ice cliffs.

Literature also suggests that supraglacial streams are actually larger in areas of thin debris-cover – which is the case in the upper ablation area – as melt rates are high there (Fyffe et al., 2019; Anderson et al., 2021b). This would support the inclusion of other parameters that show correlation with ice cliff formation (e.g. Anderson et al., 2021b), with their degree of correlation factored in. That way an entire cryokarst routine based on physical processes and measurements could be built, which considers more factors than the selective two implementations presented in this thesis.

## 5.4 Application of the model on a complex topography

In the final few experiments the model was applied to the Zmuttgletscher bed geometry, providing a more complex topography with varying slope angles. On the macroscopic scale, the accumulation area is steeper and the ablation area flatter than in the abstract geometry used before.

The sinus experiment (figure 4.18) nicely showed how the bed slope affects ice thickness and how the effects of climate changes have to be transported downstream for the debris-covered glacier. It also showed the very different dimensions of the glacier compared to the abstract geometry. The thickest parts of the glacier are found in the flat lower ablation area. The importance of this geometric difference also became apparent in the real climate history and projections experiment. Between 1250 and 2000, the debris-covered glacier showed much less of a reaction in volume and barely any in length, just showing a slow but steady advance during the entire period. This emphasizes the relevance of local conditions like bed topography on the reaction of debris-covered glaciers, in this case making it more robust to changes.

Another interesting incident was the cut-off event leading to model failure during the SSP5 run of the experiment (figure 4.20). It highlighted the potential role of fast warming combined with high-slope steps – and other areas where ice thickness is already thin per se – in the formation of cut-offs, leading to the existence of a disconnected mass of dead ice that cannot replenish the ice it is losing during a warming event. The real Zmuttgletscher also features some icefalls and already disconnected areas in the upper ablation and accumulation area, shown in figure 5.4. Hence it is thinkable that new cut-offs can form on Zmuttgletscher and other debris-covered glaciers.

**Figure 5.4:** *Southern part of the upper ablation area and accumulation area of Zmuttgletscher in July 2021, featuring multiple icefalls at high elevations and a steep step with thin ice, which is the one causing the cut-off event in the model. Photo taken by Andreas Vieli.*

The attempt at replicating the length changes of Zmuttgletscher from 1880 to 2021 (GLAMOS 1880-2021) might have been unsuccessful, but important implications can be extracted from the analysis. The experiment mainly showed that the default implementation is – at least for the example of Zmuttgletscher – highly unrealistic in terms of timing of retreat. The lag of retreat is simply too long, with adaptation to LIA cooling just levelling off in 1950 – 100 years after the end of the LIA – and no sign of retreat within the 21st century.

A combination of both major newly introduced model components, the new Østrem curve and the default-melt cryokarst version, was somewhat more successful, at the very least showing some retreat over the 20th century. However, this needs to be put into perspective, as a larger glacier with the same parameters reacted slower, only starting to retreat around 1980. A debris-free glacier being the best at explaining the retreat of Zmuttgletscher might give us an indication of one of the underlying reasons. As explained in section 2.5, Zmuttgletscher has massively increased its debris cover since the LIA, more than doubling the fraction of surface covered by debris (Mölg et al., 2019). With Zmuttgletscher only being sparsely covered with debris in the LIA, its behavior might have been more similar to a debris-free glacier. Debris cover thickness is also rather thin on Zmuttgletscher currently, with values ranging from 0 to about 70 centimeters, and the highest values found on elongated ridges, and an average thickness of ~16 centimeters (Mölg et al., 2019). Debris cover thicknesses in the model are much

higher, often reaching over one meter. An additional uncertainty comes from other local factors not considered by the model, such as geology, local climate, and variable debris input.

## 5.5 Limitations

This section summarizes some of the limitations of the model itself, of the newly added components and of the experimental approach, as well as making some suggestions for improvement and remaining research gaps.

### 5.5.1 DEBISO model

First of all, it needs to be emphasized that the DEBISO model is designed to be a simplified, efficient two-dimensional representation of debris-covered glaciers. This in itself bears some limitations, as the complexity of a glacier is reduced for simplicity. This is however an issue for all models of this type and will therefore not be discussed further.

The second issue lies within the way the models adds debris to the system and transports it downstream. Debris concentration is constant across the ice, and correspondingly debris starts melting out right below the ELA. This might not be accurate for many glaciers where the majority of debris is deposited on the upper accumulation area (Ferguson and Vieli, 2021), such as Zmuttgletscher.

Another consequence of using a debris concentration is that the total amount of debris is scaled with the size of the glacier (Ferguson and Vieli, 2021), which means that during cool periods, the amount of debris in the glacier is overestimated, constituting a positive feedback, as it leads to an overestimated debris cover further decreasing surface ablation. As a consequence, inaccuracies occur whenever glaciers of different sizes are compared, and the often observed stronger effect of advance might partly be caused by this modelling artifact.

The concept of a temporally and spatially uniform debris concentration also leads to a neglect of potential surface topography heterogeneity and the influence of debris on the shape of a glacier, for example by horizontal differences in debris cover like a higher concentration of debris towards the margins. The 2D modelling approach also neglects across-glacier surface velocity patterns redistributing debris laterally and longitudinally (Nicholson et al., 2021). Longitudinal debris structures like medial moraines can also affect the formation of supraglacial stream catchments and valleys (Mölg et al., 2020), influencing cryokarst formation. And because debris concentration is not exactly a property we can measure directly, comparing it to real glaciers can only be done indirectly through the resulting debris cover.

Many of these issues would be at least partially solved by using an actual debris input and tracking the movement through the glacier, which was done in previous studies (e.g. Rowan et al., 2015), but it would be much more computationally expensive (Ferguson and Vieli, 2021). One potential solution, adding complexity while still remaining efficient by avoiding debris transport, would be to include a factor or a curve each for across- and along-glacier debris variability, adding some – predefined or random – variability to the debris cover. This could then be modified for individual glaciers or categories of glaciers. A solution addressing the scaling issue would be a simple correction factor that lowers debris concentration by a certain amount for a given volume. Both of these approaches would however come with their own problems and limitations, and add more parameters to the model.

Ferguson and Vieli (2021) also mention limitations of the boundary condition at the terminus. Large terminal ice cliffs are observed to be rather unusual, especially for retreating glaciers. Zmuttgletscher for example does have terminal ice cliffs due to ice erosion and debris evacuation by the stream (Mölg et al., 2020), but not across the whole terminus. They also assess that because of the boundary condition grid size affects glacier extent substantially, with the default grid sized used in this thesis showing an error of about 5%, which adds another imprecision in steady state extent. As all experiments use the same grid size and extent is mostly used to show relative differences – not absolute extents – this should not affect the validity of the results in a meaningful way. The boundary condition still represents a good compromise, solving debris offloading at the terminus in a simple way, while conserving realistic terminus dynamics.

### 5.5.2 New model components

The two main additions made to the model also have their own limitations. The new Østrem curve that was fit to literature data certainly is an improvement on the default curve. However, it is still a variably good representation of individual glaciers and is based on only six studies. Data density could be better, especially for rather thick debris cover. A comprehensive review of all available measurements of debris thickness and ablation including an analysis of correlations with other properties such as region, elevation, lithology, grain size, and albedo would be a next step towards a better understanding of the debris-ablation relationship. Not only would that improve the use of a single general Østrem curve as done in this thesis, but it could then also be altered according to local conditions.

The new runoff-based melt implementation brings along a few issues as well. First of all, local yearly melt is derived from the mass balance with a simple factor. This underestimates melt in the upper ablation area, as melt at the ELA must be zero according to this method. This could be avoided by integrating a degree-day model that calculates melt over the whole glacier. This would

however add to complexity, while the existing implementation works with values given by the base model. The implementation also probably overestimates the amount of supraglacial runoff that stays on the glacier, which is highest near the terminus. Observations on Zmuttgletscher show that supraglacial streams rather occur in the upper ablation area and do not form a coherent cumulative network on the glacier surface (Anderson et al., 2021b) but rather in englacial channel networks (Fyffe et al., 2019). The distribution of cryokarst features obtained through this method is still in agreement with observations on Zmuttgletscher, as the lower ablation area features more ice cliffs from englacial channel collapse and other processes. Overall, an approach based on data correlation as proposed in section 5.3 would be advisable for future implementations, but would demand large amounts of data that are currently not available. Consequently, quantifying the role of cryokarst features in debris-covered glacier surface ablation requires new, detailed field studies (Anderson et al., 2021b).

### 5.5.3 Experimental approach

In terms of the execution of experiments, it once again has to be emphasized that all experiments were run with a specific set of mostly constant parameters to avoid an exorbitant amount of experiments. For the sake of simplicity, comparability and reproducibility most experiments were run with the same set of parameters except for the one or two variables investigated. For example, most experiments use the default Østrem curve and cryokarst version to enable comparing results with the previous work by Ferguson and Vieli (2021). Of course, the potential for a variety of further interesting combinations would have been there, such as looking at the new Østrem curve with real climate forcing or comparing debris thicknesses on the Zmuttgletscher bed geometry. Many experiments using such combinations were also conducted but not deemed significant enough to showcase in the already full results.

In the individual experiments, parameters such as the wavelength in the sinus wave experiment are often arbitrary, and were mostly selected because of the results they showcased, causing somewhat of a bias. The step-change and sinus wave experiments were however always meant to test the sensibility of the model in an abstract setting rather than a realistic one.

In the case of the real climate history and projections, results are very much dependent on the assumptions made for the projections and the quality of the underlying data from Lüthi (2014). The projections are just scenarios bound to predictions about developments in the future. Possible medium-scale changes (50-100 years) – natural or anthropogenic – are not considered. The stabilization of temperatures after 2090 is also a bold assumption, which was made to be able to analyze a finite retreat and use fixed temperature increase values given by the IPCC (Masson-Delmotte et al., 2021). Climate reconstruction from alpine glacier

extents (Lüthi, 2014) makes it on the one hand suitable for use on glaciers, but also unreliable in representing historic variability, as it gets progressively more uncertain the further back in time we go. Especially warm periods – which play a key role observed with the example between the years 1400 and 1500 – are uncertain because they originate from gaps in the data.

And as already mentioned earlier, the use of the Zmuttgletscher geometry constitutes an enormous oversimplification of the real Zmuttgletscher, and is accordingly only suitable to represent a general complex topography rather than being an accurate representation of the actual glacier.

Chapter 6

# Conclusion

This thesis has worked with the newly developed DEBISO model from Ferguson and Vieli (2021) to test and expand it, and answer three specific research questions in the process.

**How well do field measurements agree with literature and the Østrem curve used in the model?**

Data from field measurements on Zmuttgletscher on the relationship of debris cover and ablation were well in the range of literature values. The new Østrem curve that was fit to all available data showed that previous estimates might have overestimated the insulating effect of debris cover, with the default Østrem curve used in the model indicating a three times faster insulation effect compared to the data-based curve. Implementing the new curve produces significantly smaller glaciers, essentially halving the insulating effect. The geometry of a modeled debris-covered glacier is therefore very much dependent on the choice in Østrem curve.

**How do debris-covered glaciers react to real climate history and scenarios?**

In step-change, sinus wave, and real climate approximation experiments the climate sensitivity and the mechanisms of advance and retreat were analyzed. The first two of these served as abstract inputs to test out the general behavior of the model. Previous findings about debris concentration and the asymmetric response in advance and retreat are supported by the results. In the analysis of the sinus wave experiment, general relationships between ELA, volume and length were established, as it was shown that debris cover often leads to configurations where length change can be neglected. This means volume response can be approximated as the first derivative of the ELA.

Over all the experiments, the effect leading to significant lag in retreat was often observed, showing how thinning and associated processes have to be transported down the glacier, making the lag of retreat dependent on glacier size and ice velocities. The lag in retreat and the process of debris cover offloading caused by the collapse of the tongue following strong and persistent warming events lead

to a dichotomy of responses depending on the duration of the warm period. While short warm periods can be compensated very well in re-advance, debris-covered glaciers take significantly longer to re-advance after long-lasting warm periods.

Use of the IPCC's SSP1 to SSP5 projections caused varying amounts of detriment to debris-covered glaciers, with all scenarios leading to significant volume, length and debris cover losses, making potential re-advance more difficult. Analysis of glacier dynamics during advance and retreat nicely showed the formation of stagnant ice in the lower tongue as a precursor to retreat. Applying the real climate history and projections forcing to a complex bed geometry revealed that bed topography has a significant impact on the response of a glacier to changes in climate, with the Zmuttgletscher geometry used proving more robust to warming than the abstract geometry from previous experiments. The potential for the formation of cut-off features during fast retreat at steep slopes is also connected to the differential reaction between accumulation and ablation zone during warming, bearing the possibility of faster retreat than predicted by the model.

**What are the main factors in cryokarst formation? How can these be integrated into a model?**

Literature laid out a multitude of processes connected to the formation of cryokarst, including supraglacial streams and ponds, collapsing englacial channels, slope oversteepening from heterogeneous debris cover and crevasse opening. The DEBISO model includes a cryokarst routine using low driving stress as a driver of cryokarst formation. This only accounts for cryokarst features near the terminus. Observations on Zmuttgletscher showed the frequent appearance of supraglacial streams and associated ice cliffs in the upper ablation area. The implementation in this thesis thus focused on supraglacial streams, using runoff as a condition for cryokarst formation in a semi-physically based runoff accumulation routine. Results show that using this routine in combination with the default version strongly counteracts the insulation effect of debris, leading to smaller glaciers that show less lag in retreat. In a test to predict real length measurements of Zmuttgletscher, the new implementation performed well but not exceptional.

# Bibliography


Anderson, L. S. and Anderson, R. S. 2016. "Modeling debris-covered glaciers: Response to steady debris deposition." *Cryosphere* 10.3: 1105–1124. doi:10.5194/TC-10-1105-2016.

Anderson, L. S. and Anderson, R. S. 2018. "Debris thickness patterns on debris-covered glaciers." *Geomorphology* 311: 1–12. doi:10.1016/J.GEOMORPH.2018.03.014.

Anderson, L. S., Armstrong, W. H., Anderson, R. S., and Buri, P. 2021a. "Debris cover and the thinning of Kennicott Glacier, Alaska: In situ measurements, automated ice cliff delineation and distributed melt estimates." *Cryosphere* 15.1: 265–282. doi:10.5194/TC-15-265-2021.

Anderson, L. S., Armstrong, W. H., Anderson, R. S., Scherler, D., and Petersen, E. 2021b. "The Causes of Debris-Covered Glacier Thinning: Evidence for the Importance of Ice Dynamics From Kennicott Glacier, Alaska." *Frontiers in Earth Science* 9.680995. doi:10.3389/FEART.2021.680995.

Bahr, D. B., Pfeffer, W. T., Sassolas, C., and Meier, M. F. 1998. "Response time of glaciers as a function of size and mass balance: 1. Theory." *Journal of Geophysical Research: Solid Earth* 103.B5: 9777–9782. doi:10.1029/98JB00507.

Benn, D. I., Bolch, T., Hands, K., Gulley, J., Luckman, A., Nicholson, L. I., Quincey, D., Thompson, S., Toumi, R., and Wiseman, S. 2012. "Response of debris-covered glaciers in the Mount Everest region to recent warming, and implications for outburst flood hazards." *Earth-Science Reviews* 114.1-2: 156–174. doi:10.1016/J.EARSCIREV.2012.03.008.

Benn, D., Thompson, S., Gulley, J., Mertes, J., Luckman, A., and Nicholson, L. 2017. "Structure and evolution of the drainage system of a Himalayan debris-covered glacier, and its relationship with patterns of mass loss." *Cryosphere* 11.5: 2247–2264. doi:10.5194/TC-11-2247-2017.

Bolch, T., Kulkarni, A., Kääb, A., Huggel, C., Paul, F., Cogley, J. G., Frey, H., Kargel, J. S., Fujita, K., Scheel, M., Bajracharya, S., and Stoffel, M. 2012. "The state and fate of himalayan glaciers." *Science* 336.6079: 310–314. doi:10.1126/SCIENCE.1215828.

Brook, M. S., Hagg, W., and Winkler, S. 2013. "Debris cover and surface melt at a temperate maritime alpine glacier: Franz Josef Glacier, New

Zealand." *New Zealand Journal of Geology and Geophysics* 56.1: 27–38. doi:10.1080/00288306.2012.736391.

Brun, F., Buri, P., Miles, E. S., Wagnon, P., Steiner, J., Berthier, E., Ragettli, S., Kraaijenbrink, P., Immerzeel, W. W., and Pellicciotti, F. 2016. "Quantifying volume loss from ice cliffs on debris-covered glaciers using high-resolution terrestrial and aerial photogrammetry." *Journal of Glaciology* 62.234: 684–695. doi:10.1017/JOG.2016.54.

Brun, F., Wagnon, P., Berthier, E., Shea, J. M., Immerzeel, W. W., Kraaijenbrink, P. D., Vincent, C., Reverchon, C., Shrestha, D., and Arnaud, Y. 2018. "Ice cliff contribution to the tongue-wide ablation of Changri Nup Glacier, Nepal, central Himalaya." *Cryosphere* 12.11: 3439–3457. doi:10.5194/TC-12-3439-2018.

Buri, P., Miles, E. S., Steiner, J. F., Ragettli, S., and Pellicciotti, F. 2021. "Supraglacial Ice Cliffs Can Substantially Increase the Mass Loss of Debris-Covered Glaciers." *Geophysical Research Letters* 48.6: e2020GL092150. doi:10.1029/2020GL092150.

Buri, P., Pellicciotti, F., Steiner, J. F., Miles, E. S., and Immerzeel, W. W. 2016. "A grid-based model of backwasting of supraglacial ice cliffs on debris-covered glaciers." *Annals of Glaciology* 57.71: 199–211. doi:10.3189/2016AOG71A059.

Dobhal, D. P., Mehta, M., and Srivastava, D. 2013. "Influence of debris cover on terminus retreat and mass changes of Chorabari Glacier, Garhwal region, central Himalaya, India." *Journal of Glaciology* 59.217: 961–971. doi:10.3189/2013JoG12J180.

Ferguson, J. C. and Vieli, A. 2021. "Modelling steady states and the transient response of debris-covered glaciers." *Cryosphere* 15.7: 3377–3399. doi:10.5194/TC-15-3377-2021.

Fountain, A. G. and Walder, J. S. 1998. "Water flow through temperate glaciers." *Reviews of Geophysics* 36.3: 299–328. doi:10.1029/97RG03579.

Fyffe, C. L., Brock, B. W., Kirkbride, M. P., Mair, D. W., Arnold, N. S., Smiraglia, C., Diolaiuti, G., and Diotri, F. 2019. "Do debris-covered glaciers demonstrate distinctive hydrological behaviour compared to clean glaciers?" *Journal of Hydrology* 570: 584–597. doi:10.1016/J.JHYDROL.2018.12.069.

Gardelle, J., Berthier, E., Arnaud, Y., and Kääb, A. 2013. "Region-wide glacier mass balances over the Pamir-Karakoram-Himalaya during 1999-2011." *The Cryosphere* 7: 1263–1286. doi:10.5194/tc-7-1263-2013.

Gardner, A. S., Moholdt, G., Cogley, J. G., Wouters, B., Arendt, A. A., Wahr, J., Berthier, E., Hock, R., Pfeffer, W. T., Kaser, G., Ligtenberg, S. R., Bolch,

T., Sharp, M. J., Hagen, J. O., Van Den Broeke, M. R., and Paul, F. 2013. "A reconciled estimate of glacier contributions to sea level rise: 2003 to 2009." *Science* 340.6134: 852–857. doi:10.1126/SCIENCE.1234532.

GLAMOS 1880-2021. "The Swiss Glaciers 1880-2018/19, Glaciological Reports No 1-140, Yearbooks of the Cryospheric Commission of the Swiss Academy of Sciences (SCNAT), published since 1964 by VAW / ETH Zurich." 2021.

Grab, M., Mattea, E., Bauder, A., Huss, M., Rabenstein, L., Hodel, E., Linsbauer, A., Langhammer, L., Schmid, L., Church, G., Hellmann, S., Deleze, K., Schaer, P., Lathion, P., Farinotti, D., and Maurer, H. 2021. "Ice thickness distribution of all Swiss glaciers based on extended ground-penetrating radar data and glaciological modeling." *Journal of Glaciology* 67.266: 1074–1092. doi:10.1017/JOG.2021.55.

Groos, A. R., Mayer, C., Smiraglia, C., Diolaiuti, G., and Lambrecht, A. 2017. "A First Attempt to Model Region-Wide Glacier Surface Mass Balances in the Karakoram: Findings and Future Challenges." *Geogr. Fis. e Dinam. Quat.* 40: 137–159. doi:10.4461/GFDQ.2017.40.10.

Hagg, W., Mayer, C., Lambrecht, A., and Helm, A. 2008. "Sub-debris melt rates on southern inylchek glacier, central tian shan." *Geografiska Annaler: Series A, Physical Geography* 90 A.1: 55–63. doi:10.1111/J.1468-0459.2008.00333.X.

Hartmeyer, I., Delleske, R., Keuschnig, M., Krautblatter, M., Lang, A., Christoph Otto, J., and Schrott, L. 2020. "Current glacier recession causes significant rockfall increase: The immediate paraglacial response of deglaciating cirque walls." *Earth Surface Dynamics* 8.3: 729–751. doi:10.5194/ESURF-8-729-2020.

Heimsath, A. M. and McGlynn, R. 2008. "Quantifying periglacial erosion in the Nepal high Himalaya." *Geomorphology* 97.1-2: 5–23. doi:10.1016/J.GEOMORPH.2007.02.046.

Jarosch, A. H. and Gudmundsson, M. T. 2012. "A numerical model for meltwater channel evolution in glaciers." *Cryosphere* 6.2: 493–503. doi:10.5194/TC-6-493-2012.

King, O., Turner, A. G., Quincey, D. J., and Carrivick, J. L. 2020. "Morphometric evolution of Everest region debris-covered glaciers." *Geomorphology* 371: 107422. doi:10.1016/J.GEOMORPH.2020.107422.

Kirkbride, M. P. and Deline, P. 2013. "The formation of supraglacial debris covers by primary dispersal from transverse englacial debris bands." *Earth Surface Processes and Landforms* 38.15: 1779–1792. doi:10.1002/ESP.3416.

Kneib, M., Miles, E. S., Buri, P., Molnar, P., McCarthy, M., Fugger, S., and Pellicciotti, F. 2021. "Interannual Dynamics of Ice Cliff Populations on Debris-Covered Glaciers From Remote Sensing Observations and Stochastic Modeling." *Journal of Geophysical Research: Earth Surface* 126.10. doi:10.1029/2021JF006179.

Konrad, S. and Humphrey, N. 2000. "Steady-state flow model of debris-covered glaciers (rock glaciers)." *Debris-Covered Glaciers (Proceedings of a workshop held at Seattle, Washington, USA, September 2000)*. vol. 264. Seattle, WA, USA, 2000, 255–263.

Lüthi, M. P. 2014. "Little Ice Age climate reconstruction from ensemble reanalysis of Alpine glacier fluctuations." *The Cryosphere* 8: 639–650. doi:10.5194/tc-8-639-2014.

Masson-Delmotte, V., Zhai, P., Chen, Y., Goldfarb, L., Gomis, M. I., Matthews, J. B. R., Berger, S., Huang, M., Yelekçi, O., Yu, R., Zhou, B., Lonnoy, E., Maycock, T. K., Waterfield, T., Leitzell, K., and Caud, N. 2021. "IPCC, 2021: Summary for Policymakers." *Climate Change 2021: The Physical Science Basis. Contribution of Working Group I to the Sixth Assessment Report of the Intergovernmental Panel on Climate Change* .

Mattson, L. E., Gardner, J. S., and Young, G. J. 1993. "Ablation on Debris Covered Glaciers: an Example from the Rakhiot Glacier, Punjab, Himalaya." *Snow and Glacier Hydrology (Proceedings of the Kathmandu Symposium, November 1992)* 218: 289–296.

Mihalcea, C., Mayer, C., Diolaiuti, G., Lambrecht, A., Smiraglia, C., and Tartari, G. 2006. "Ice ablation and meteorological conditions on the debris-covered area of Baltoro glacier, Karakoram, Pakistan." *Annals of Glaciology* 43: 292–300. doi:10.3189/172756406781812104.

Miles, E. S., Pellicciotti, F., Willis, I. C., Steiner, J. F., Buri, P., and Arnold, N. S. 2016. "Refined energy-balance modelling of a supraglacial pond, Langtang Khola, Nepal." *Annals of Glaciology* 57.71: 29–40. doi:10.3189/2016AOG71A421.

Mölg, N., Bolch, T., Walter, A., and Vieli, A. 2019. "Unravelling the evolution of Zmuttgletscher and its debris cover since the end of the Little Ice Age." *Cryosphere* 13.7: 1889–1909. doi:10.5194/tc-13-1889-2019.

Mölg, N., Ferguson, J., Bolch, T., and Vieli, A. 2020. "On the influence of debris cover on glacier morphology: How high-relief structures evolve from smooth surfaces." *Geomorphology* 357: 107092. doi:10.1016/j.geomorph.2020.107092.

Moore, P. L. 2018. "Stability of supraglacial debris." *Earth Surface Processes and Landforms* 43.1: 285–297. doi:10.1002/ESP.4244.

Nicholson, L. and Benn, D. I. 2006. "Calculating ice melt beneath a debris layer using meteorological data." *Journal of Glaciology* 52.178: 463–470. doi:10.3189/172756506781828584.

Nicholson, L., Wirbel, A., Mayer, C., and Lambrecht, A. 2021. "The Challenge of Non-Stationary Feedbacks in Modeling the Response of Debris-Covered Glaciers to Climate Forcing." *Frontiers in Earth Science* 9: 1126. doi:10.3389/FEART.2021.662695.

Nicholson, L. I., McCarthy, M., Pritchard, H. D., and Willis, I. 2018. "Supraglacial debris thickness variability: Impact on ablation and relation to terrain properties." *Cryosphere* 12.12: 3719–3734. doi:10.5194/TC-12-3719-2018.

Nuimura, T., Fujita, K., Yamaguchi, S., and Sharma, R. R. 2012. "Elevation changes of glaciers revealed by multitemporal digital elevation models calibrated by GPS survey in the Khumbu region, Nepal Himalaya, 1992-2008." *Journal of Glaciology* 58.210: 648–656. doi:10.3189/2012JOG11J061.

Østrem, G. 1959. "Ice Melting under a Thin Layer of Moraine, and the Existence of Ice Cores in Moraine Ridges." *Geografiska Annaler* 41.4: 228–230. doi:10.1080/20014422.1959.11907953.

Pellicciotti, F., Stephan, C., Miles, E., Herreid, S., Immerzeel, W. W., and Bolch, T. 2015. "Mass-balance changes of the debris-covered glaciers in the Langtang Himal, Nepal, from 1974 to 1999." *Journal of Glaciology* 61.226: 373–386. doi:10.3189/2015JOG13J237.

Reid, T. D. and Brock, B. W. 2014. "Assessing ice-cliff backwasting and its contribution to total ablation of debris-covered Miage glacier, Mont Blanc massif, Italy." *Journal of Glaciology* 60.219: 3–13. doi:10.3189/2014JOG13J045.

Reid, T. D. and Brock, B. W. 2010. "An energy-balance model for debris-covered glaciers including heat conduction through the debris layer." *Journal of Glaciology* 56.199: 903–916. doi:10.3189/002214310794457218.

Reznichenko, N. V., Davies, T. R., and Alexander, D. J. 2011. "Effects of rock avalanches on glacier behaviour and moraine formation." *Geomorphology* 132.3-4: 327–338. doi:10.1016/J.GEOMORPH.2011.05.019.

Richardson, J. M. and Brook, M. S. 2010. "Ablation of debris-covered ice: Some effects of the 25 September 2007 Mt Ruapehu eruption." *Journal of the Royal Society of New Zealand* 40.2: 45–55. doi:10.1080/03036758.2010.494714.

Rounce, D. R., Hock, R., McNabb, R. W., Millan, R., Sommer, C., Braun, M. H., Malz, P., Maussion, F., Mouginot, J., Seehaus, T. C., and Shean, D. E. 2021. "Distributed Global Debris Thickness Estimates Reveal Debris

Significantly Impacts Glacier Mass Balance." *Geophysical Research Letters* 48.8: e2020GL091311. doi:10.1029/2020GL091311.

Rowan, A. V., Egholm, D. L., Quincey, D. J., and Glasser, N. F. 2015. "Modelling the feedbacks between mass balance, ice flow and debris transport to predict the response to climate change of debris-covered glaciers in the Himalaya." *Earth and Planetary Science Letters* 430: 427–438. doi:10.1016/j.epsl.2015.09.004.

Sakai, A., Nakawo, M., and Fujita, K. 2002. "Distribution Characteristics and Energy Balance of Ice Cliffs on Debris-covered Glaciers, Nepal Himalaya." *Arctic, Antarctic, and Alpine Research* 34.1: 12–19. doi:10.1080/15230430.2002.12003463.

Sakai, A., Takeuchi, N., Fujita, K., and Masayoshi, N. 2000. "Role of supraglacial ponds in the ablation process of a debris-covered glacier in the Nepal Himalayas." *Debris-Covered Glaciers (Proceedings of a workshop held at Seattle, Washington, USA, September 2000)* 265: 119–130.

Steiner, J. F., Buri, P., Miles, E. S., Ragettli, S., and Pellicciotti, F. 2019. "Supraglacial ice cliffs and ponds on debris-covered glaciers: spatio-temporal distribution and characteristics." *Journal of Glaciology* 65.252: 617–632. doi:10.1017/JOG.2019.40.

Steiner, J. F., Pellicciotti, F., Buri, P., Miles, E. S., Immerzeel, W. W., and Reid, T. D. 2015. "Modelling ice-cliff backwasting on a debris-covered glacier in the Nepalese Himalaya." *Journal of Glaciology* 61.229: 889–907. doi:10.3189/2015JOG14J194.

Vacco, D. A., Alley, R. B., and Pollard, D. 2010. "Glacial advance and stagnation caused by rock avalanches." *Earth and Planetary Science Letters* 294.1-2: 123–130. doi:10.1016/J.EPSL.2010.03.019.

Van Woerkom, T., Steiner, J. F., Kraaijenbrink, P. D., Miles, E. S., and Immerzeel, W. W. 2019. "Sediment supply from lateral moraines to a debris-covered glacier in the Himalaya." *Earth Surface Dynamics* 7.2: 411–427. doi:10.5194/ESURF-7-411-2019.

Vaughan, D. G. 1993. "Relating the occurrence of crevasses to surface strain rates." *Journal of Glaciology* 39.132: 255–266. doi:10.3189/S0022143000015926.

Vincent, C., Wagnon, P., Shea, J. M., Immerzeel, W. W., Kraaijenbrink, P., Shrestha, D., Soruco, A., Arnaud, Y., Brun, F., Berthier, E., and Sherpa, S. F. 2016. "Reduced melt on debris-covered glaciers: Investigations from Changri Nup Glacier, Nepal." *Cryosphere* 10.4: 1845–1858. doi:10.5194/TC-10-1845-2016.

Watson, S. C., Quincey, D. J., Carrivick, J. L., and Smith, M. W. 2017. "Ice cliff dynamics in the Everest region of the Central Himalaya." *Geomorphology* 278: 238–251. doi:10.1016/J.GEOMORPH.2016.11.017.

Appendix A

# Additional Figures

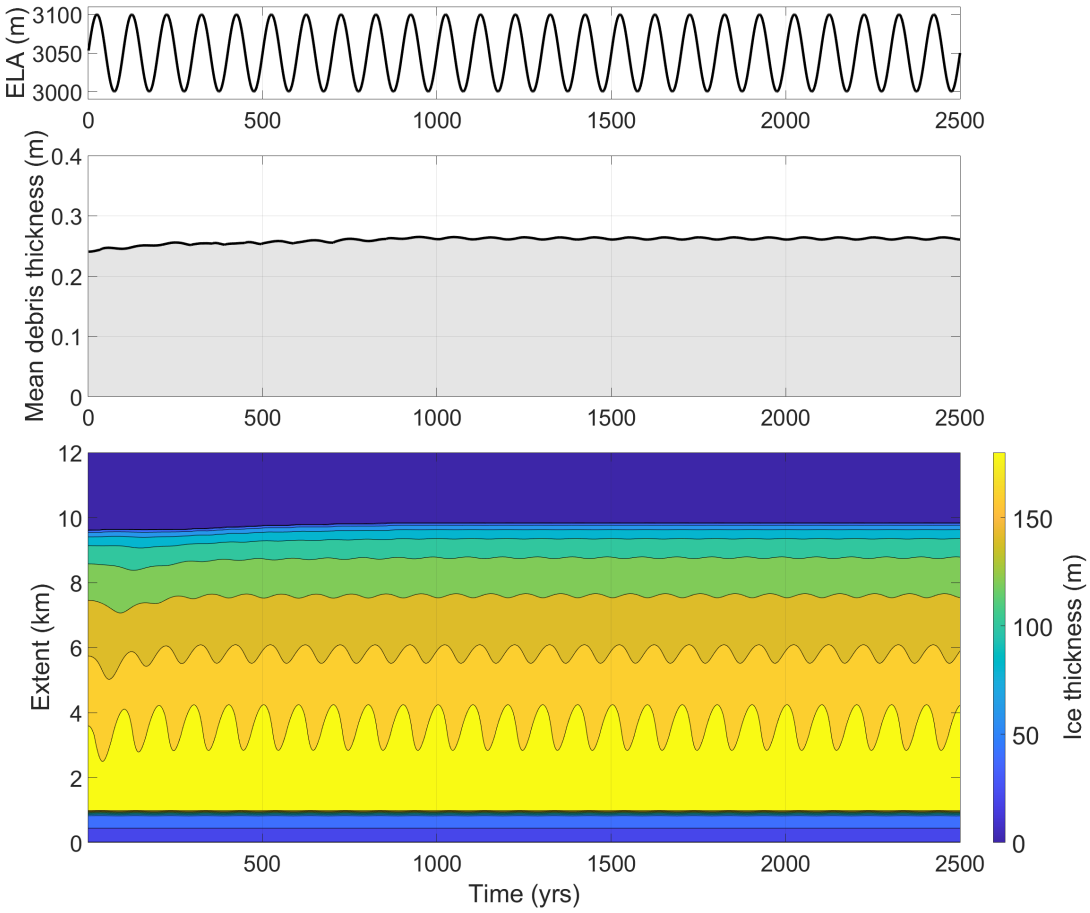


**Figure A.1:** *ELA, debris cover thickness and ice thickness contour plot of experiment B3 with a 100 year wavelength and a 50 meter amplitude.*

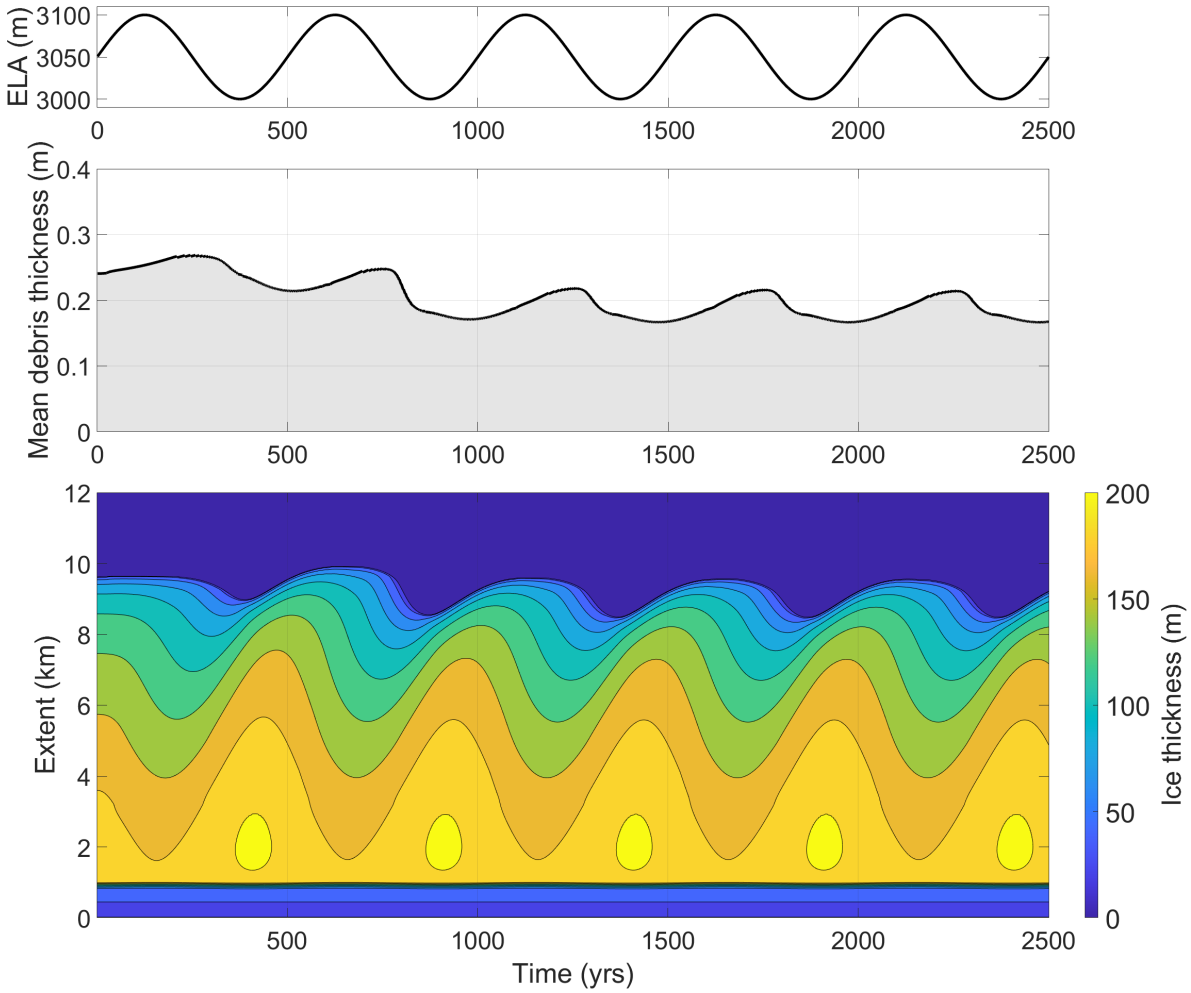


**Figure A.2:** *ELA, debris cover thickness and ice thickness contour plot of experiment B3 with a 500 year wavelength and a 50 meter amplitude.*

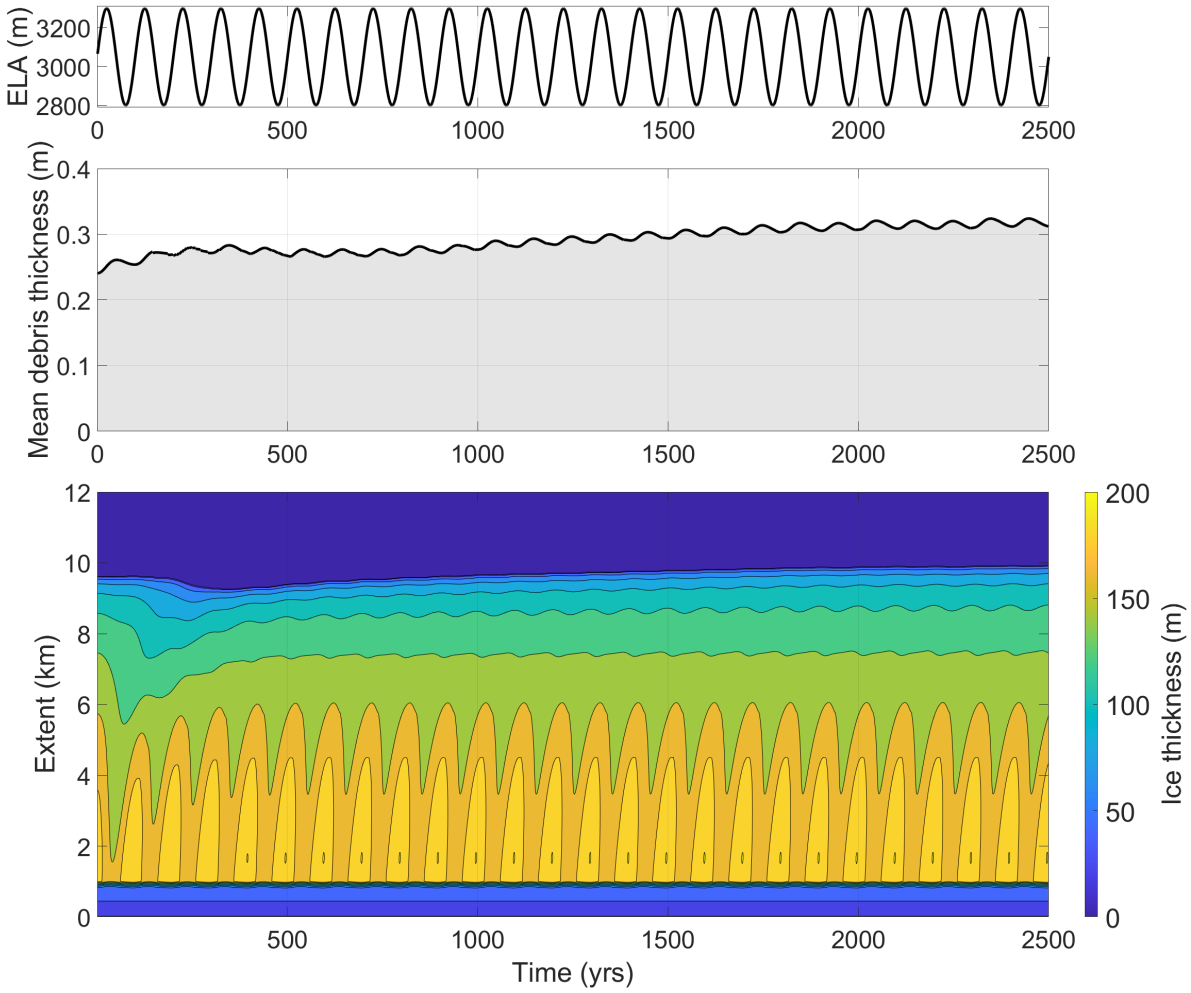


**Figure A.3:** *ELA, debris cover thickness and ice thickness contour plot of experiment B3 with a 100 year wavelength and a 250 meter amplitude.*

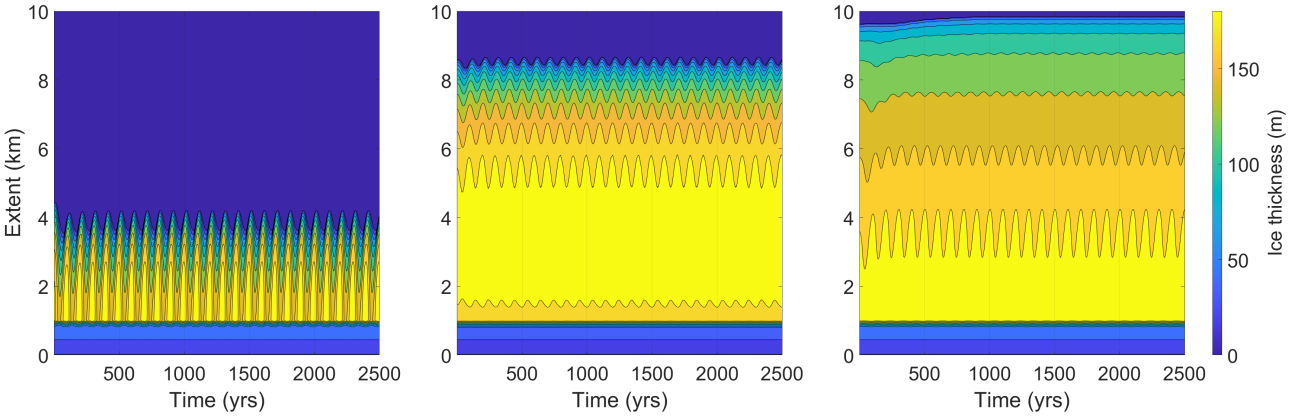


**Figure A.4:** *Ice thickness contour plots of experiment B3 ($\lambda$ = 100 years, $A$ = 50 meters) conducted on a small debris-free glacier (a), a large debris-free glacier (b), and a large debris-covered glacier (c). It is meant to show that the stable glacier extent found for debris-covered glaciers is not a results of its size (and therefore slower response) but rather of the insulation effect on the terminus through debris cover.*

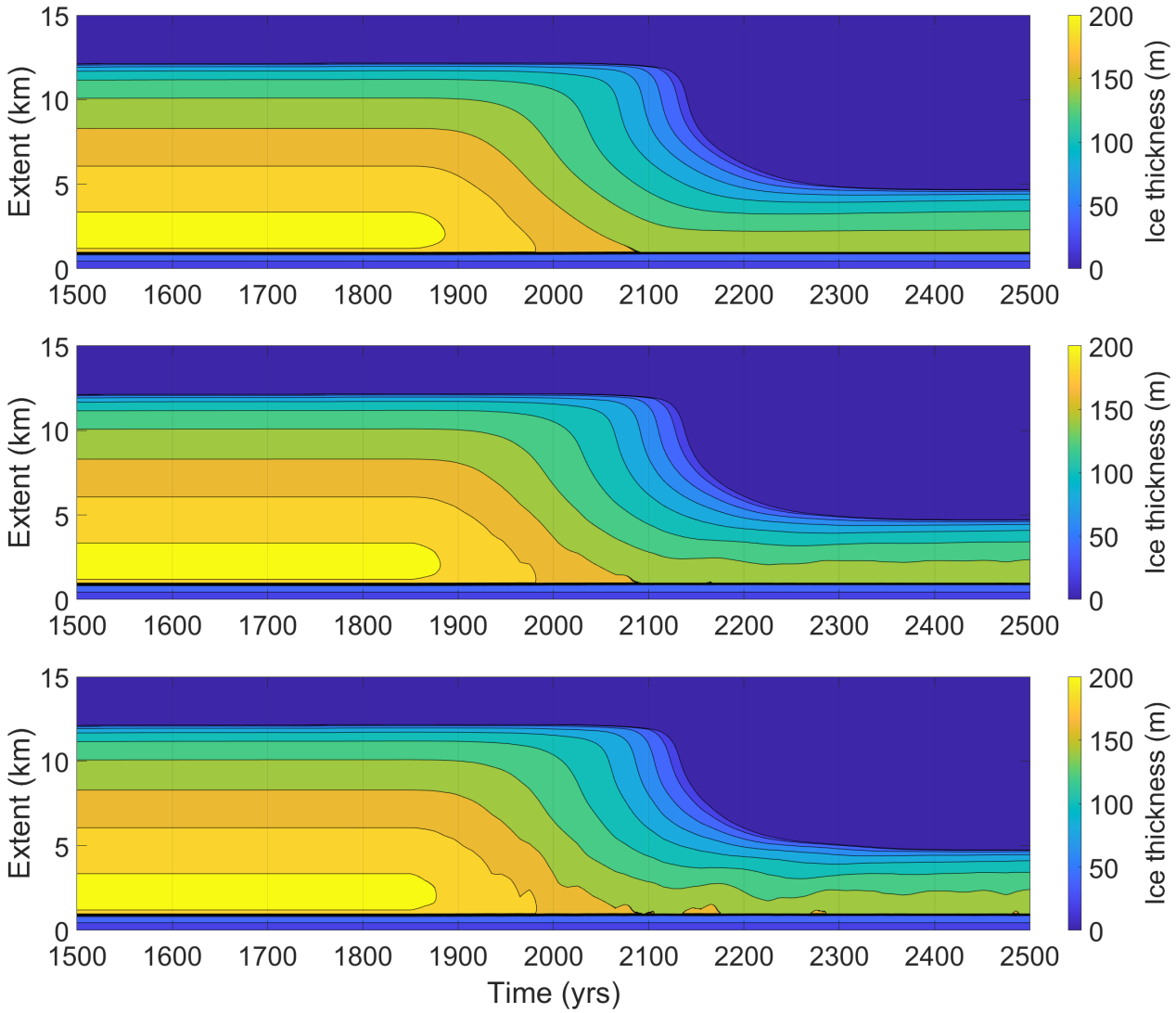


**Figure A.5:** *Linear increase experiment (B4) on a debris-covered glacier. The plots show a contour representation of ice thickness of the default linear increase climate (a), linear increase with a mean variability of 20 meters (b) and a linear increase with a mean variability of 50 meters (c). Variability is calculated in 10 year steps.*

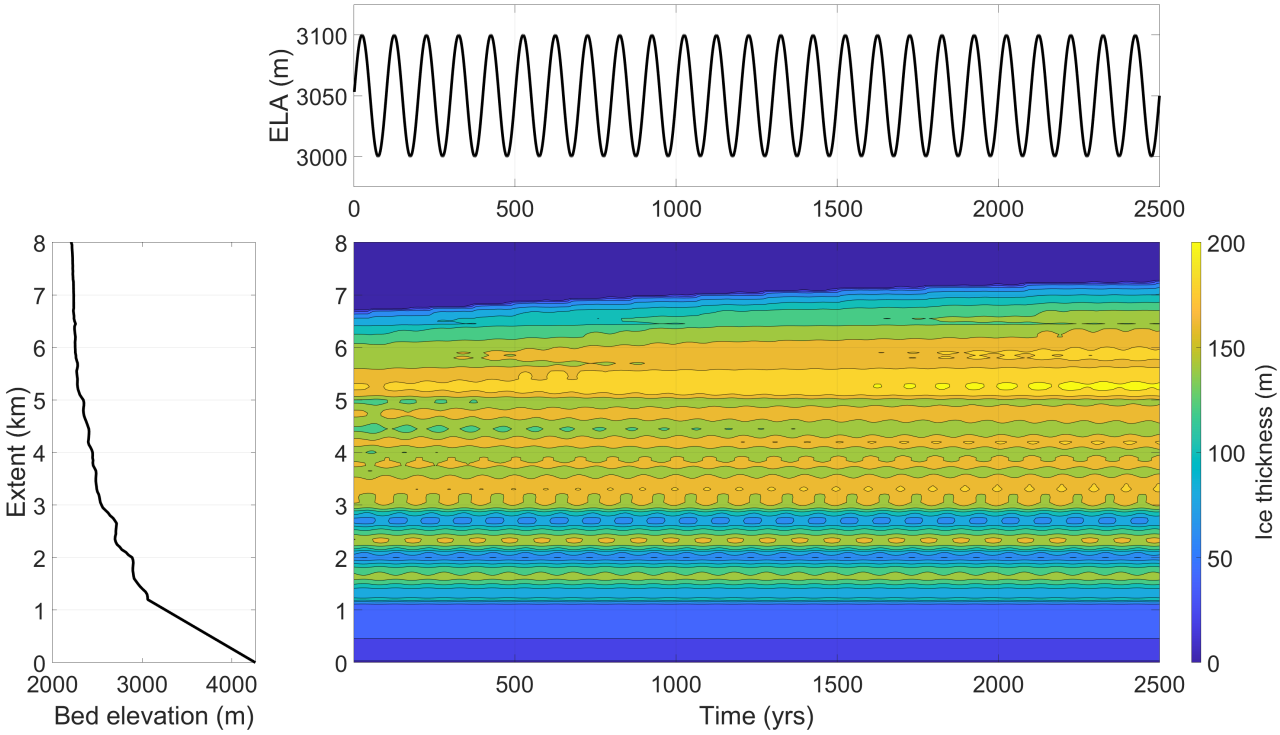


**Figure A.6:** *Sinus wave experiment (D1) on the Zmuttgletscher geometry, using $\lambda = 100$ years and $A = 50$ meters. Plots show ELA, bed topography, and a contour representation of ice thickness over time and space.*

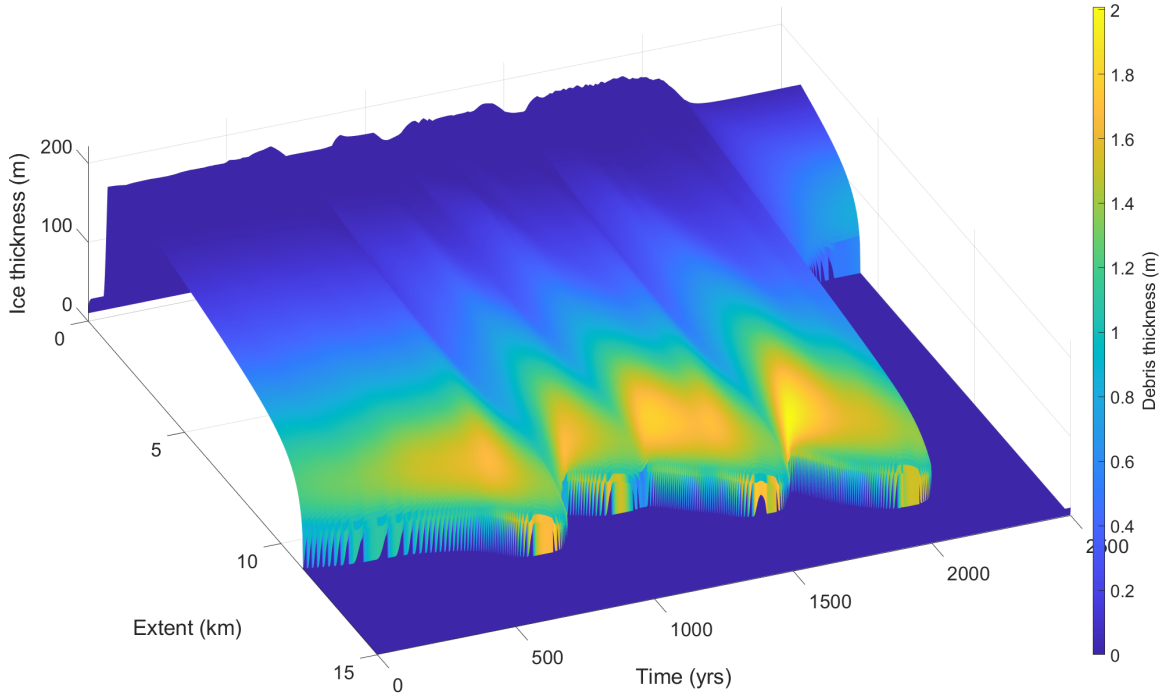


**Figure A.7:** *Contour representation of debris cover thickness on a 3D surface plot of model time, glacier length, and ice thickness in the real climate history and projections experiment (B5), using the SSP2 projection. The high debris cover anomalies after small retreat events are well visible, as well as artifacts from the boundary condition at the terminus.*

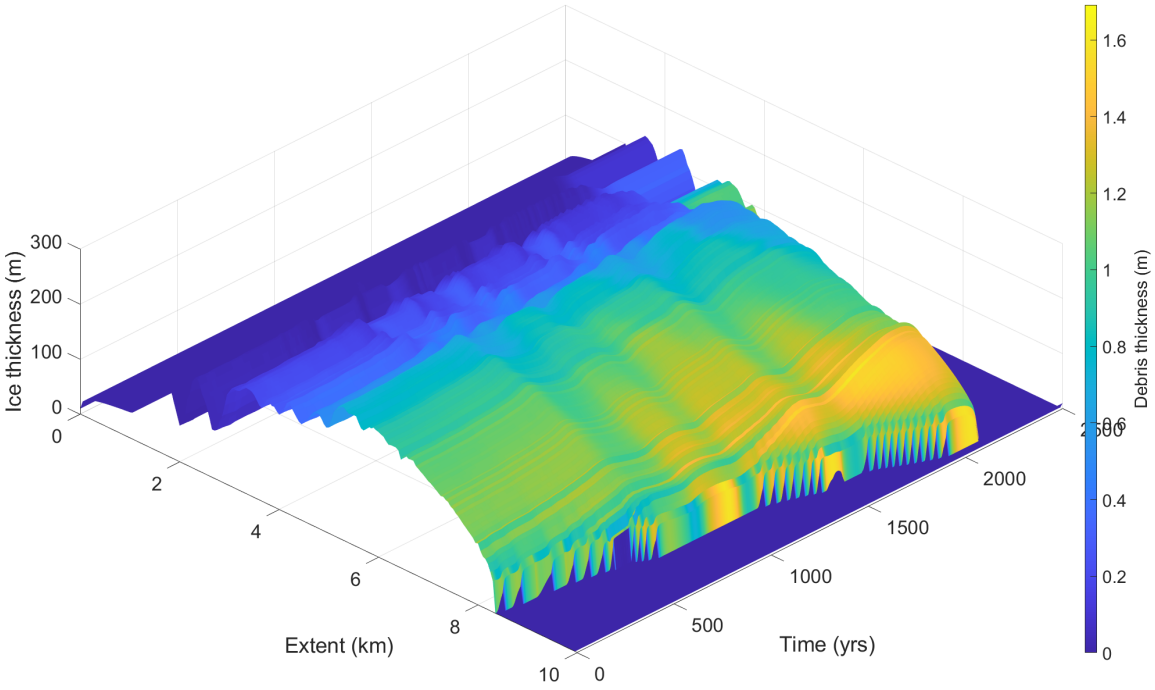


**Figure A.8:** *Contour representation of debris cover thickness on a 3D surface plot of model time, glacier length, and ice thickness in the real climate history and projections experiment on the Zmuttgletscher bed geometry (D2), using the SSP2 projection. We can observe the relatively thick tongue and the much more slow and steady advance without any signs of retreat between years 0 and 2000, contrary to the more reactive glacier on the abstract geometry (figure A.7).*

Appendix B

# Matlab code for the new cryokarst implementation

```
if c.cryo == 1 % cryokarst effect

    % cryokarst formation near terminus, by driving stress
    dx = x(2) - x(1);
    K = length(H);
    s = H+b;
    sgrad = 0*s;
    sgrad(2:K-1) = (s(3:K) - s(2:K-1))/dx(1);
    sgrad(1) = sgrad(2);
    taud = -c.rho*c.g*H.*sgrad;
    taud(H<=0.0) = 0.0;

    fac = c.lambdam*(c.maxth - taud)/(c.maxth-c.minth);
    fac(taud > c.maxth) = 0;
    fac(taud < c.minth) = c.lambdam;
    fac(H <=c.Ht) = 0;

    % cryokarst formation in the whole ablation area, by discharge

    % melt parameter value; only one of three active at once
    maxm = 50*dx; % default
    maxm = 500*dx;
    maxm = 200*dx;

    facm = c.lambdam*m*dx/maxm;
    facm(abs(m) > maxm) = c.lambdam;
    facm(abs(m) < 0) = 0;
    facm(H <=c.Ht) = 0;

    % effect on mass balance; only one of three active at once
    a = (1-fac).*a + fac.*aH; % default implementation
    a = (1-facm.').*a + facm.'.*aH; % melt factor solo
    a = (1-(fac+fam.')).*a + (fac+facm.').*aH; % default and melt ADDITIVE
```

Appendix C

# Personal declaration

---

I hereby declare that the submitted thesis is the result of my own, independent work. All external sources are explicitly acknowledged in the thesis.

Uster, 28.04.2022 Florian Hardmeier